Julia Brunner, BSc

Electron transferring flavoproteins link the degradation of D-2-hydroxyglutarate and D-lactate with energy production both in humans and yeast

MASTERARBEIT

Zur Erlangung des akademischen Grades

Master of Science

Masterstudium Biochemie und Molekulare Biomedizin

eingereicht an der

Technischen Universität Graz

Betreuer

Univ.-Prof. Dr. rer. nat. Peter Macheroux

Dr. rer. nat. Marina Toplak, BSc MSc

Institut für Biochemie

Graz, October 2019

Affidavit

I declare that I have authored this thesis independently, that I have not used other than the declared sources/resources, and that I have explicitly indicated all material which has been quoted either literally or by content from the sources used. The text document uploaded to TUGRAZonline is identical to the present master‘s thesis.

Eidestattliche Erklärung

Ich erkläre an Eides statt, dass ich die vorliegende Arbeit selbstständig verfasst, andere als die angegebenen Quellen/Hilfsmittel nicht benutzt, und die den benutzten Quellen wörtlich und inhaltlich entnommenen Stellen als solche kenntlich gemacht habe. Das in TUGRAZonline hochgeladene Textdokument ist mit der vorliegenden Masterarbeit identisch.

Date/Datum

Signature/Unterschrift

Acknowledgements

First and foremost, I would like to thank Prof. Dr. Peter Macheroux for the opportunity to work in his department, as well as for allowing me to work on this project and therefore helping me gain more experience. His guidance during the times when the project gave was very challening helped me to gain a better understanding on how to deal with problems occurring during research.

I would also like to thank my supervisor Marina Toplak for working on the project with me. Due to our teamwork lead to many successes and we were also able to overcome many difficulties we faces due to many of our interesting discussions, which made the project even more interesting and enjoyable. Working alongside her I was able to learn a lot of new things, which will definitely help me in my future career.

Additionally I also want to thank Julia Schmidt for her help and support during the second part of my project.

Furthermore, I would like to thank the entire biochemistry institute for their open arms and for welcoming me to be a part of their team. Their openness created a great work environment and made my experience at the institute even better.

Last, but certainly not least, I would also like to thank my friends and family for being by my side and encouraging me to follow my passion. I am grateful for their continuous interest in my project, which lead to many interesting talks. They always cheered me on and I am very thankful to them for that.

Abstract

Electron transferring flavoproteins (ETFs) are a group of proteins found in all organisms of life. They function as electron carriers, deliver electrons to the electron transport chain and therefore play an important role in energy production.

The aim of this thesis was to gain more knowledge on the characteristics of the ETF from *Saccharomyces cerevisiae* (yETF) and of its electron donor D-lactate dehydrogenase (Dld2), as well as their putative interaction. Furthermore, human D-2-hydroxyglutarate dehydrogenase in humans (hD2HGDH) was found to be a human protein homologous to Dld2 and was therefore tested for its ability to function as an electron donor for hETF.

Analyses of the electron transfer system in *Saccharomyces cerevisiae* using Dld2 and yETF have shown different biochemical and kinetic properties compared to the electron transfer system found in humans. Using D-2-hydroxyglutarate (D-2HG) as the preferred substrate, the conversion of the substrate using Dld2 leads to two electrons being transferred to yETF in a single step. Therefore, the electron transfer in *Saccharomyces cerevisiae* does not show the expected transfer of single electrons to ETF, like it is known for the human system and all previously tested eukaryotic ETFs. Considering the biochemical properties of yETF, it may also transfer two electrons at once to the following receptor enzyme, Cir2p, which would again be different compared to the homologous human system, as only single electrons get transferred from hETF to hETF-QO.

Additionally, experiments on hD2HGDH have shown that while this enzyme is a protein homologue of Dld2, the electron transfer from hD2GDH to hETF is slower than the electron transfer from Dld2 to yETF. Under steady-state conditions using DCPIP as final electron acceptor, this may be explained by the number of electrons transferred at once; while Dld2 transfers two electrons in a single step, hD2HGDH transfers one electron after the other. Nevertheless, the rates we determined in our assay are in the same range as shown for the electron transfer from other client dehydrogenases to hETF.

In the course of this thesis, new information about the electron transfer processes occurring in *Saccharomyces cerevisiae* could be gathered and information about its energy metabolism could be obtained. Additionally, hD2HGDH was identified as electron donor for hETF, making it the fourteenth enzyme found in humans to carry out this function.

Zusammenfassung

Elektronen-transferierende Flavoproteine (ETFs) sind eine Klasse von Proteinen, die in allen Organismen des Lebens gefunden werden können. Sie haben die Aufgabe, Elektronen, die sie von einem Elektronendonor erhalten, zur Elektronentransportkette weiterzuleiten und tragen daher entscheidend zur Energieproduktion bei.

Das Ziel dieser Arbeit war es, die biochemischen Eigenschaften von ETF aus *Saccharomyces cerevisiae* und dessen Elektronendonor D-Laktat dehydrogenase (Dld2) zu untersuchen, sowie die Interaktion zwischen ihnen zu erforschen. Zusätzlich wurde auch die D-2-Hydroxyglutarat dehydrogenase (D2HGDH), welche im Menschen zu finden ist, analysiert. Dieses Enzym ist homolog zu Dld2, weswegen überprüft wurde, ob hD2HGDH die Fähigkeit hat als Elektronendonor für menschliches ETF (hETF) zu wirken.

Der Elektronentransfer in *Saccharomyces cerevisiae* mittels Dld2 und yETF unterscheidet sich anhand der biochemischen und kinetischen Eigenschaften von dem Elektrontransfer in menschlichen Zellen. Das bevorzugte Substrat von Dld2, D-2-Hydroxyglutarat (D-2HG), stellt Elektronen für Dld2 zur Verfügung, welche anschließend in Form von zwei Elektronen an yETF transferiert werden. Dies unterscheidet sich von hETF, sowie von anderen getesteten eukaryotischen ETFs, da auf diese nur einzelne Elektronen übertragen werden können. Aufgrund der biochemischen Eigenschaften lässt sich vermuten, dass yETF zwei Elektronen in einem Schritt auf das Rezeptorenzym Cir2p übertragen kann, was sich von dem homologen menschlichen System unterscheiden würde, bei dem einzelne Elektronen übertragen werden.

hD2HGDH, das menschliche homologe Protein zu Dld2, transferiert Elektronen zu hETF mit Raten, die mit den Raten anderer Dehydrogenasen, welche mit hETF interagieren, übereinstimmen. Zusätzlich zeigen Experimente unter „steady-state“ Bedingungen und mittels künstlichen Elektronenakzeptoren, dass dieser Transfer langsamer stattfindet als der Elektronentransfer von Dld2 zu yETF. Dies könnte sich durch die Zahl an transferierenden Elektronen in einem Schritt erklären, da Dld2 zwei Elektronen auf einmal und hD2HGDH ein Elektron nach dem anderen transferiert.

Alles in allem konnten im Laufe dieser Arbeit neue Informationen über den Elektronentransfer, sowie über die Energieproduktion in *Saccharomyces cerevisiae* erhalten werden. Zusätzlich konnte hD2HGDH als Elektronendonor für hETF identifiziert werden, welches nun das vierzehnte entdeckte Enzym im Menschen ist, welches diese Funktion trägt.

Table of Content

1 Introduction 1

1.1 Electron transport chain 1

1.2 Flavoproteins 2

1.3 Electron transferring flavoproteins 4

1.3.1 General aspects 4

1.3.2 Electron transfer 5

1.3.3 Diseases associated with the electron transferring flavoprotein 6

1.4 Mitochondrial matrix flavoprotein dehydrogenases 6

1.5 Electron transport in *Saccharomyces cerevisiae* 7

1.6 D-2-hydroxyglutarate metabolism in *Saccharomyces cerevisiae* 8

1.7 D-2-hydroxyglutarate in humans 9

1.8 Outline of this thesis 10

1.9 References 12

2. Closing the gap: Yeast electron transferring flavoprotein links the oxidation of D-lactate and D-α-hydroxyglutarate to energy production via the respiratory chain 15

2.1 Abstract 17

2.2 Introduction 17

2.3 Experimental Procedures 19

2.3.1 Materials 19

2.3.2 Cloning and recombinant production of yETF (E. coli) 19

2.3.3 Cloning and recombinant production of Dld2 (K. phaffii) 20

2.3.4 Protein denaturation and determination of the extinction coefficient of yETF and Dld2 22

2.3.5 Photoreduction of yETF and Dld2 22

2.3.6 Expression, purification and photoreduction of hETF-βY16F 22

2.3.7 Determination of the redox potential of yETF and Dld2 22

2.3.8 Analysis of time-dependent modification in yETF by HPLC 23
2.3.9 Homology modeling of yETF 24
2.3.10 Site directed mutagenesis 24
2.3.11 Reductive and oxidative half reaction (Dld2) 25
2.3.12 Qualitative analysis of the electron transfer from Dld2 to yETF 25
2.3.13 Steady state kinetics (Dld2) 26
2.3.14 Steady state analysis of the electron transfer from Dld2 onto yETF 26
2.3.15 Titration of yETF and Dld2 with α-ketoglutarate 26
2.4 Results 27
2.4.1 Production, purification and biochemical characterization of yETF 27
2.4.2 Comparison of the yeast ETF to the human homolog 29
2.4.3 Biochemical characterization of Dld2 32
2.4.4 Kinetic properties of Dld2 and electron transfer to yETF 34
2.5 Discussion 38
2.5.1 Biochemical characterization of yETF 38
2.5.2 Kinetic characterization of Dld2 39
2.5.3 Two-electron transfer from Dld2 to yETF 42
2.6 Author contributions 42
2.7 Conflict of interest 42
2.8 Acknowledgements 42
2.9 References 43
3. Biochemical characterization of human D-2-hydroxyglutarate dehydrogenase and two disease related variants reveals the molecular cause of D-2-hydroxyglutaric aciduria... 48
Abstract 50
3.1 Introduction 51
3.2 Materials and Methods 52
3.2.1 Materials 52

3.2.2 Cloning and recombinant production of hD2HGDH 53
3.2.3 Recombinant production and purification of hETF 55
3.2.4 Protein denaturation and determination of the extinction coefficient of hD2HGDH 55
3.2.5 Photoreduction of hD2HGDH 55
3.2.6 Determination of the redox potential of hD2HGDH 55
3.2.8 Multiple sequence alignment 56
3.2.9 Reductive and oxidative half-reaction 57
3.2.10 Electron transfer from hD2HGDH to hETF 57
3.2.11 Steady-state kinetics (hD2HGDH) 58
3.2.12 Steady-state analysis of the electron transfer from hD2HGDH to hETF 58
3.2.13 Site-directed mutagenesis 58
3.2.14 Co-production of GB1-hD2HGDH variants and the groES-groEL complex ... 59
3.2.15 Production of GB1-hD2HGDH variants in the presence of increased riboflavin levels in the culture medium 59
3.2.16 CD-spectroscopy 60
3.2.17 Limited proteolysis 60
3.3 Results 60
3.3.1 Production, purification and biochemical characterization of hD2HGDH 60
3.3.2 Kinetic characterization of hD2HGDH 63
3.3.3 Electron transfer from hD2HGDH to hETF 66
3.3.4 Production, purificationand characterization of two pathogenic variants of hD2HGDH 68
3.4 Discussion 71
3.4.1 Kinetic characterization of hD2HGDH 71
3.4.2 Electron transfer to hETF 73
3.4.3 Disease related variants 74
3.5 Conclusions 76

3.6 Author contributions 76
3.7 Conflict of interest 76
3.8 Acknowledgements 76
3.9 References 77
4. Supplement: 8-formyl FAD modification in yETF variants 82
4.1 Methods 82
4.1.1 Site directed mutagenesis 82
4.2 Results 83
4.2.1 Photoreduction of yETF variants 83
4.2.2 Formation of 8-formyl-FAD in yETF variants 83
4.3 Conclusion 85

1 Introduction

1.1 Electron transport chain

The electron transport chain, also known as the respiratory chain, is a complex system of proteins found in the mitochondria of all eukaryotic cells and plays an essential role in energy metabolism/production. Upon degradation of glucose and other sugars, high energy metabolites such as NADH and $FADH_2$ are generated, which donate electrons to the respiratory chain. The latter consists of five membrane-bound complexes. Complex I, an NADH dehydrogenase and complex II, a succinate dehydrogenase, "receive" electrons from NADH and $FADH_2$, respectively. The electrons are then passed on to ubiquinone, which can "move" through the inner mitochondrial membrane and delivers them further to complex III, the ubiquinol cytochrome c oxidoreductase. Using cytochrome c, the electrons are in the end transferred to complex IV, a cytochrome c oxidase, which in turn produces water. Additionally, complex I, III and IV couple electron transfer with the translocation of protons to the intermembrane space. The resulting proton gradient is then used by complex V, an ATP synthase, to produce energy in form of ATP [1].

The respiratory chain, starting from the donation of electrons up to the production of ATP, is shown in Figure 1.

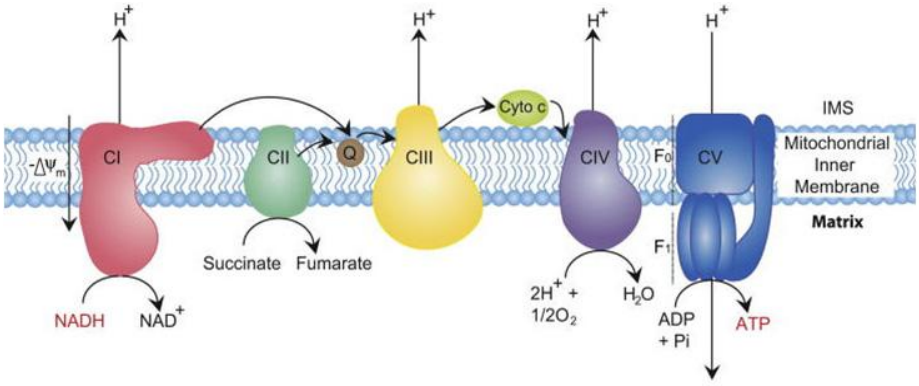

Figure 1: Overview of components of the respiratory chain [2]**.** Electrons are delivered to complex I and II by oxidizing NADH and $FADH_2$, respectively. In a chain-like reaction, the electrons are then transferred to ubiquinone, complex III and complex IV, which coincides with the formation of a proton gradient and ultimately results in the production of ATP.

Though not shown in Figure 1, electrons can also be transferred to the electron transport chain via the electron transferring flavoprotein (ETF) and the electron transferring flavoprotein-ubiquinone oxidoreductase (ETF-QO). The latter is a membrane-bound protein, which directly reduces ubiquinone, the electron carrier transferring electrons to complex III [3].

1.2 Flavoproteins

Flavoproteins are a group of proteins utilizing the vitamin B_2 (riboflavin) derivatives flavin mononucleotide (FMN) and/or flavin adenine dinucleotide (FAD) as a cofactor [4].

Due to the tricyclic heteroaromatic isoalloxazine ring of these cofactors, flavoproteins possess the ability to accept and donate up to two electrons [5], which enables them to catalyze reduction, oxidation, oxygenation and electron transfer reactions. [6]

There are three possible redox states a flavoprotein can adopt – oxidized, radical, and reduced state (Figure 2, Figure 3). Oxidized flavins are electron-deficient, therefore giving them the ability to accept up to two electrons. The radical state, which is also known as the semiquinone state, can be formed from an oxidized flavin if one single electron is transferred to the isoalloxazine ring [7]. Interestingly, semiquinones can be present in an anionic form or a neutral form [8], which can be distinguished based on their spectral characteristics around 350-400 nm and 500-600 nm, respectively (Figure 3) [9]. The reduced state, which is also known as the hydroquinone state, in contrast, can be formed by the reduction of an oxidized flavin resulting from the uptake of two electrons. The different redox states of flavins are shown in Figure 2.

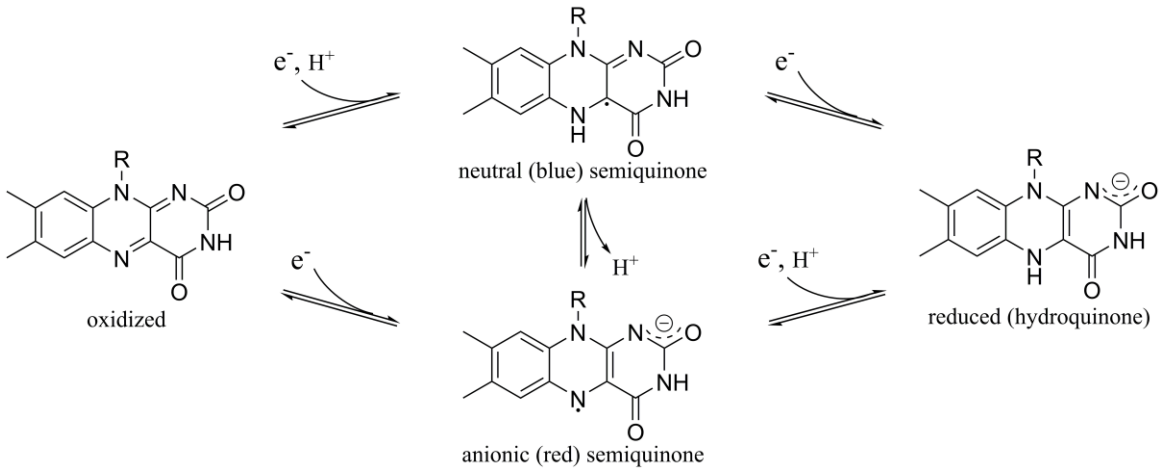

Figure 2: Flavin redox states. One electron reduction of the oxidized FAD leads to the formation of a semiquinone, which may be present in an anionic (red) or neutral (blue) state, whereas uptake of two electrons results in the formation of a hydroquinone, referred to as the fully reduced state of FAD.

Interestingly, semiquinones cannot be observed in all flavoproteins. The reason therefore is that not all of them provide a chemical environment required to efficiently stabilize a radical intermediate. The detailed analysis of the UV-visible absorption characteristics of a flavoprotein under certain conditions can hence give information about its possible electron transfer properties. Starting from an oxidized flavin, a two electron transfer is reflected by the simultaneous decrease in intensity of the characteristic flavin peaks at 360 and 450 nm (Figure 3 dashed line). If an anionic flavin semiquinone is formed, an increase of the 360 nm peak is observed, while a decrease of the peak at 450 nm is monitored [9] (Figure 3). A neutral flavin semiquinone, however, shows a wide absorbance band from 500-650 nm, with a maximum at 580 nm (Figure 3 dotted line).

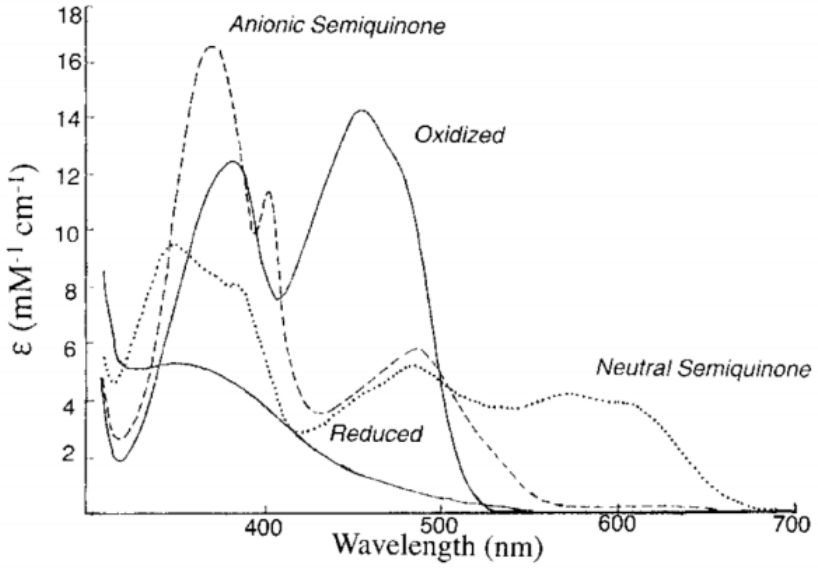

Figure 3: UV/Vis absorption spectra of a protein-bound flavin in its different redox states [10]**.** The solid lines show the oxidized and reduced states. The dashed line indicates an anionic semiquinone, while the dotted line represents a neutral semiquinone.

1.3 Electron transferring flavoproteins

1.3.1 General aspects

Electron transferring flavoproteins (ETF) are mitochondrial matrix proteins, which transfer electrons to a membrane-bound electron acceptor, called ETF-ubiquinone oxidoreductase, and thereby help to introduce electrons into the electron transport chain [11]. These proteins exist in all organisms as heterodimeric flavoproteins, consisting of a large α- and a small β-subunit. The FAD-cofactor bound at the subunit interface [12] is very crucial for their biochemical properties and enables these proteins to serve as electron carriers. While the structure of ETFs varies depending on the organism, the amino acid residues, which bind the flavin cofactor, are conserved [12].

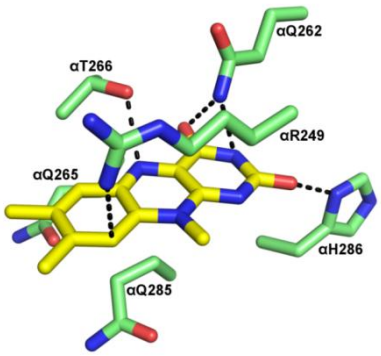

Figure 4: Conserved amino acid residues surrounding the isoalloxazine ring. The dashed lines indicate the possible interactions between FAD and the amino acid residues in its vicinity.

As ETFs are redox active due to the flavin cofactor, they can accept electrons from flavoprotein dehydrogenases, which are involved in different catabolic pathways [13]. In order to be able to do so, ETFs can adopt two conformations – an open, productive one, as well as a closed, unproductive conformation. While they are usually present in their closed form in "free" solution, ETFs tend to be in their open, productive state once they are in close proximity to a flavoprotein dehydrogenase. This is important since in the productive state the ETF's flavin cofactor is more exposed to the surface, which facilitates the acceptance of electrons [14].

1.3.2 Electron transfer

The interaction of a "reduced" flavoprotein dehydrogenase with ETF leads to the transfer of electrons to ETF, which consequently results in the reduction of the FAD cofactor bound to ETF. Reduced ETF can later on be re-oxidized by delivering the electrons to ETF-QO, a mitochondrial membrane protein. ETF-QO has two cofactors (a $[4Fe\text{-}4S]^{2+,1+}$ cluster and an FAD), which allow the electron transfer to occur. The iron-sulfur cluster is closer to the surface and thus serves as the primary acceptor for electrons delivered from ETFs. The cluster, in turn, shares these electrons with the FAD cofactor [15]. Once three electrons are transferred from ETFs to ETF-QO the latter is considered fully reduced and is able to interact with and reduce ubiquinone, allowing for the electrons to be used for energy production [16].

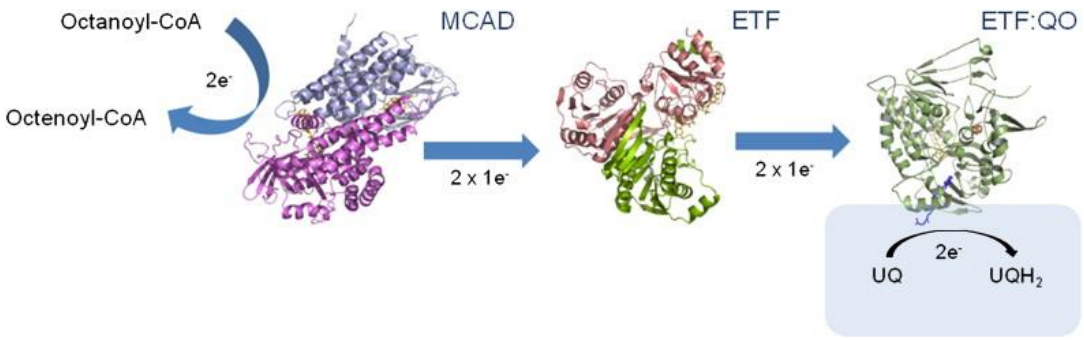

Figure 5: Electron transfer from MCAD (medium-chain acyl CoA dehydrogenase) to ETF and to its electron acceptor ETF-QO [17]**.** MCAD receives electrons by oxidizing octanoyl-CoA, leading to the reduction of MCAD's cofactor. The electrons are then donated to ETF in two steps. ETF, in turn delivers the electrons one at a time to ETF-QO, which further transfers them to ubiquinone and thereby introduces them into the respiratory chain.

1.3.3 Diseases associated with the electron transferring flavoprotein

Since ETF, its client dehydrogenases and ETF-QO are essential proteins for the production of energy, malfunction of this system can have serious consequences. For example, it may lead to the inherited disorder multiple acyl-coenzyme A (CoA) dehydrogenase deficiency (MADD), which is also known as glutaric aciduria type II [18]. This disorder results from the inactivity of either ETF or ETF-QO, which is caused by mutations in the genes encoding ETF-QO or one of the subunits of ETF. Depending on the severity of the disorder, clinical phenotypes can range from a lethal neonatal onset type, which is characterized by severe congenital anomalies, to the adult onset type [19]. Some patients suffering from an adult onset type of MADD can be treated with riboflavin, which leads to the patients having a normal life-span [19]. However, the majority of MADD patients cannot be treated successfully due to the severity of the disorder, resulting in a strongly shortened life-span [20].

1.4 Mitochondrial matrix flavoprotein dehydrogenases

Mitochondrial matrix flavoprotein dehydrogenases play important roles in energy metabolism. They catalyze oxidation reaction in various catabolic processes, such as in the β-oxidation of fatty acids, in the degradation of amino acids and/or in the degradation of choline (a process only occurring in humans and other mammals) [16] and link the reoxidation of their flavin cofactor to electron transfer to ETFs [17].

In humans, there are 13 (14) known flavoprotein dehydrogenases, which transfer electrons to hETF [12 + chapter 2]. These dehydrogenases are involved in the metabolic processes mentioned above and are structurally rather distinct. In order to be able to interact with all of these dehydrogenases hETF, therefore, has evolved a flexible mechanism, allowing it to switch its conformation from the closed, unproductive conformation to the open, productive state in the presence of a client dehydrogenase [14].

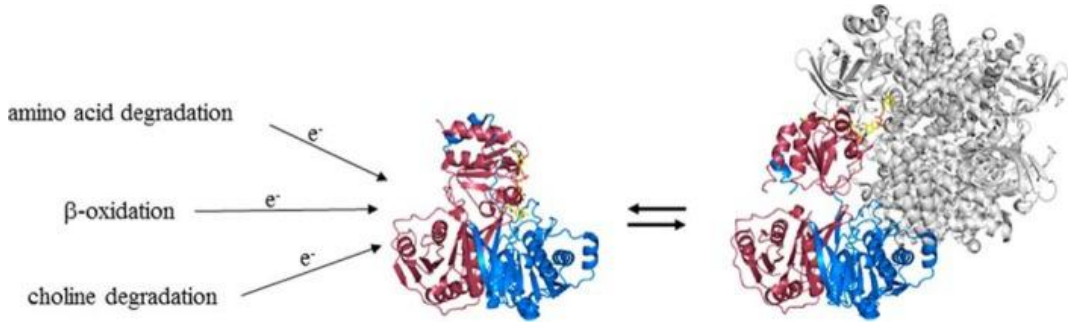

Figure 6: Interaction of human flavin dehydrogenases with hETF [16]**.** The mitochondrial matrix flavoprotein dehydrogenase can receive electrons via amino acid degradation, β-oxidation and/or choline degradation. After accepting the electrons, the dehydrogenase is able to interact with hETF, leading to the electron transfer from the dehydrogenase to ETF.

1.5 Electron transport in *Saccharomyces cerevisiae*

Electron transport in *Saccharomyces cerevisiae* operates based on the same principle as it does in other eukaryotic species; however, the amount of flavoprotein dehydrogenases involved in electron transport differs from other organisms. Humans, for instance, utilize 13 (14) different flavoprotein dehydrogenases [12 + chapter 2], which provide electrons to the respiratory chain. In contrast to that, only one dehydrogenase is suspected to act as an electron donor for the ETF in *S. cerevisiae* [21]. The reason for the difference in the quantity of client dehydrogenases can be found in the rather distinct organization of the catabolic processes in these organisms. In *S. cerevisiae*, fatty acid β-oxidation only occurs in peroxisomes, while it takes place in peroxisomes, as well as in the mitochondria in humans [22]. Therefore, the electrons are not provided to the respiratory chain, but are, alongside with protons, transferred to oxygen [23].

The generation of electrons is also achieved by the degradation of branched-chain amino acids. In mammals, four flavin dependent dehydrogenases are involved in the degradation – short branched chain acyl-CoA, iso-valeryl-CoA, iso-butyryl-CoA, and glutaryl-CoA

dehydrogenase [16]. However, the degradation of branched-chain amino acids in *S. cerevisiae* follows a different pathway. The amino acids leucine, isoleucine and valine are degraded to the "fusel" alcohols isoamyl alcohol, amyl alcohol and isobutyl alcohol, respectively [23, 24, 25]. The formation of these "fusel" alcohols does not require a dehydrogenation but a decarboxylation step, which can be carried out by pyruvate decarboxylase or α-ketoisocaproate decarboxylase [25].

Therefore, *S. cerevisiae* only has one dehydrogenase, D-lactate dehydrogenase (Dld2), which is suspected to act as the electron donor for its ETF (yETF) [21]. Dld2 is located in the mitochondrial matrix and it is thought to "receive" electrons by converting D-lactate and D-2-hydroxyglutarate to pyruvate and α-ketoglutarate, respectively [27].

1.6 D-2-hydroxyglutarate metabolism in *Saccharomyces cerevisiae*

In recent studies, D-2-hydroxyglutarate (D-2HG) has been shown to be a key-metabolite for energy production in *Saccharomyces cerevisiae* [27]. D-2HG is mainly present in the cytosol [28] and can be converted to α-ketoglutarate, which in turn can be shuttled across the inner mitochondrial membrane, leading to the introduction into the citric acid cycle. However, α-ketoglutarate in the mitochondria can also be re-converted to D-2HG, allowing it to serve as substrate for Dld2, a dehydrogenase suspected to be involved in energy production via respiratory chain [21].

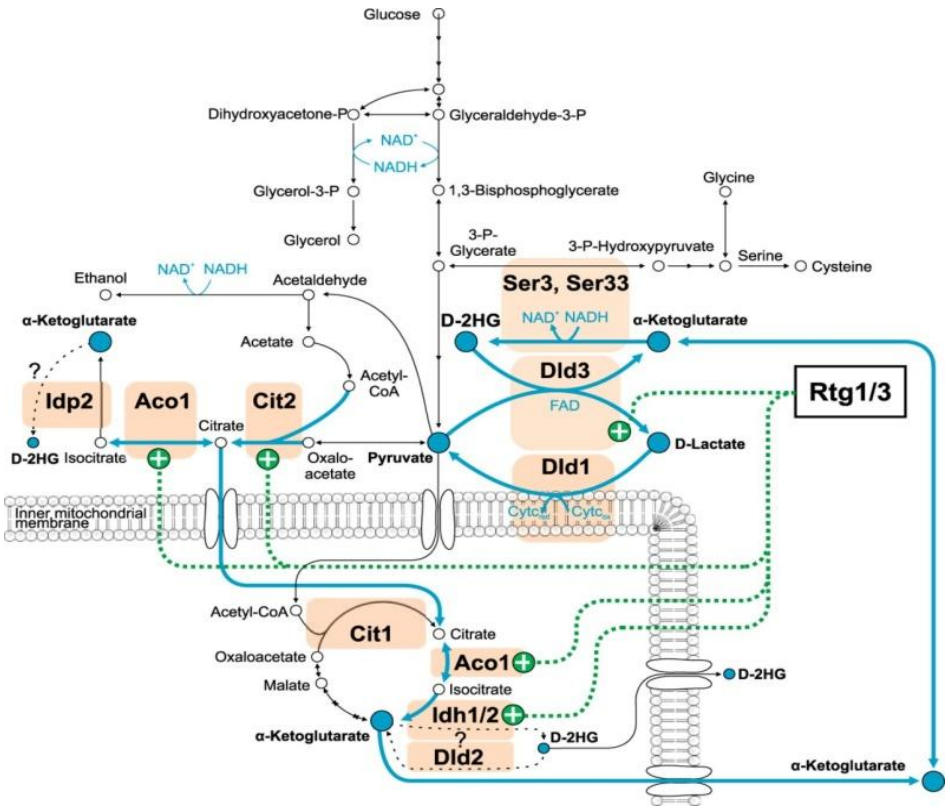

Figure 7: Metabolic network of *S. cerevisiae* showing the formation and degradation of D-2HG [27]**.** D-2HG is formed via enzymatic reactions using α-ketoglutarate in the cytosol, as well as in the mitochondria. The transport of D-2HG from cytosol to mitochondria is carried out by a transport system, which shuttles α-ketoglutarate across the membrane.

Although D-2HG can function as an energy source for *S. cerevisiae*, it is generally considered an oncometabolite, since an accumulation of D-2HG in the cell can lead to the inhibition of specific H3K36 histone demethylases, resulting in the alteration of gene expression. At the same time, the increase in H3K36 methylation may cause the repression of inhibitors controlling cell proliferation, therefore altering the cell growth [29].

1.7 D-2-hydroxyglutarate in humans

In humans it has been shown that an accumulation of 2-hydroxyglutarate can lead to various health issues, such as D-2-hydroxyglutaric aciduria (D-2HGA), a neurometabolic disorder [30]. D-2HGA is characterized by increased D-2HG (D-2-hydroxyglutarate) levels in the urine and may result in developmental delay, hypotonia and seizures [31] and is mainly caused by mutations in the *d2hgdh* gene [30].

The mutations in the gene result in the pathogenic amino acid substitutions in the mature protein, leading to the dysfunction of the enzyme D-2-hydroxyglutarate dehydrogenase (D2HGDH) [32]. The latter is a so far uncharacterized flavoprotein located in the mitochondria. However, in *Arabidopsis thaliana* it has been shown, that D2HGDH catalyzes the oxidation of D-lactate and D-2HG to pyruvate and α-ketoglutarate, respectively. It is further believed that *At*D2HGDH is able to transfer electrons to ETF [33], suggesting that D2HGDH may be a so far unexplored client enzyme of the human ETF.

1.8 Outline of this thesis

In this master's thesis studies of the energy metabolism in *Saccharomyces cerevisiae* in particular of the processes involving the electron-transferring flavoprotein (ETF) are summarized. Additionally, an enzyme suspected to act as an electron donor for the electron-transferring flavoprotein in *Homo sapiens* was analyzed.

Saccharomyces cerevisiae is known as a model organism, which is used to study and understand different cellular processes. A previous study had shown that upon exposure of hETF to alkaline conditions the cofactor bound to the protein gets irreversibly oxidized to its 8-formyl form [16]. To gain more information on the reaction mechanism leading to this modification, yETF variants were generated which mimic the protein pocket of hETF wild type, as well as of human ETF variants which rapidly generate 8-formyl-FAD modification as described by *Augustin et al. 2018* [16]. hETF (variants) showing a strong tendency toward 8-formylation strongly stabilized the anionic FAD semiquinone. Therefore, the redox state of FAD in yETF, as well as the degree of 8-formyl-FAD modification was examined (chapter 4. Supplement: 8-formyl FAD modification in yETF variants).

Following the comparison, the biochemical properties of yETF were further analyzed. ETFs of different organisms show a difference in their electron transfer. Since this process is strongly determined by the reduction potential of the protein-bound FAD, the latter was determined using stopped-flow spectrometry.

Additionally, D-lactate dehydrogenase (Dld2), the only known electron donor of yETF [21], was examined. Dld2 has the ability to oxidize D-α-hydroxyglutarate and D-lactate to α-ketoglutarate and pyruvate, respectively, and donates the electrons it receives during these

conversions to yETF. To acquire a broader knowledge on Dld2, its biochemical characteristics as well as the difference of its interaction with the two substrates were studied. The determination of the redox potential of Dld2 also provided insights into its putative interaction with yETF.

The kinetic properties of the interaction between Dld2 and yETF were also analyzed. Parameters were determined using both D-α-hydroxylutarate and D-lactate to find out if usage of a different substrate leads to different kinetic properties. Additionally, it was determined if Dld2 donates the electrons to yETF one by one or both electrons at once.

Furthermore, after taking a deeper look into the sequence of Dld2, a human protein homologous to Dld2 was found – D-2-hydroxyglutarate dehydrogenase (D2HGDH). This enzyme catalyzes the conversion of D-2-hydroxyglutarate to α-ketoglutarate; however an involvement of the enzyme in the energy production via ETF had not been reported thus far. Therefore, human D2HGDH (hD2HGDH) was produced recombinationally and its interaction with hETF was tested.

Lastly, two pathogenic variants of hD2HGDH were produced, their kinetic activity was tested and their structural properties were analyzed. However, the experiments addressing the pathogenic variants were not part of this thesis and were carried out by my supervisor Marina Toplak.

Experiments surrounding yETF and its electron donor Dld2 are shown in chapter 2. "*Closing the gap: Yeast electron transferring flavoprotein links the oxidation of D-lactate and D-α-hydroxyglutarate to energy production via the respiratory chain*". This article was published in the FEBS Journal in 2019. Additionally, chapter 3. "*Biochemical characterization of human D-2-hydroxyglutarate dehydrogenase and two disease related variants reveals the molecular cause of D-2-hydroxyglutaric aciduria*", which focuses on the analysis of hD2HGDH, was published in Biochimica et Biophysica Acta (BBA) in July 2019.

1.9 References

[1] Y. Hatefi, "*The mitochondrial electron transport and oxidative phosphorylation system*," Annu. Rev. Biochem., vol. 54, no. 1, pp. 1015–1069, 1985.

[2] L. D. Osellame, T. S. Blacker, and M. R. Duchen, "*Cellular and molecular mechanisms of mitochondrial function*," Best Pract. Res. Clin. Endocrinol. Metab., vol. 26, no. 6, pp. 711–723, Dec. 2012.

[3] J. Zhang, F. E. Frerman, and J.-J. P. Kim, "*Structure of electron transfer flavoprotein-ubiquinone oxidoreductase and electron transfer to the mitochondrial ubiquinone pool.*," Proc. Natl. Acad. Sci. U. S. A., vol. 103, no. 44, pp. 16212–7, Oct. 2006.

[4] I. A. Rodionova, M. W. Vetting, X. Li, S. C. Almo, A. L. Osterman, and D. A. Rodionov, "*A novel bifunctional transcriptional regulator of riboflavin metabolism in Archaea.*," Nucleic Acids Res., vol. 45, no. 7, pp. 3785–3799, Apr. 2017.

[5] J. T. Pinto and A. J. L. Cooper, "*From cholesterogenesis to steroidogenesis: role of riboflavin and flavoenzymes in the biosynthesis of vitamin D.*," Adv. Nutr., vol. 5, no. 2, pp. 144–63, Mar. 2014.

[6] P. Chaiyen and N. S. Scrutton, "*Special Issue: Flavins and Flavoproteins*," FEBS J., vol. 282, no. 16, pp. 3001–3002, Aug. 2015.

[7] V. Massey and G. Palmer, "*On the Existence of Spectrally Distinct Classes of Flavoprotein Semiquinones. A New Method for the Quantitative Production of Flavoprotein Semiquinones* *," Biochemistry, vol. 5, no. 10, pp. 3181–3189, Oct. 1966.

[8] T. C. Lehman and C. Thorpe, "*A new form of mammalian electron-transferring flavoprotein*," Arch. Biochem. Biophys., vol. 292, no. 2, pp. 594–599, 1992.

[9] P. Macheroux, "*UV-visible spectroscopy as a tool to study flavoproteins.*," Methods Mol. Biol., vol. 131, pp. 1–7, 1999.

[10] V. Massey, "*The Chemical and Biological Versatility of Riboflavin*," Biochem. Soc. Trans., vol. 28, no. 4, pp. 283–296, 2000.

[11] R. R. Ramsay, D. J. Steenkamp, and M. Husain, "*Reactions of electron-transfer flavoprotein and electron-transfer flavoprotein: ubiquinone oxidoreductase.*," Biochem. J., vol. 241, pp. 883–892, 1987.

[12] D. L. Roberts, D. Salazar, J. P. Fulmer, F. E. Frerman, and J. J. P. Kim, "*Crystal structure of Paracoccus denitrificans electron transfer flavoprotein: Structural and electrostatic analysis of*

a conserved flavin binding domain," Biochemistry, vol. 38, no. 7, pp. 1977–1989, 1999.

[13] S. Cortassa, M. A. Aon, and S. J. Sollott, "*Control and Regulation of Substrate Selection in Cytoplasmic and Mitochondrial Catabolic Networks. A Systems Biology Analysis.*," Front. Physiol., vol. 10, p. 201, 2019.

[14] H. S. Toogood, A. Van Thiel, N. S. Scrutton, and D. Leys, "*Stabilization of non-productive conformations underpins rapid electron transfer to electron-transferring flavoprotein*," J. Biol. Chem., vol. 280, no. 34, pp. 30361–30366, 2005.

[15] M. A. Swanson, R. J. Usselman, F. E. Frerman, G. R. Eaton, and S. S. Eaton, "*The iron-sulfur cluster of electron transfer flavoprotein-ubiquinone oxidoreductase is the electron acceptor for electron transfer flavoprotein,*" Biochemistry, vol. 47, no. 34, pp. 8894–8901, 2008.

[16] P. Augustin et al., "*Oxidation of the FAD cofactor to the 8-formyl-derivative in human electron-transferring flavoprotein*," J. Biol. Chem., vol. 293, no. 8, pp. 2829–2840, 2018.

[17] N. J. Watmough and F. E. Frerman, "*The electron transfer flavoprotein: Ubiquinone oxidoreductases,*" Biochimica et Biophysica Acta - Bioenergetics, vol. 1797, no. 12. pp. 1910–1916, 2010.

[18] M. Schiff, R. Froissart, R. K. J. Olsen, C. Acquaviva, and C. Vianey-Saban, "*Electron transfer flavoprotein deficiency: Functional and molecular aspects*," Mol. Genet. Metab., vol. 88, no. 2, pp. 153–158, 2006.

[19] L. L. Goh, Y. Lee, E. S. Tan, J. S. C. Lim, C. W. Lim, and R. Dalan, "*Patient with multiple acyl-CoA dehydrogenase deficiency disease and ETFDH mutations benefits from riboflavin therapy: a case report.*," BMC Med. Genomics, vol. 11, no. 1, p. 37, 2018.

[20] S. C. Grünert, "*Clinical and genetical heterogeneity of late-onset multiple acyl-coenzyme A dehydrogenase deficiency.*," Orphanet J. Rare Dis., vol. 9, p. 117, Jul. 2014.

[21] V. Gudipati, K. Koch, W. D. Lienhart, and P. Macheroux, "*The flavoproteome of the yeast Saccharomyces cerevisiae*," Biochim. Biophys. Acta - Proteins Proteomics, vol. 1844, no. 3, pp. 535–544, 2014.

[22] W. H. Kunau, V. Dommes, and H. Schulz, "*beta-oxidation of fatty acids in mitochondria, peroxisomes, and bacteria: a century of continued progress.*," Prog. Lipid Res., vol. 34, no. 4, pp. 267–342, 1995.

[23] S. A. Henry, S. D. Kohlwein, and G. M. Carman, "*Metabolism and regulation of glycerolipids in the yeast Saccharomyces cerevisiae.*," Genetics, vol. 190, no. 2, pp. 317–49, Feb. 2012.

[24] J. R. Dickinson et al., "*A 13C nuclear magnetic resonance investigation of the metabolism of leucine to isoamyl alcohol in Saccharomyces cerevisiae*," J. Biol. Chem., vol. 272, no. 43, pp. 26871–26878, 1997.

[25] J. R. Dickinson, S. J. Harrison, J. A. Dickinson, and M. J. E. Hewlins, "*An investigation of the metabolism of isoleucine to active amyl alcohol in Saccharomyces cerevisiae*," J. Biol. Chem., vol. 275, no. 15, pp. 10937–10942, 2000.

[26] J. R. Dickinson, S. J. Harrison, and M. J. E. Hewlins, "*An investigation of the metabolism of valine to isobutyl alcohol in Saccharomyces cerevisiae,*" J. Biol. Chem., vol. 273, no. 40, pp. 25751–25756, 1998.

[27] J. Becker-Kettern et al., "*Saccharomyces cerevisiae Forms D-2-Hydroxyglutarate and Couples Its Degradation to D-Lactate Formation via a Cytosolic Transhydrogenase*," J. Biol. Chem., vol. 291, no. 12, pp. 6036–6058, 2016.

[28] E. Albers, L. Gustafsson, C. Niklasson, and G. Liden, "*Distribution of 14C-labelleed carbon from glucose and glutamate during anaerobic growth of Saccharomyces cerevisiae*," Microbiology, vol. 144, no. 6, pp. 1683–1690, Jun. 1998.

[29] R. Janke, A. T. Iavarone, and J. Rine, "*Oncometabolite D-2-Hydroxyglutarate enhances gene silencing through inhibition of specific H3K36 histone demethylases*.," Elife, vol. 6, 2017.

[30] E. A. Struys *et al.*, "*Mutations in the d-2-Hydroxyglutarate Dehydrogenase Gene Cause d-2-Hydroxyglutaric Aciduria*," Am. J. Hum. Genet., vol. 76, no. 2, pp. 358–360, Feb. 2005.

[31] M. Kranendijk, E. A. Struys, G. S. Salomons, M. S. Van der Knaap, and C. Jakobs, "*Progress in understanding 2-hydroxyglutaric acidurias*.," J. Inherit. Metab. Dis., vol. 35, no. 4, pp. 571–87, Jul. 2012.

[32] A.-P. Lin et al., "*D2HGDH regulates alpha-ketoglutarate levels and dioxygenase function by modulating IDH2*.," Nat. Commun., vol. 6, p. 7768, Jul. 2015.

[33] W. L. Araújo et al., "*Identification of the 2-hydroxyglutarate and isovaleryl-CoA dehydrogenases as alternative electron donors linking lysine catabolism to the electron transport chain of Arabidopsis mitochondria.*," Plant Cell, vol. 22, no. 5, pp. 1549–63, May 2010.

2. Closing the gap: Yeast electron transferring flavoprotein links the oxidation of D-lactate and D-α-hydroxyglutarate to energy production via the respiratory chain

Closing the gap: Yeast electron transferring flavoprotein links the oxidation of D-lactate and D-α-hydroxyglutarate to energy production via the respiratory chain

Marina Toplak, Julia Brunner, Chaitanya Tabib and Peter Macheroux*

Institute of Biochemistry, Graz University of Technology, Petersgasse 12/2, A-8010 Graz, Austria

Running title: Electron transferring flavoprotein and D-lactate dehydrogenase 2 from *S. cerevisiae*

*to whom correspondence should be addressed:
Prof. Dr. Peter Macheroux
Graz University of Technology
Institute of Biochemisty
Petersgasse 12/2
A-8010 Graz, Austria
Tel.: +43-316-873 6450
Fax: +43-316-873 6952
Email: peter.macheroux@tugraz.at

Keywords: D-α-hydroxyglutarate, electron transferring flavoprotein, enzyme kinetics, flavin adenine dinucleotide (FAD), *Saccharomyces cerevisiae*.

Abbreviations: DCPIP, 2,6-dichlorophenol indophenol; Dld2, D-lactate dehydrogenase 2 from *Saccharomyces cerevisiae*; ETF, electron transferring flavoprotein; hETF, ETF from *Homo sapiens*; ETF-QO, ETF-ubiquinone oxidoreductase; 2HG, D-2-hydroxyglutarate or D-α-hydroxyglutarate; yETF, ETF from *Saccharomyces cerevisiae*; PCMH, p-cresol methylhydroxylase.

2.1 Abstract

Electron transferring flavoproteins (ETFs) have been found in all kingdoms of life, mostly assisting in shuttling electrons to the respiratory chain for ATP production. While the human (h) ETF has been studied in great detail, very little is known about the biochemical properties of the homologous protein in the model organism *Saccharomyces cerevisiae* (yETF). In view of the absence of client dehydrogenases, *e.g.* the acyl-CoA dehydrogenases involved in β-oxidation of fatty acids, D-lactate dehydrogenase 2 (Dld2) appeared to be the only relevant enzyme that is serviced by yETF for electron transfer to the mitochondrial electron transport chain. However, this hypothesis was never tested experimentally. Here, we report the biochemical properties of yETF and Dld2 as well as the electron transfer reaction between the two proteins. Our study revealed that Dld2 oxidizes D-α-hydroxyglutarate more efficiently than D-lactate exhibiting k_{catapp}/K_{Mapp} values of 1200± 300M^{-1} s^{-1} and 11 ± 2 M^{-1} s^{-1}, respectively. As expected, substrate-reduced Dld2 very slowly reacted with oxygen or the artificial electron acceptor 2,6-dichlorophenol indophenol (DCPIP). However, photoreduced Dld2 was rapidly re-oxidized by oxygen, suggesting that the reaction products, *i.e.*α-ketoglutarate and pyruvate, "lock" the reduced enzyme in an unreactive state. Interestingly, however, we could demonstrate that substrate-reduced Dld2 rapidly transfers electrons to yETF. Therefore, we conclude that formation of a product-reduced Dld2 complex suppresses electron transfer to dioxygen but favors the rapid reduction of yETF, thus preventing the loss of electrons and the generation of reactive oxygen species.

2.2 Introduction

Since the discovery of the first electron transferring flavoprotein (ETF) by Crane et al.[1] in 1956, a variety of other proteins belonging to the same family have been identified in all kingdoms of life. In prokaryotes as well as eukaryotes most of them function as housekeeping proteins by coupling the degradation of fatty and amino acids (in humans also of choline) with energy production via the respiratory chain [2]–[4]. This feature is based on the ability of ETFs to accept electrons from various dehydrogenases involved in catabolic pathways and the transfer to an integral membrane protein, ETF-ubiquinone oxidoreductase (ETF-QO), which in turn reduces ubiquinone, a key metabolite of the respiratory chain, and thus directly influence the generation of ATP. In some cases, however, ETF is part of a specialized system, for example in *Methylophilus methylotrophus* and *Peptostreptococcus elsdenii*. In these

bacteria reduced trimethylamine dehydrogenase and NADH, respectively, serve as the predominant source for electrons, as these organisms lack the metabolic pathways mentioned above and, therefore, rely on other carbon sources (methanol or trimethylamine and D-lactate, respectively) for energy production [5]–[9].In other cases, reduced ETFs transfer electrons to acyl-CoA dehydrogenases, which subsequently catalyze the reduction of short chain α,β-unsaturated fatty acids [7].The cellular role of the electron transferring flavoprotein of *Saccharomyces cerevisiae* (yETF) appears to be similar to bacterial homologs because only one enzyme is currently suspected to deliver electrons, *i.e.* D-lactate dehydrogenase (Dld2), whereas, yETF was reported to deliver the electrons to an ETF-QO homolog, named Cir2p, and thus shares this feature with other eukaryotic organisms [10], [11].

The mitochondrial matrix protein Dld2 was first discovered in a yeast-two-hybrid assay, which was used to identify actin interacting proteins (therefore it was initially called Aip2)[12]–[14]. In the course of subsequent *in vivo* characterizations, however, it was shown that the protein catalyzes the oxidation of D-lactate to pyruvate. Interestingly, recent studies by Becker-Kettern *et al.* revealed that Dld2was also able to oxidize D-α-hydroxyglutarate to α-ketoglutarate [15]. In fact, according to steady-state experiments (with truncated Dld2) D-α-hydroxyglutarate was oxidized with a higher efficiency compared to D-lactate[15]. In any case, the oxidation of the two substrates results in the reduction of the flavin cofactor, which needs to be regenerated for turnover. Although the natural electron acceptor of reduced Dld2 remains elusive, the presence of a gene encoding an electron transferring flavoprotein suggested this protein to serve as the electron acceptor, which then further transfers the electrons to a quinone-dependent dehydrogenase in the inner mitochondrial membrane (Cir2p).

To study the possible interaction and the electron transfer between Dld2 and yETF, we produced both proteins in *Komagataella phaffii* and *Escherichia coli*, respectively. In a detailed biochemical characterization of yETF, we could show that it exhibits spectral and electrochemical properties strongly diverging from its human counterpart [16], despite high sequence identity (47 %) and structural similarity. Because we identified only a single amino acid residue in the active site of yETF to be different in comparison with the human homolog (βPhe19 vs βTyr16), we asked the question whether the replacement of this particular phenylalanine by tyrosine could restore the biochemical properties of hETF [16], [17]. Therefore, we also generated a βPhe19Tyr variant, as well as two double variants (βPhe19Tyr-αAsn269Ala and βPhe19Tyr-βGlu169Ala), with an additional amino acid

exchange targeting the well-studied salt bridge at the surface of the human protein (equivalent to human αAsn259Ala and βGlu165Ala variants, respectively)[18].

To better understand the catalytic properties of full length Dld2, we performed a detailed kinetic characterization of the enzyme involving steady-state and pre steady-state experiments with both substrates, *i.e.* D-α-hydroxyglutarate and D-lactate. As previously reported by Becker-Kettern *et al.*[15], steady-state experiments revealed a higher catalytic efficiency and lower K_{Mapp} with D-α-hydroxyglutarate, but also a lower turnover. In our pre steady-state experiments, however, D-α-hydroxyglutarate was shown to reduce Dld2 about 10-times faster than D-lactate, which indicated that the oxidative half-reaction was rate limiting under steady-state conditions using DCPIP as electron acceptor. Finally, we could show that substrate-reduced Dld2 rapidly transfers electrons to yETF, suggesting that product binding to the reduced Dld2 suppresses reaction with oxygen but not with yETF. Thus, our study revealed that (i) Dld2 is in fact a more efficient D-α-hydroxyglutaric acid dehydrogenase, (ii) electron transfer is controlled by product binding to reduced Dld2 and (iii) yETF is the natural electron acceptor of Dld2.

2.3 Experimental Procedures

2.3.1 Materials

All chemicals and media ingredients were purchased from Sigma-Aldrich (St. Louis, MO, USA), Roth (Karlsruhe, Germany), Merck (Darmstadt, Germany), Fluka (Buchs, Switzerland) or Becton, Dickinson and Company (Franklin, Lakes, NJ, USA) and were of the highest grade commercially available.

All restriction enzymes used were ordered form Thermo Scientific/Fermentas (St. Leon-Rot, Germany) or New England Biolabs (Ipswich, MA, USA) and Ni-sepharose column material was obtained from GE Healthcare (Chalfont St. Giles, UK).

2.3.2 Cloning and recombinant production of yETF (E. coli)

To produce yETF in *Escherichia coli* the respective gene was purchased from Thermo Scientific, codon optimized for the *E. coli* organism. The received gene was subcloned to the *E coli* pJET vector and then, digested with *Nco*I and *Not*I to produce sticky ends on the DNA string. For gene expression the *yETF* gene subsequently was inserted into the vector pETM11-His TEV Appa, which added nucleotides coding for an N-terminal hexahistidine tag

to the gene sequence. Proper insertion of the gene was confirmed by sequencing, before transforming the recombinant plasmid with *E. coli* Rosetta (DE3)-pLysS cells for gene expression.

For expression, LB medium containing 50 µg/mL kanamycin as well as 20 µg/mL chloramphenicol for selection was inoculated with an overnight culture to an optical density at 600 nm (OD_{600}) of approximately 0.1. Then, cultures were left to grow to an OD_{600} of about 0.7 at 37°C and 140 rpm, before adding 100 µM IPTG to induce gene expression. To maximize the protein yield, the cultures were incubated at 20 °C and 140 rpm overnight.

Harvested cells were resuspended and lysed in binding buffer (50 mM HEPES, 15 mM imidazole, pH 7 + 1 mM DTT) by sonication with a Labsonic L sonication probe (B. Braun Biotech, Berlin, Germany) for 2 x 5 min. After centrifugation at 38,500 g for 1 h (4 °C), the cleared cell lysate was loaded onto a Ni-NTA column equilibrated with binding buffer. After removing unspecifically bound protein with wash buffer (50 mM HEPES, 15 mM imidazole, pH 7 containing 1 mM DTT), yETF was eluted with elution buffer (50 mM HEPES, 500 mM imidazole, pH 7 containing 1 mM DTT). To confirm the presence of the desired protein in the fractions as well as to determine the quality of the purification SDS-PAGE analysis was used. Fractions containing yETF were pooled and dialyzed against 50 mM HEPES pH 7 + 1 mM DTT for three hours. Then, the protein was concentrated to approximately 100 µM using Centripreps® 30 kDa MWCO (Merck Millipore, Burlington, MA, USA), flash frozen with liquid nitrogen and stored at -80 °C until further use.

2.3.3 Cloning and recombinant production of Dld2 (K. phaffii)

For recombinant expression of Dld2 in *Komagataella phaffii*, the respective gene was purchased from Thermo Scientific. On ordering, the sequence, flanked with the restriction sites *Xho*I (5') and *Not*I (3'), was optimized for *Komagataella phaffii*. Additionally, a nucleotide sequence coding for an octahistidine tag was added to the 3'-end of the gene, to allow purification by Ni-NTA affinity chromatography.

The received DNA string was cloned into the *Komagataella phaffii* vector pPICZα, using the *Xho*I and *Not*I restriction sites and successful insertion was confirmed by sequencing. Having linearized the plasmid DNA using *Sac*I, electroporation was carried out, according to the instructions provided by the EasySelect™ ExpressionKit (Invitrogen), to transform KM71H cells with our construct of interest. Additionally, the cells were transformed with pPICK-PDI

plasmid DNA to allow co-expression of the protein disulfide isomerase of *Saccharomyces cerevisiae*.

Small-scale expression in 96 well plates was performed as described by Weis et al. [19] in order to identify stably and well-expressing clones. Clones, which displayed the high signal intensity when analyzing the expression supernatants with dot blot, were later used in large-scale expression.

Large-scale expression was performed in a BBI CT5-2 fermenter (Sartorius, Göttingen, Germany) as described in [20]. After an induction time of 24 h (a total of 250 g MeOH were added), the pH was set to 8 and cells and medium were separated by centrifugation at 3,500 g for 30 min. As Dld2 was, despite the presence of an α-factor, not properly secreted, the protein had to be purified from the cell pellets. Therefore, the pellets (cell wet weight: about 1.2-1.5 kg per fermenter) were suspended in an equal volume of lysis buffer (50 mM HEPES, 150 mM NaCl, 10 mM imidazole pH 8 + 2 mM DTT and 2 mM PMSF) and lysed using zirconium oxide beads in a Merkenschlager (Braun Biotech International, Melsungen, Germany).

After centrifugation of the suspension (38,500 g for 1 h), the cleared lysate was incubated with 15 mL of equilibrated Ni-Sepharose™ (GE Healthcare) Fast Flow column material at 4°C for approximately 1.5 h. Then, the supernatant was decanted and the column material was packed into an empty column and washed with approximately 150 mL wash buffer (50 mM HEPES, 150 mM NaCl, 20 mM imidazole, pH 8), before eluting Dld2 with elution buffer (50 mM HEPES, 150 mM NaCl, 300 mM imidazole, pH 8). SDS-PAGE was used to identify fractions containing the protein, which, subsequently were pooled and concentrated.

To obtain Dld2 of satisfactory purity a second purification step was needed, which required the buffer to be exchanged to 50 mM HEPES, 150 mM NaCl, pH 8 using a Sephadex G-25 PD10 desalting column (GE Healthcare). Then, the protein solution was applied to a MonoQ™ 5/50 GL column (GE Healthcare), attached to an ÄKTA system (GE Healthcare) and equilibrated with buffer A (50 mM HEPES, 150 mM NaCl, pH 8). After a short wash with buffer A, the protein was eluted using a linear gradient of buffer A and buffer B (50 mM HEPES, 1 M NaCl, pH 8) (flow: 1 mL/min, linear gradient: 0 → 100 % buffer B in 40 minutes). Fractions containing pure Dld2 (the protein eluted at approximately 40 to 55 % buffer B) were pooled and concentrated using Centripreps® 30 kDa MWCO (Merck Millipore). The concentrated protein was flash frozen using liquid nitrogen and stored at -80 °C until further use.

2.3.4 Protein denaturation and determination of the extinction coefficient of yETF and Dld2

To determine the extinction coefficient of yETF, a spectrum of native as well as of denatured yETF was recorded as suggested by Macheroux[21]. Assuming that the spectrum of the denatured protein equals the one of free FAD, the extinction coefficient of free FAD (11,300 M^{-1} cm^{-1} at 450 nm) could be used to calculate the extinction coefficient of yETF at 450 nm (11,600 M^{-1} cm^{-1}) and 469 nm (9,900 M^{-1} cm^{-1}; independent of flavin modification), respectively.

The extinction coefficient of Dld2 was determined as described for yETF. From the absorbance at 450 nm recorded for native and denatured enzyme, an extinction coefficient of 12,700 M^{-1} cm^{-1} at 450 nm was calculated for Dld2.

2.3.5 Photoreduction of yETF and Dld2

Photoreduction was performed under anoxic conditions as described by Massey *et al.* (1978)[22]. For yETF, a solution containing 30 µM protein, 1 mM EDTA, 2 µM methylviologen and 1 µM 5-deaza-FMN was rendered anaerobic and transferred to a sealable quartz cuvette. After recording a UV-*visible* absorption spectrum from 300 to 800 nm, the sample was irradiated and additional spectra were recorded at a constant temperature of 15 °C, until no further spectral changes were observed. Then, the lid was removed under aerobic conditions to initiate reoxidation of the protein, which again was monitored spectrophotometrically.

Photoreduction of Dld2 was performed as described for yETF, just the amount of EDTA (2.5 mM), 5-deaza-FMN (2.5 µM) and methylviologen (6 µM) was adapted, as the sample turned out to be difficult to reduce.

2.3.6 Expression, purification and photoreduction of hETF-βY16F

Cloning and expression of the hETF-variant βY16F was carried out as described previously [16]. Photoreduction was carried out as described for yETF (see above).

2.3.7 Determination of the redox potential of yETF and Dld2

The redox potential of yETF was studied under anoxic conditions using a stopped flow device from Hi-Tech (SF-61DX2; TgK-Scientific, Bradford-on-Avon, UK) placed in an anaerobic

glove box (Belle Technology, Cambridge, UK) by applying the dye equilibrium method based on the xanthine/xanthine oxidase system, as reported by Massey [23]. Two solutions, one containing ~50 µM yETF, 500 µM xanthine and 5 µM methyl viologen and a second one with ~40 µM indigo carmine (A_{610}: ~0.5; E°:-125 mV) and ~200 nM xanthine oxidase, were prepared in 50 mM HEPES pH 7 + 1 mM DTT and mixed using the stopped flow device. Then, reduction of the flavin and the dye was monitored by recording 500 absorption spectra (350 to 700 nm) with a KinetaScan T diode array detector (MG-6560) within 2 h (four measurements). From these data a Nernst plot was generated by plotting the log ([ox]/[red]) of the protein as a function of the log ([ox]/[red]) of the dye - to determine the log($yETF_{ox}$/$yETF_{red}$) and the log(dye_{ox}/dye_{red}) the relative absorption changes at 460 nm and 610 nm, respectively, were used. Using the resulting intercept the redox potential of yETF could be determined as described by Minnaert [24].

To determine the redox potential of Dld2, two solutions, one containing ~20 µM Dld2, 500 µM xanthine and 5 µM methyl viologen and a second one with ~20 µM phenosafranin (A_{520}: ~0.2; E°: -252 mV) and ~200 nM xanthine oxidase, were prepared in 50 mM HEPES, 150 mM NaCl pH 7 and mixed using the stopped flow device. Then, reduction of the flavin and the dye was monitored by recording 500 absorption spectra (350 to 700 nm) with a KinetaScan T diode array detector (MG-6560) within 25 min (seven measurements). From these data a Nernst plot was generated by plotting the log ([ox]/[red]) of the enzyme as a function of the log ([ox]/[red]) of the dye - to determine the log($Dld2_{ox}$/$Dld2_{red}$) and the log(dye_{ox}/dye_{red}) the relative absorption changes at 450 nm and 520 nm, respectively, were used. Using the resulting intercept the redox potential of yETF could again be determined as described by Minnaert [24].

2.3.8 Analysis of time-dependent modification in yETF by HPLC

To analyze the degree and type of modification of the flavin bound to yETF, the protein was diluted to a concentration of approximately 50 µM at pH 8.5 and incubated at 25 °C for 24 h. Samples were taken after 0 and 24 h and inactivated by heat denaturation (10 min at 80-90°C). After 10 min of centrifugation at 13,300 rpm, the supernatant was transferred to HPLC-vials for following HPLC-DAD analysis with a Dionex Ultimate 3000 HPLC instrument (Thermo Fisher Scientific) equipped with an Atlantis® dC18 column (5 µm, 4.6 x 250 mm, Waters, Milford, MA, USA) equilibrated with H_2O/0.1 % TFA, 7 % acetonitrile. For all measurements, 100 µL of sample was injected and separation was carried out at a constant

temperature of 25 °C and a flow rate of 1 mL min^{-1} by applying the following gradient: 0 - 10 min, 7 - 9 % acetonitrile; 10 - 25 min, 10 % acetonitrile; 25 - 30 min, 12 % acetonitrile; 30 -32 min, 95 % acetonitrile; 32 – 40 min, 7 % acetonitrile. Elution of the different flavin species was monitored with a diode array detector (DAD; λ = 280, 370, 450, 460 nm, full spectrum).

2.3.9 Homology modeling of yETF

A homology model of yETF was generated using the SWISS-MODEL server [25]–[27]. Since yETF was found to share the highest sequence coverage and identity with hETF (PDB: 1efv[4]) the crystal structure of the latter protein was chosen as template. Additionally, the flavin cofactor was modeled into the predicted structure of yETF by aligning the two proteins and copying the flavin moiety from hETF to the active site of the yeast homolog.

2.3.10 Site directed mutagenesis

To get more information about the role of various active site residues found in yETF, variants were generated from the pETM11-yETF wild type construct, using PCR based mutagenesis. All required nucleotide exchanges were introduced using forward and reverse primers carrying the desired mutations (for primers see Table 4). Constructs confirmed by sequencing were transformed with *E. coli* Rosetta (DE3)-pLysS cells, to allow expression and purification as described for yETF wild type.

Table 4: Mutagenesis primers used for the generation of the various yETF-variants, with the codon triplets carrying the desired mutations shown in bold.

Variant	Type	Primer Sequence
βF19Y	fwd.	5'– GCGTATTCTGGTTCCGGTTAAACGTGTTGTTGAT**TAT**CAGATTAAACCG –3'
	rev.	5'– CGGTCAGGGTTTTATTCACACGCGGTTTAATCTG**ATA**ATCAACAACACG –3'
αN269A	fwd.	5'– CGTGCAAGCGTTGATAATGGCCTGTGTGAT**GCT**AGCCTGCAGATTGG –3'
	rev.	5'– GCAACAACTTTACCGGTCTGACCAATCTGCAGGCT**AGC**ATCACACAGG –3'
βE169A	fwd.	5'– CTGGATAATGGTCGTGTTCAGGTTACCCGT**GCA**ATCGATGATGGTG –3'
	rev.	5'– GGCTTGCTTCAATAACTTCTTCACCATCATCGAT**TGC**ACGGGTAACC –3'

2.3.11 Reductive and oxidative half reaction (Dld2)

To study the pre steady-state kinetics of Dld2, time dependent spectral changes of the flavin absorption were recorded under anoxic conditions using a stopped flow device (Hi-Tech, TgK Scientific), placed in a glove box (Belle Technology), and monitored with a KinetikaScan T diode array detector (MG-6560). The following analysis was performed by fitting the data points recorded at 450 nm with the Kinetic Studio Software (TgK Scientific).

For the determination of the reductive rate of Dld2, its flavin reduction was studied in the presence of seven different D-α-hydroxyglutarate (final concentration: 50 µM to 1500 µM) and nine D-lactate (final concentration: 1 mM to 100 mM) concentrations. A 20 µM enzyme solution and the substrate solutions were prepared in 50 mM HEPES, 150 mM NaCl pH 7, before mixing them in the stopped flow device and recording the spectral changes between 350 and 700 nm (measurements were performed 4-times at each substrate concentration). The extracted observed rate constants were plotted as a function of the respective substrate concentrations to obtain a hyperbolic curve, which allowed determination of the reduction rates (k_{red}) as well as of the dissociation constants (K_D).

To study the effect of product binding on the rate or reoxidation, one sample of reduced Dld2 (20 µM) was generated using photoreduction (see above) and a second one by adding about 1.5 eq of D-α-hydroxyglutarate. Then, both samples were mixed with air saturated buffer (20°C) in a stopped flow device and spectral changes between 350 nm and 700 nm were monitored for 1.5 - 3s and 25 - 50 min, respectively. To obtain bimolecular reoxidation rates, the observed rate constants were divided by the final oxygen concentration in the reaction mixture (final concentration: 140 µM).

2.3.12 Qualitative analysis of the electron transfer from Dld2 to yETF

To analyze the possible electron transfer from Dld2 to yETF, yETF was diluted to a final concentration of ~10 µM using 50 mM HEPES pH 7 + 1 mM DTT and mixed with 1 mM of D-α-hydroxyglutarate. After recording an initial UV-visible absorption spectrum between 300 and 800 nm, Dld2 was added to a final concentration of 10 nM and changes in the absorption characteristics of yETF were monitored over time.

2.3.13 Steady state kinetics (Dld2)

To study the kinetic parameters of Dld2 under steady state conditions, a coupled assay with DCPIP as final electron acceptor was used. Solutions containing varying final concentrations of D-α-hydroxyglutarate (25 µM to 1000µM) or D-lactate (1 mM to 250 mM) were prepared in 50 mM HEPES, 150 mM NaCl pH 7 and mixed with 125 µM DCPIP. After 10 minutes of incubation at 25°C, Dld2 was added to a final concentration of 100 nM and absorbance changes at 600 nm were recorded for 120s. By plotting the extracted initial rates as a function of the corresponding substrate concentrations the kinetic parametersK_{Mapp} andk_{catapp} could be determined.

2.3.14 Steady state analysis of the electron transfer from Dld2 onto yETF

Steady state parameters for the electron transfer of Dld2 onto wild type yETF were determined by performing a coupled assay with DCPIP as final electron acceptor. Therefore, buffer (50 mM HEPES pH 7 containing 1 mM DTT), Dld2 (10 nM), yETF (0.875 to 28 µM) and DCPIP (125 µM) were mixed and incubated at 25 °C for 10 minutes. Then, the reaction was started by adding 1 mM D-α-hydroxyglutarate, the substrate of Dld2, and the decrease in absorption at 600 nm was monitored at 25°C for 120 s (measurements at each yETF concentration were performed in triplicate). To determine the kinetic parameters K_{Mapp} and k_{catapp} the extracted initial velocities (normalized to enzyme concentration) were plotted as a function of the respective yETF concentrations yielding a hyperbolic curve, which was fitted using the program Origin 7 (OriginLab, Northampton, MA, USA).

2.3.15 Titration of yETF and Dld2 with α-ketoglutarate

To study the binding of α-ketoglutarate to yETF and Dld2,800 µL of protein diluted to a final concentration of about 10 µM using 50 mM HEPES pH 7 + 1 mM DTT and 50 mM HEPES, 150 mM NaCl pH 7, respectively, were transferred to a quartz cuvette (reference just 800 µL of buffer) and a UV-*visible* absorption spectrum between 300 and 800 nm was recorded. Then, 10 µL aliquots of 2.5 mM α-ketoglutarate were added to both the reference and the measurement cuvette and further spectra were recorded after an incubation time of 1 min following the addition of the metabolite.

2.4 Results

2.4.1 Production, purification and biochemical characterization of yETF

Recombinant production of yETF in *Escherichia coli* and subsequent purification using Ni-NTA affinity chromatography yielded about 3-5 mg of pure heterodimeric protein (Figure 1A, lane 6) per g wet cell weight, which allowed its detailed biochemical characterization. Like other flavoproteins yETF exhibits a characteristic UV-*visible* absorption spectrum with maxima at 377 nm and 441 nm, which are slightly shifted upon denaturation (Figure 1B, *black* and *red* line, respectively). The maxima at 373 nm and 447 nm observed in the absorption spectrum of denatured yETF further indicate the presence of an FAD chromophore, which is also present in all other electron transferring flavoproteins studied so far [6], [17], [28]–[31].

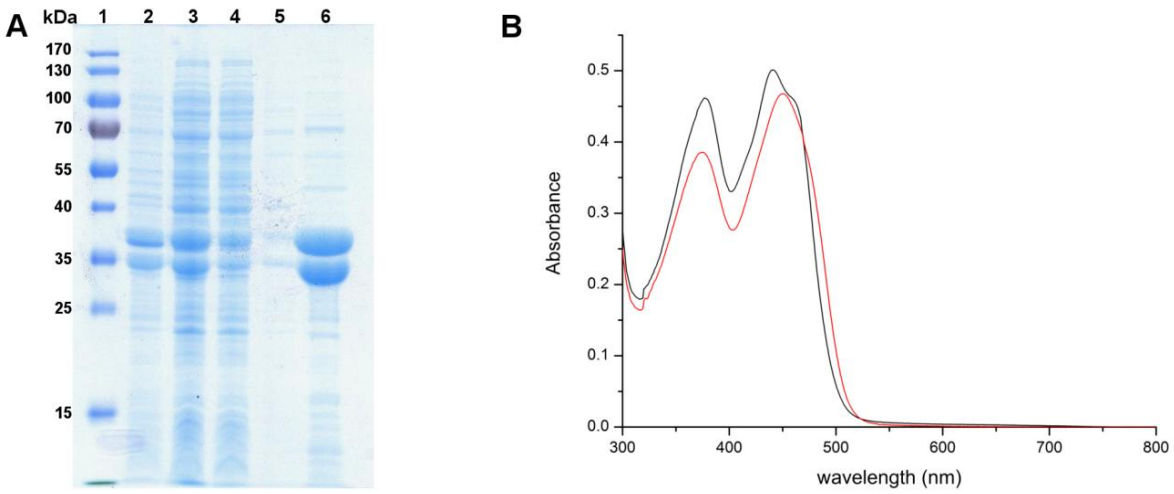

Figure 1: SDS-PAGE analysis of the different steps in yETF purification (A) and UV-*visible* absorption spectrum of native (*black* line) and denatured (*red* line) yETF (B). A, SDS-PAGE analysis of the different fractions collected during purification of yETF wild type using Ni-NTA affinity chromatography. In lane 1 PageRuler® prestained protein ladder (Thermo Fisher Scientific), in lane 2 the cell pellet after lysis, in lane 3 the cell lysate, in lane 4 the column flow through, in lane 5 the wash fraction and in lane 6 the elution fraction (α-subunit of yETF at 38 kDa; β-subunit at 37 kDa) is shown. **B**, UV-*visible* absorption spectra of yETF diluted to a final concentration of 40 µM with 50 mM HEPES pH 7 + 1 mM DTT (*black* line) and denatured using 2 % SDS (*red* line) were recorded between 300 and 800 nm at 25 °C. Based on the extinction coefficient of free FAD (denatured, *red* line) at 450 nm (11,300 M^{-1} cm^{-1}), the extinction coefficient of yETF wild type at 450 nm (11,600 M^{-1} cm^{-1}) and 469 nm (9,900 M^{-1} cm^{-1}) could be determined.

Though all ETFs share the same cofactor, their electrochemical properties are tuned to the electron transfer pathway they service. Eukaryotic ETFs were found to efficiently stabilize the anionic flavin semiquinone state and therefore mainly receive single electrons from their donor systems [28], while the protein-bound FAD cofactor in bacterial ETF from *Megasphera elsdenii* was shown to undergo two-electron reduction when accepting electrons[7]. To study the ability of yETF to stabilize the radical intermediate state, photoreduction and redox potential experiments were conducted. Upon illumination of oxidized yETF (Figure 2A, *black* line) under anoxic conditions, a short-lived anionic semiquinone (Figure 2A,*red* line) was observed, which could easily be further reduced to the hydroquinone form (Figure 2A, *blue* line). In the course of the reoxidation, no stable semiquinone intermediate was detected.

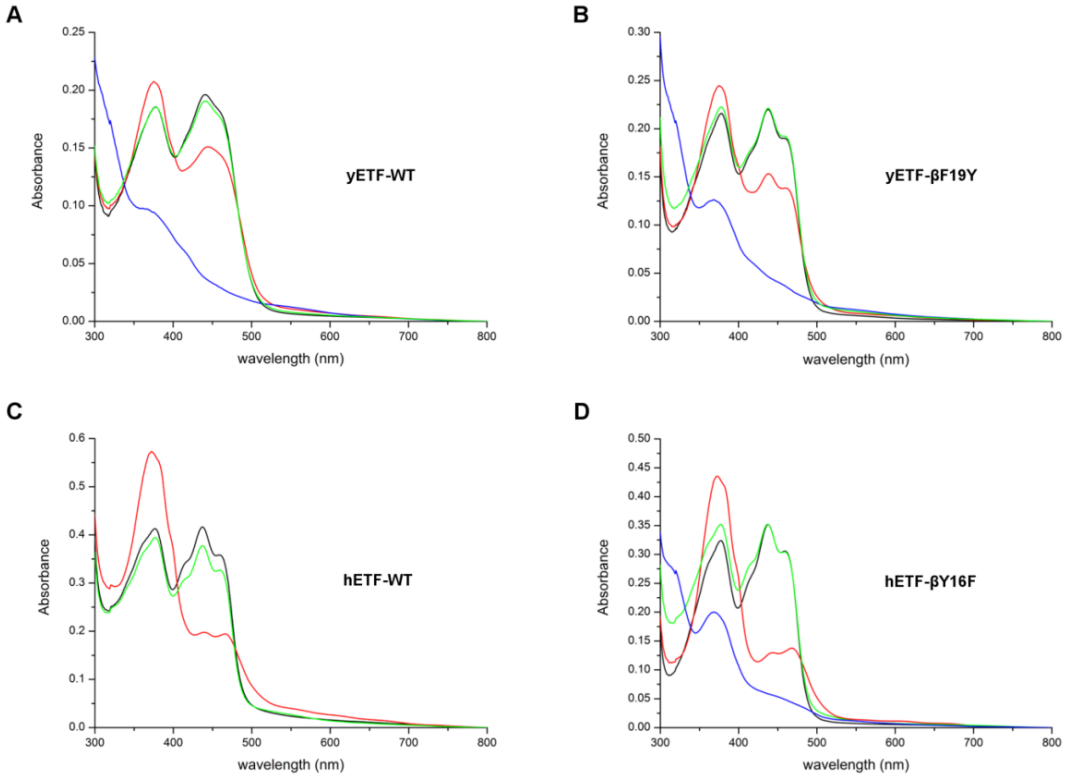

Figure 2: Photoreduction of yETF wild type (A) and yETF-βPhe19Tyr (B) as well as of hETF wild type (C) and hETF-βTyr16Phe (D) under anoxic conditions. UV-visible absorption spectra (300-800 nm) of yETF wild type and yETF-βPhe19Tyr as well as of hETF wild type and hETF-βTyr16Phe, diluted to a final concentration of 30 µM using 50 mM HEPES pH 7 containing 1 mM DTT, recorded during anaerobic photoreduction. The four spectra in each panel correspond to the different flavin redox states observed for yETF wild type (**A**), yETF-βPhe19Tyr (**B**), hETF wild type (**C**) and hETF-βTyr16Phe (**D**) in the course of the photoreduction: oxidized FAD (start spectrum, *black* line), anionic semiquinone (*red* line), reduced (*blue* line) and reoxidized FAD (*green* line).

When determining the redox potential of yETF, by applying the dye equilibration method [23], no stabilization of the flavin radical was observed, at all. The flavin chromophore and the reporting dye (indigo carmine; E°: -125 mV) were reduced almost synchronously (Figure 3), allowing the generation of a Nernst plot by plotting the $\log(yETF_{ox}/yETF_{red})$ as a function of the $\log(dye_{ox}/dye_{red})$. From the intercept a midpoint potential of -101 ± 2 mV (oxidized to reduced) was calculated, which is more negative compared to eukaryotic ETFs, *i.e.* around -20 mV [32], [33], but more positive than of the prokaryotic ETF from *Megasphera* (*Peptostreptococcus)elsdenii* (-259 mV)[34]. Therefore, yETF can be considered a better electron acceptor than the ETF from *Megasphera elsdenii*, but a weaker electron acceptor than the eukaryotic homologs.

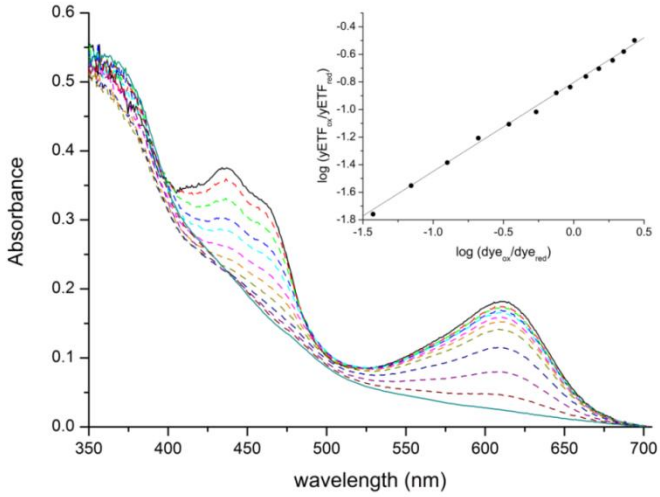

Figure 3: Determination of the redox potential of yETF wild type. Spectral changes of yETF (~25 µM) and indigo carmine (~20 µM; E°: -125 mV) observed in the course of the reduction reaction (2 h), indicating full reduction of the FAD cofactor and the dye and therefore a 2-electron transfer onto yETF. All measurements were carried out in 50 mM HEPES pH 7 + 1 mM DTT at a constant temperature of 25 °C. ***Inset***, Nernst plot obtained from a single measurement by plotting the $\log(yETF_{ox}/yETF_{red})$ as a function of the $\log(dye_{ox}/dye_{red})$ - to determine the $\log(yETF_{ox}/yETF_{red})$ and the $\log(dye_{ox}/dye_{red})$ the relative absorption changes at 460 and 610 nm, respectively, were used. From the intercept a redox potential of -101 ± 2 mV was calculated (from four determinations).

2.4.2 Comparison of the yeast ETF to the human homolog

Based on the X-ray structure of hETF, we have built a homology model of yETF indicating conservation of the overall fold (Figure 4A) and composition of the amino acid residues forming the FAD-binding pocket (Figure 4B). The only obvious difference found in the active

site of the model is the change of Tyr16 in hETF to Phe19 in yETF in the β-subunit (Figure 4B).

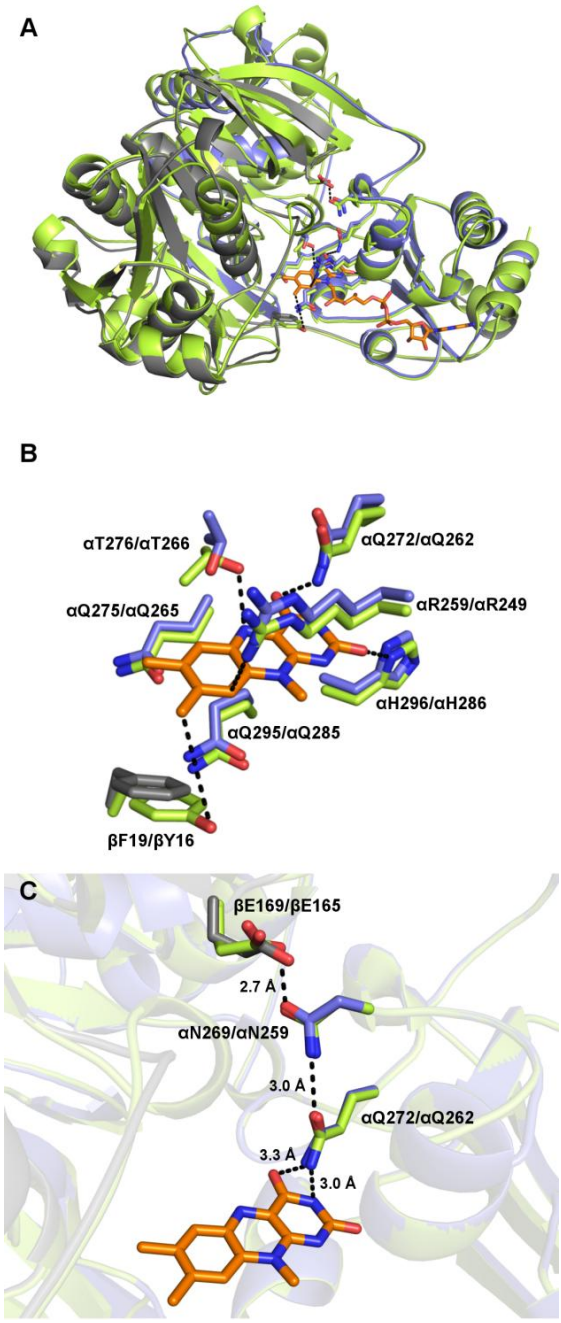

Figure 4: Structural comparison of yETF and hETF. A, Overall structure comparison of yETF (*blue*: α-subunit, *grey*: β-subunit; model based on hETF) and hETF (*green*; PDB: 1efv). **B**, Comparison of the active site residues of yETF (*blue*: α-subunit, *grey*: β-subunit) and hETF (*green*). The FAD cofactor (*orange*) and the important amino acid residues are shown as sticks (*blue* and *grey*: yETF; *green*: hETF) and are labeled as follows: yETF/hETF. **C**, Close-up view of the well-studied salt-bridge formed between βGlu169 and αAsn269, which was shown to determine the dynamics of hETF (βGlu165 and αAsn259, respectively). The third residue displayed as sticks is αGln272, which is in H-bonding distance to both αAsn269 and the N3-C4=O locus of the flavin cofactor.

Recently, we have shown that the FAD cofactor of hETF is oxidized at the 8α-position to yield 8-formyl FAD upon incubation under slightly alkaline conditions[16]. Interestingly, this reaction is promoted by βTyr16 in hETF[16], [35], [36] and thus we hypothesized that yETF may be resistant toward oxidation of the FAD cofactor. To test our hypothesis, we transferred purified yETF to 50 mM HEPES pH 8.5 containing 1 mM DTT and incubated the sample at 25 °C for 24 h. After denaturation of the protein, the free cofactor was analyzed on HPLC-DAD, which indeed revealed no 8-formyl modification of the flavin cofactor. Instead, a mix of other flavin derivatives, which could not be identified due to their low abundance and insufficient purity, was found (Table 1).

Table 1: Cofactor modification in yETF wild type and variants after 24 h of incubation at pH 8.5: yETF wild type and the variants were diluted to a final concentration of ~50 µM using 50 mM HEPES pH 8.5 + 1 mM DTT and incubated at 25°C for 24 h. After denaturation of the proteins their cofactor was analyzed with HPLC-DAD. Total cofactor modification (%) refers to the amount of flavin cofactor altered upon incubation under alkaline conditions (column 2). Columns 3 and 4 provide a more detailed analysis of the obtained results - the fraction of flavin species that could be clearly identified as 8-formyl FAD (based on retention time and flavin spectrum) is given in column three, whereas the amount of unknown flavin species is summarized in column 4.

protein	total cofactor modification [%]	8f-FAD [%]	unknown modification [%]
WT	12	0	12
βF19Y	13	0	13
αN269A	26	26	0
βF19Y-αN269A	42	31	11
βE169A	36	0	0
βF19Y-βE169A	n.d.*	yes*	n.d*

* as this variant is very unstable, cofactor modification cannot be assessed/quantified reliably

In order to determine whether the tyrosine to phenylalanine replacement in yETF renders the 8α-methyl group stable toward oxidation, we generated the hETF-like variant yETF-βPhe19Tyr. In the modification assay, however, this variant behaved rather similarly compared with wild-type yETF by exhibiting an equal amount of overall flavin modification and not being able to form 8f-FAD (Table 1). This finding, of course, raised the question which other factors are important for the oxidation reaction at this position. Since the cleavage

of the salt bridge (between αAsn259 and βGlu165), which was shown to strongly influence the flexibility of the human protein [18], resulted in a much higher degree of formylation[16], we also generated two single variants (αAsn269Ala and βGlu169Ala) and two double variants (βPhe19Tyr-αAsn269Ala and βPhe19Tyr-βGlu169Ala) targeting this interaction (Figure 4C). Although these variants exhibited a slightly higher degree of overall cofactor modification (Table 1), neither one of the variants showed 8α-oxidation comparable with hETF.

Similarly, also the spectral properties remained almost unaffected by the amino acid replacements. Photoreduction of the single and the double variants, like for the wild type protein first yielded a short lived anionic semiquinone, which was further reduced to the flavin hydroquinone (Figure 2B). This finding is in contrast to the homologous human proteins (wild type,αAsn259Alaand βGlu165Alavariant), which strongly stabilize the flavin semiquinone and, therefore, do not allow full reduction of their FAD cofactor in the photoreduction experiment (Figure 2C and [16]).

2.4.3 Biochemical characterization of Dld2

To obtain satisfactory amounts of full length Dld2 from *Saccharomyces cerevisiae*, recombinant expression was carried out in *Komagataella phaffii*. Despite the presence of an α-factor (secretion signal), the protein was not secreted to the culture medium, which required its purification from the cell pellet and yielded about 2-3mg of pure enzyme per kg of wet cell weight. In its pure form, Dld2 exhibits absorption maxima at 383 nm and 454 nm, which are shifted to 375 and 450 nm, respectively, when the protein is denatured using 2% SDS, confirming the presence of an FAD cofactor (Figure5A).

To obtain information about the electrochemical properties of Dld2, we performed a photoreduction and determined the redox potential of the enzyme. Photochemical reduction of Dld2 required the use of high amounts of the redox mediators 5-deaza FMN (2.5 µM) and methylviologen (6 µM) and yielded fully reduced enzyme after about half an hour of irradiation. Neither in the course of the reduction, nor upon reoxidation was a flavin radical observed (Figure 5B), however, we found that under aerobic conditions Dld2 was reoxidized within a few seconds, which is in contrast to what one would expect from a dehydrogenase.

Like for yETF, the redox potential of Dld2 was determined by applying the xanthine/xanthine oxidase method first reported by Massey [23]. The redox dye phenosafranine (E°: -252 mV) and the enzyme were reduced almost synchronously without the appearance of any radical intermediate species, indicating a two electron transfer onto Dld2 and the dye (Figure 5C).

This finding is in line with the photoreduction experiment and the slope near unity obtained when plotting the log of the relative absorption changes of Dld2 (450 nm) as a function of the log of the relative absorption changes of phenosafranine (520 nm). From the intercepta redox potential of -246 ±2 mV was calculated, which is clearly much more negative than that of yETF (midpoint potential: -101 mV) and thus in line with electron transfer from Dld2 to yETF.

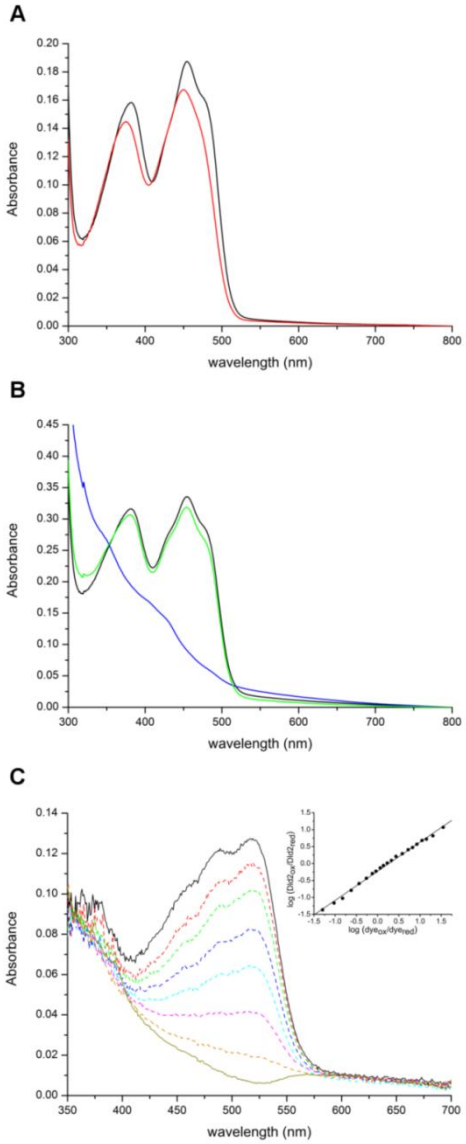

Figure 5: UV-*visible* absorption spectrum (A), photoreduction (B) and determination of the redox potential (C) of Dld2. A, UV-visible absorption spectra of Dld2 diluted to a final concentration of 10 µM with 50 mM HEPES, 150 mM NaCl pH 7 (*black* line) and denatured using 2 % SDS (*red* line) were recorded between 300 and 800 nm at 25 °C. Based on the extinction coefficient of free FAD (denatured, *red* line) at 450 nm (11,300 $M^{-1}cm^{-1}$), the extinction coefficient of Dld2 at 450 nm (12,700 $M^{-1}cm^{-1}$) could be determined. **B**, UV-*visible* absorption spectra (300-800 nm) of oxidized (*black* line), fully reduced (*blue* line) and reoxidized (*green* line) Dld2 (diluted to a final concentration of 30 µM using 50 mM HEPES, 150 mM NaCl pH 7) recorded during

anaerobic photoreduction. **C**, Time dependent spectral changes of Dld2 (~10 µM) and phenosafranine (~10 µM; E°: -252 mV) observed in the course of the reduction reaction (25 min), indicating full reduction of the FAD cofactor and the dye and therefore a 2-electron transfer onto Dld2. All measurements were carried out in 50 mM HEPES, 150 mM NaCl pH 7 at a constant temperature of 25 °C. ***Inset***, Nernst plot obtained from a single measurement by plotting the $\log(Dld2_{ox}/Dld2_{red})$ as a function of the $\log(dye_{ox}/dye_{red})$ - to determine the $\log(Dld2_{ox}/Dld2_{red})$ and the $\log(dye_{ox}/dye_{red})$ the relative absorption changes at 450 and 520 nm, respectively, were used. From the intercept a redox potential of -246 ± 2 mV was calculated (from seven determinations).

2.4.4 Kinetic properties of Dld2 and electron transfer to yETF

To learn more about the kinetic properties of full length Dld2 from *S. cerevisiae*, we conducted pre steady-state experiments in a stopped-flow apparatus. By studying the rate of flavin reduction in the presence of different substrate concentrations (50-1500 µM D-α-hydroxyglutarate; 1 to 100 mM D-lactate), observed rates were measured and plotted as a function of substrate concentration. Using a hyperbolic fit, limiting rate constants (k_{red}) and dissociation constants (K_D) for both substrates were determined (Figure 6A and B, Table 2).

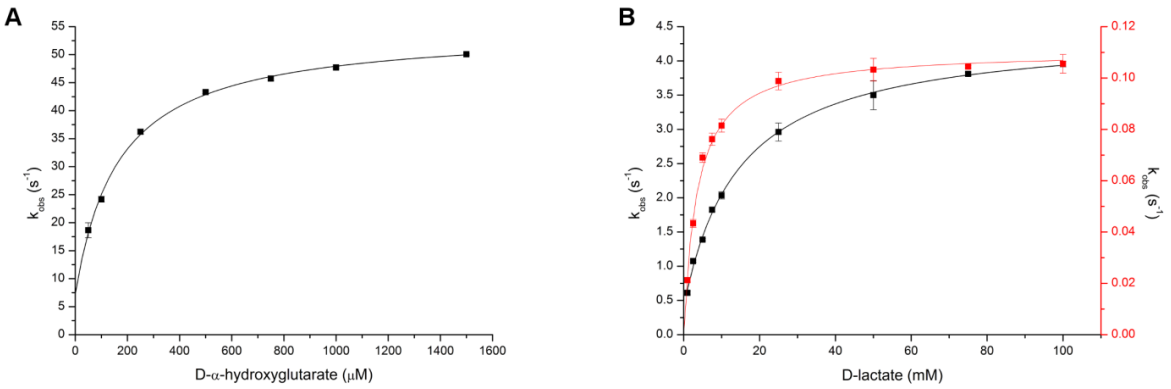

Figure 6: Rapid reaction kinetics of Dld2 using D-α-hydroxyglutarate (A) and D-lactate (B) as substrate. The reductive half reaction of Dld2 was studied by mixing Dld2 (~10 µM final concentration) with varying concentrations of D-α-hydroxyglutarate (final concentrations: 50 – 1500 µM) and D-lactate (final concentrations: 1 -100 mM) in 50 mM HEPES, 150 mM NaCl pH 7 at 25 °C. The observed rate constants (k_{obs}) were plotted as a function of the substrate concentration to give a hyperbolic curve that allowed the determination of the reductive rate (k_{red}) and the dissociation constant (K_D) of Dld2 with D-α-hydroxyglutarate (K_D = 170 ± 20 µM, k_{red} = 47 ± 1 s^{-1}, observed rate constants at each substrate concentration were determined in triplicate; standard deviations are indicated by error bars) and D-lactate (K_D = 15 ± 1 mM, k_{red} = 4.1 ± 0.1 s^{-1}, observed rate constants at each substrate concentration were determined in triplicate), respectively. In the course of the reduction of Dld2 with D-lactate a second slower phase was observed, which was analyzed in the same way to yield a K_D= 3.5 ± 0.2 mM and a k_{red} = 0.11 ± 0.00 s^{-1}(panel B, *red* line).

Table 2: Kinetic parameters of Dld2 determined with D-α-hydroxyglutarate and D-lactate under pre steady-state and steady state conditions. In the course of the pre steady-state experiment 10 µM Dld2 (in reaction) were mixed with varying concentrations of D-α-hydroxyglutarate (final concentrations: 50 – 1500 µM) and D-lactate (final concentrations: 1 -100 mM) in 50 mM HEPES, 150 mM NaCl pH 7 and spectral changes were monitored for 1.5-150 s. From the absorbance changes at 450 nm observed rate constants were extracted and plotted as function of the corresponding substrate concentrations to obtain reductive rates (k_{red}) as well as dissociation constants (K_D) for the interaction of Dld2 with both substrates.

Kinetic characterization of Dld2 under steady-state conditions was performed using DCPIP as final electron acceptor. Dld2 (100 nM), DCPIP (125 µM) and varying final concentrations of D-α-hydroxyglutarate (25 µM to 1000 µM) or D-lactate (1 mM to 250 mM) were mixed in 50 mM HEPES, 150 mM NaCl pH 7 and absorbance changes at 600 nm were recorded for 120 s. By plotting the initial rates as function of the substrate concentrations, additionally $k_{cat_{app}}$ and $K_{M_{app}}$ values for the interaction of Dld2 with both accepted substrates were obtained.

kinetic parameters	**D-α-hydroxyglutarate**	**D-lactate**
k_{red}[s^{-1}]	47 ± 1	4.1 ± 0.1
k_{-1}[s^{-1}]	7.3 ± 1.7	0.4 ± 0.1
K_D [mM]	0.17 ± 0.02	15 ± 1
$k_{cat_{app}}$[s^{-1}]	0.42 ± 0.02	1.2 ± 0.1
$K_{M_{app}}$[mM]	0.35 ± 0.05	110 ± 10
$k_{cat_{app}}/K_{M_{app}}$[$M^{-1}$ s^{-1}]	1200 ± 300	11 ± 2

The rate of reduction was 47 ± 1 s^{-1} and 4.1 ± 0.1 s^{-1} for D-α-hydroxyglutarate and D-lactate with dissociation constants of 0.17 ± 0.02mM and 15 ± 1mM, respectively. Thus, D-α-hydroxyglutarate is oxidized more efficiently by the enzyme than D-lactate. The graphs in Figure 6A and B also indicate reversibility of the electron transfer reaction because the hyperbolic fit to the data yielded y-axis intercepts of k_{-1}= 7.3 ± 1.7 s^{-1} and 0.4 ± 0.1 s^{-1} (~6% of k_{red}) for D-α-hydroxyglutarate (~10% of k_{red}) and D-lactate, respectively.

Interestingly, detailed analysis of the reduction reaction further revealed that flavin reduction proceeded in two distinct phases (Figure 6B and Figure 7A and B).

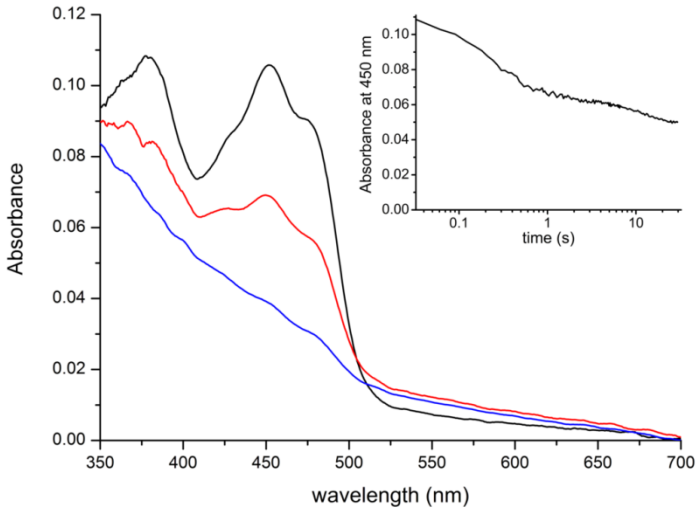

Figure 7: Spectral changes monitored in the course of the rapid reaction kinetics of Dld2 with D-lactate. A, Spectral changes recorded within 3 s, when mixing Dld2 (final concentration: 10 µM) with D-lactate (final concentration: 100 mM) in 50 mM HEPES, 150 mM NaCl pH7. In a first, fast phase, oxidized Dld2 (*black* line) is partially reduced to yield the spectrum shown in *red*, before undergoing full reduction (*blue* line) in a second much slower phase. ***Inset***, Two distinct phases of flavin reduction observed in the course of the rapid reaction kinetics experiment involving Dld2 (final concentration: 10 µM) and D-lactate (final concentration: 100 mM). Absorbance changes at 450 nm were plotted as a function of time (logarithmic time scale) to determine the rate of flavin reduction in both phases.

In the case of D-α-hydroxyglutarate the second phase was about 200-times slower than the first and thus exact quantification of the rate was not possible. In the case of D-lactate, the second phase was determined to0.11± 0.00 s^{-1} and exhibited a dissociation constant of 3.5 ± 0.2 mM. Next, we determined kinetic parameters for steady-state conditions using DCPIP as an artificial electron acceptor under aerobic conditions. The turnover rates with D-α-hydroxyglutarate and D-lactate were 0.42 ± 0.02 s^{-1} and 1.2 ± 0.1 s^{-1}, respectively. However, the observed K_{Mapp} was much lower for D-α-hydroxyglutarate (350 ± 50 µM) than for D-lactate (110 ± 10 mM) resulting in a higher catalytic efficiency for D-α-hydroxyglutarate (1200 ± 300$M^{-1}s^{-1}$ *vs* 11 ± 2$M^{-1}s^{-1}$).A summary of kinetic parameters is provided in Table 2. The large difference between the rate of reduction and the turnover rate suggested that the oxidative rate is rate limiting, which prompted us to analyze the rate of reoxidation of photoreduced and substrate-reduced Dld2 using molecular oxygen as electron acceptor. Interestingly, photoreduced Dld2 was reoxidized about 5000-times faster than the enzyme reduced with D-α-hydroxyglutarate (k_{ox} = 3.3 · 10^4 ± 0.2 · 10^4 M^{-1} s^{-1}*vs* 7 ± 1 M^{-1} s^{-1}). This

result suggested that the reaction product (*i.e.*α-ketoglutarate or pyruvate) tightly binds to the enzyme, thereby inhibiting the reoxidation by molecular oxygen. The addition of α-ketoglutarate (or pyruvate) to photoreduced Dld2, either before or after the photoreduction, however, had no effect on the rate of reoxidation. Equally, titration of α-ketoglutarate (or pyruvate) to oxidized Dld2 did not produce any changes in the UV-*visible* absorption spectrum of the FAD-cofactor, suggesting that the products only bind to the enzyme when generated in the course of the oxidation reaction. This interesting behavior prompted us to investigate the reoxidation of reduced Dld2 using its putative natural electron acceptor yETF. First, we incubated yETF (10 µM) with catalytic amounts of Dld2 (10 nM) and an excess of D-α-hydroxyglutarate (1 mM) and monitored the reduction of yETF by UV-*visible* absorption spectrometry. As shown in Figure 8A, yETF was reduced directly from the oxidized state to the fully reduced (hydroquinone) state within 4 minutes, which is in agreement with earlier experiments that have demonstrated the preferential two-electron reduction of yETF.

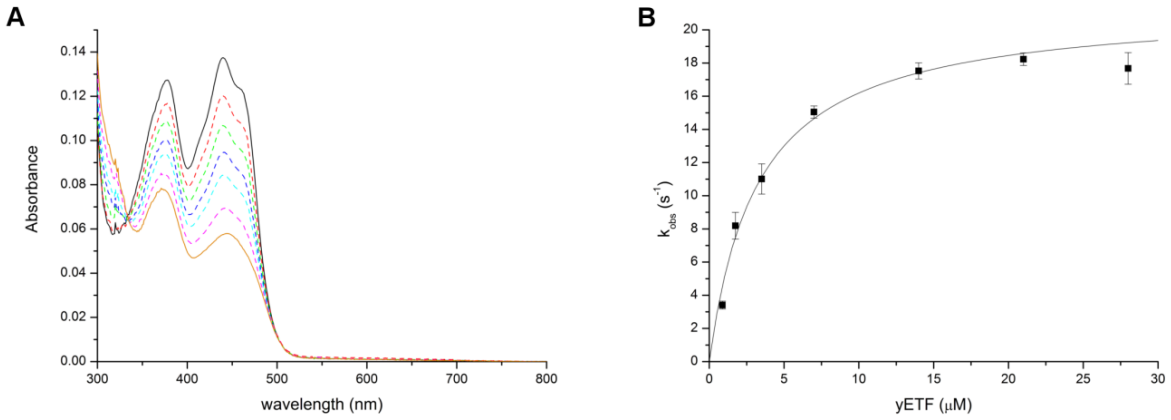

Figure 8: Electron transfer from Dld2 onto yETF. A, yETF was diluted to a final concentration of 10 µM using 50 mM HEPES pH 7 + 1 mM DTT (*black* spectrum) and mixed with 1 mM D-α-hydroxyglutarate and 10 nM Dld2 at 25 °C. Then, time-dependent spectral changes were monitored until no further changes were observed. The *black* spectrum corresponds to fully oxidized yETF, while the *orange* line represents the final spectrum recorded after 4 min. All other spectra recorded in the course of the reaction are shown using *dashed* lines. **B**, Steady state turnover assays involving 1 mM D-α-hydroxyglutarate, 10 nM Dld2, yETF (0.875 – 28 µM) and 125 µM DCPIP as final electron acceptor were carried out in 50 mM HEPES pH 7 containing 1 mM DTT at 25 °C. Initial rates (normalized to enzyme concentration) were extracted from the absorbance changes recorded at 600 nm and plotted as a function of the yETF concentration. By applying a hyperbolic fit, the kinetic parameters $K_{M_{app}}$ and $k_{cat_{app}}$ were determined ($K_{M_{app}}$ = 3.3 ± 0.4 µM, $k_{cat_{app}}$ = 21 ± 1 s^{-1}; initial rates at each yETF concentration were determined in triplicate; standard deviations are indicated by error bars).

For a more detailed kinetic characterization, steady state measurements using DCPIP as final electron acceptor were performed(Figure 8B, Table 3) yielding an apparent k_{catapp} of 21 ± 1 s^{-1} and K_{Mapp} of 3.3 ± 0.4 µM, which confirm an efficient electron transfer from Dld2 to yETF (catalytic efficiency: $6 \cdot 10^6 \pm 1 \cdot 10^6$ M^{-1} s^{-1}). Thus, electron transfer to the cognate electron acceptor, yETF, is several orders of magnitude faster than the reoxidation by either oxygen or DCPIP.

Table 3: Kinetic parameters determined for the electron transfer from Dld2 onto yETF under steady-state conditions.

The steady-state parameters for the electron transfer were determined in a coupled assay involving 1mM D-α-hydroxyglutarate, 10 nM Dld2, 125 µM DCPIP and varying concentrations of yETF in 50 mM HEPES pH 7 containing 1mM DTT (when using D-lactate as substrate for Dld2 its reduction became rate limiting). By monitoring the decolorization of DCPIP at 600 nm for 120 s initial rates could be obtained and plotted as function of the yETF concentrations to yield the kinetic parameters $k_{catapp}$and K_{Mapp}.

kinetic parameters	D-α-hydroxyglutarate	D-lactate
k_{catapp}[s^{-1}]	21 ± 1	0.8 ± 0.4
K_{Mapp}[µM]	3.2 ± 0.4	rate ETF-concentration independent

2.5 Discussion

2.5.1 Biochemical characterization of yETF

Successful production of recombinant yETF and full length Dld2 from *S. cerevisiae* in *E. coli* and *K. phaffii*, respectively, enabled us to study their biochemical properties and the presumed electron transfer from Dld2 to yETF. Despite the extensive sequence similarity in the FAD binding pocket, we found that the properties of yETF diverge significantly from the human ortholog. The most salient differences concern the reduction behavior of yETF as evidenced by the absence of the anionic flavin semiquinone and the much more negative redox potential (-101 mV and -20 mV for yETF and hETF, respectively). Thus far, all ETFs characterized showed the preferential one-electron reduction of FAD to yield the anionic semiquinone including mammalian and bacterial proteins [7], [16], [37], [38]. In fact, the formation of the anionic semiquinone is thought to be critical for electron transfer from client dehydrogenases

[39]. Because of the obvious difference in the single active site residue provided by the β-chain (βTyr16 in hETF and βPhe19 in yETF), we hypothesized that this amino acid exchange in yETF may be responsible for the distinct reduction behavior. In order to investigate this possibility, we generated the βTyr16Phe and βPhe19Tyr variant for hETF and yETF, respectively. While the replacement of βTyr16 by Phe in hETF strongly affected the stabilization of the anionic semiquinone, enabling full reduction of the protein in the course of the photoreduction experiment, the βPhe19Tyr variant of yETF did not behave like hETF (Figure 2, *panels* A-D). Similarly, we have recently reported that replacement of βTyr16 by Phe impedes the oxidation of the 8α-methyl to the 8-formyl-group and, therefore, we have also tested the propensity of wild-type yETF and the βPhe19Tyr variant to form 8-formyl-FAD. Surprisingly, we have found that neither the wild-type yETF nor the βPhe19Tyr variant formed 8-formyl-FAD. Even the introduction of further amino acid replacements (*i.e.* in the variants βPhe19Tyr-αAsn269Ala and βPhe19Tyr-βGlu169Ala) that significantly enhanced the rate of oxidation at the 8α-methyl group in hETF wild-type [16] did not result in increased formation of the 8-formyl group. Thus, it appears that the redox properties of the FAD cofactor as well as the reactivity of the 8α-methyl group is not simply governed by amino acid residues in the direct vicinity of the isoalloxazine ring but also by other factors such as amino acids in the second shell and the overall dynamics of the protein, which for example may influence the accessibility of the FAD cofactor. This view is in accordance with observations by Salazar *et al.* (1997), who reported that the redox properties of ETFs are not solely affected by the amino acids found in the vicinity of the flavin moiety [17].

2.5.2 Kinetic characterization of Dld2

Recently, the determination of steady-state kinetic parameters by Becker-Kettern *et al.* revealed very slow turnover numbers for the oxidation of D-lactate (1.3 s^{-1}) and D-α-hydroxyglutarate (0.18 s^{-1}) using *N*-terminally truncated Dld2 [15]. Thus, we decided to reinvestigate the steady-state kinetics of Dld2 using full-length Dld2 recombinantly produced in *K. phaffii* (see Experimental Procedures). However, we virtually obtained very similar values fork_{catapp} for D-lactate and D-α-hydroxyglutarate of 1.2 and 0.42 s^{-1}, respectively, suggesting that the truncation at the N-terminus does not compromise the catalytic properties of the enzyme. In order to identify the rate-limiting step during turnover, we then investigated pre steady-state kinetics using stopped-flow absorption spectrophotometry. This clearly showed that the reductive half reaction with D-lactate and D-α-hydroxyglutarate proceeds at a

limiting rate of 4.1 ± 0.1s^{-1} and 47 ± 1s^{-1}, respectively (Table 2). In the case of D-α-hydroxyglutarate, the reductive rate is thus three orders of magnitude faster than the observed turnover. This result indicated that the oxidative half reaction is rate limiting. Surprisingly, when photoreduced Dld2 was reacted with dioxygen, we also found a rapid rate of reoxidation of $3.3 \cdot 10^4 \pm 0.2 \cdot 10^4$ M^{-1} s^{-1}. However, substrate-reduced Dld2 reacted much slower with dioxygen. In the case of D-α-hydroxyglutarate, the rate of reoxidation was only 7 M^{-1} s^{-1}, *i.e.* 5000-times slower as observed for the photoreduced enzyme. This suggested that the reaction product, pyruvate or α-ketoglutarate, forms a complex with the reduced enzyme and thereby impedes re-oxidation by dioxygen. Interestingly, addition of either pyruvate or α-ketoglutarate to photoreduced enzyme exhibited no effect on the rate of re-oxidation with dioxygen. Thus, we conclude that during the oxidation of the substrate the formed product stabilizes a conformation of the enzyme in which access to the reduced FAD is denied. A similar behavior has been observed for other client enzymes of electron transferring flavoproteins. In the case of acyl-CoA dehydrogenases, reduced either by dithionite or by light irradiation, a very fast reoxidation was observed. If, however, the reaction product or a substrate/product mimic is bound to the protein, oxygen reactivity was reduced by a factor of 3,000-4,000[40]–[42]. Wang *et al.* hypothesized that this effect is caused by the tight binding of enoyl-CoA (and derivatives), which results in a significantly more hydrophobic active site and, therefore, prohibits the stabilization of superoxide radical species required for flavin reoxidation[41]. Since α-ketoglutarate and pyruvate are far less hydrophobic, it is difficult to imagine that oxygen reactivity is controlled by the same mechanism. Therefore, we suggest that product binding to Dld2 reduces the accessibility for oxygen to the active site and thereby impedes the reaction with the reduced FAD cofactor.

The occurrence of a product-reduced enzyme complex is also supported by an increase in the long-wavelength absorption (~510-625 nm) during the reductive half-reaction (Figure 7), indicating the formation of a charge-transfer complex between α-ketoglutarate or pyruvate and reduced Dld2.In keeping with this interpretation, we also observed that the long wavelength absorption disappeared during re-oxidation of substrate-reduced Dld2 with dioxygen. The formation of the charge-transfer complex is apparently connected to the fast phase of reduction, which was also previously observed for acyl-CoA dehydrogenases. It was postulated for the latter enzymes that formation of a charge transfer complex is indicative of tight product binding, which is used to shift the reaction equilibrium toward enoyl-CoA formation [42], [43]. Tight binding of the enoyl-CoA product was argued to be necessary

because the acyl-CoA substrates have a very similar or even more positive redox potential than the FAD cofactor bound to the acyl-CoA dehydrogenases, making acyl-CoA oxidation rather unfavorable[43].Because the redox potential of the D-lactate/pyruvate couple (-190 mV) is more positive than the midpoint potential of Dld2, it is plausible that charge-transfer formation and tight product binding play a similar role in the yeast enzyme. In addition, the rather high k_{-1}-rates observed in the rapid reaction kinetics are in line with this hypothesis.

The slow re-oxidation of substrate-reduced Dld2 by oxygen and DCPIP prompted us to investigate re-oxidation using the cognate electron acceptor, yETF. Initial experiments clearly demonstrated that yETF is rapidly reduced by catalytic amounts of Dld2 utilizing D-α-hydroxyglutarate as the substrate (Figure 8A). Further steady-state experiments established that the rate of electron transfer increased hyperbolically with the concentration of yETF, reaching a limiting value of 21 s^{-1} and thus approaching the rate of reduction of Dld2 with D-α-hydroxyglutarate. In other words, electron transfer from the product-reduced enzyme complex to yETF is fast in contrast to reoxidation with oxygen or DCPIP and, therefore, product binding suppresses the undesired transfer of electrons to oxygen. The exact mechanism by which yETF obtains the electrons from the reduced enzyme are not clear yet but two scenarios are possible: (i) binding of yETF to the product-reduced enzyme complex leads to the rapid release of the product and subsequently to electron transfer to yETF or (ii) binding of yETF directly leads to electron transfer and to product dissociation from the re-oxidized enzyme. As Dld2 very much behaves like acyl-CoA dehydrogenases, it is tempting to speculate that also the mechanism of electron transfer to ETF is similar. In acyl-CoA dehydrogenases the rapid reoxidation of the enzyme by hETF [40] was assumed to be promoted by a lower p*K*a-value of the reduced FAD cofactor in the product complex [44]–[46]. In addition, tight product binding, as discussed above, shifts the equilibrium toward the reduced FAD cofactor and therefore electron transfer to ETF is more likely to occur prior to product release [44]–[46].Since Dld2 and the acyl-CoA dehydrogenases are structurally very distinct, *p*-cresol methylhydroxylase- (PCMH-) fold *vs* acyl-CoA dehydrogenase fold, and the chemical properties of their respective reaction products are rather different, further studies will be required to clearly resolve the exact mechanism of electron transfer from substrate-reduced Dld2 to yETF.

2.5.3 Two-electron transfer from Dld2 to yETF

It should also be noted that reduction of yETF by Dld2 apparently involves the transfer of two electrons (Figure 8A), which is in agreement with the large difference in redox potential of the two proteins (E° =-101 and -246 mV for yETF and Dld2, respectively). This finding is in line with our observations that yETF only weakly stabilizes the anionic semiquinone during photoreduction, and the reduction of Dld2, either by light irradiation or substrate, directly leads to the hydroquinone without the occurrence of a stable flavin semiquinone. This observation was rather surprising because all eukaryotic ETFs investigated so far were reported to operate through single electron transfer from the client dehydrogenase to the ETF [3], [7], [40], [47], [48]. Furthermore, it was demonstrated that disproportionation of the flavin semiquinone to the oxidized and hydroquinone state occurs upon interaction with ETF-QO, which is required for successful electron transfer [17], [47]. Presently, the mechanism of electron transfer between yETF and its *in vivo* electron acceptor, Cir2p, is unknown. Previous studies involving various ETFs and their corresponding electron acceptors have indicated that electron transfer requires the transfer of single electrons and therefore relies on the stabilization of the flavin semiquinone [49]–[51]. Owing to the electrochemical properties of yETF, it is thus conceivable that the mechanism of electron transfer to Cir2p is also different compared to the previously investigated electron transfer systems in eukaryotic cells.

2.6 Author contributions

MT, JB and CT prepared the constructs for heterologous gene expression; MT and JB expressed the genes, purified the produced proteins and performed biochemical experiments; MT, JB and PM designed the biochemical and kinetic experiments and interpreted the data; MT, JB and PM wrote the manuscript.

2.7 Conflict of interest

The authors declare no conflict of interest.

2.8 Acknowledgements

We are grateful to Dr. Majd Lahham for his support during the initial phase of the project. This work was supported by the Austrian Science Fund (FWF) through grant W901 (Doctoral Program “Molecular Enzymology”). The authors are also grateful for the support by the interuniversity program in natural sciences (NAWI Graz).

2.9 References

[1] F. L. Crane, S. Mii, J. G. Hauge, D. E. Green, and H. Beinert, "*On the mechanism of dehydrogenation of fatty acyl derivatives of coenzyme A. I. The general fatty acyl coenzyme A dehydrogenase.*," J. Biol. Chem., vol. 218, no. 2, pp. 701–706, 1956.

[2] M. Weidenhaupt, P. Rossi, C. Beck, H. M. Fischer, and H. Hennecke, "*Bradyrhizobium japonicum possesses two discrete sets of electron transfer flavoprotein genes: FixA, fixB and etfS, etfL*," Arch. Microbiol., vol. 165, no. 3, pp. 169–178, 1996.

[3] D. J. Steenkamp and M. Husain, "*The effect of tetrahydrofolate on the reduction of electron transfer flavoprotein by sarcosine and dimethylglycine dehydrogenases.*," Biochem. J., vol. 203, no. 3, pp. 707–715, 1982.

[4] D. L. Roberts, F. E. Frerman, and J. J. Kim, "*Three-dimensional structure of human electron transfer flavoprotein to 2.1-A resolution.*," Proc. Natl. Acad. Sci. U. S. A., vol. 93, no. 25, pp. 14355–60, 1996.

[5] M. H. Jang, N. S. Scrutton, and R. Hille, "*Formation of W3A1 electron-transferring flavoprotein (ETF) hydroquinone in the trimethylamine dehydrogenase-ETF protein complex,*" J. Biol. Chem., vol. 275, no. 17, pp. 12546–12552, 2000.

[6] F. Talfournier et al., "*αArg-237 in Methylophilus methylotrophus (sp. W3A1) electron-transferring flavoprotein affords ∼200-millivolt stabilization of the FAD anionic semiquinone and a kinetic block on full reduction to the dihydroquinone*," J. Biol. Chem., vol. 276, no. 23, pp. 20190–20196, 2001.

[7] C. D. Whitfield and S. G. Mayhew, "Purification and properties of electron-transferring flavoprotein from Peptostreptococcus elsdenii," *J. Biol. Chem.*, vol. 249, no. 9, pp. 2801–2810, 1974.

[8] S. R. Elsden, F. M. Gilchrist, D. Lewis, and B. E. Volcani, "*Properties of a fatty acid forming organism isolated from the rumen of sheep.*," J. Bacteriol., vol. 72, no. 5, pp. 681–689, 1956.

[9] O. Jenkins, D. Byrom, and D. Joned, "*Methylophilus : a new genus of methanol-utilizing bacteria*," Int. J. Syst. Bacteriol., vol. 37, no. 4, pp. 446–448, 1987.

[10] V. Gudipati, K. Koch, W. D. Lienhart, and P. Macheroux, "*The flavoproteome of the yeast Saccharomyces cerevisiae*," Biochim. Biophys. Acta - Proteins Proteomics, vol. 1844, no. 3, pp. 535–544, 2014.

[11] J. Lopes, M. J. Pinto, A. Rodrigues, F. Vasconcelos, and R. Oliveira, "*The Saccharomyces*

cerevisiae genes, AIM45, YGR207c/CIR1 and YOR356w/CIR2, are involved in cellular redox state under stress conditions," Open Microbiol. J., vol. 4, pp. 75–82, 2010.

[12] D. C. Amberg, E. Basart, and D. Botstein, "*Defining protein interactions with yeast actin in vivo*," Nat. Struct. Biol., vol. 2, no. 1, pp. 28–35, 1995.

[13] N. S. Hachiya, Y. Sakasegawa, A. Jozuka, S. Tsukita, and K. Kaneko, "*Interaction of D-lactate dehydrogenase protein 2 (Dld2p) with F-actin: Implication for an alternative function of Dld2p*," Biochem. Biophys. Res. Commun., vol. 319, no. 1, pp. 78–82, 2004.

[14] N. S. Hachiya, Y. Sakasegawa, H. Sasaki, A. Jozuka, S. Tsukita, and K. Kaneko, "*Oligomeric Aip2p/Dld2p forms a novel grapple-like structure and has an ATP-dependent F-actin conformation modifying activity in vitro,*" Biochem. Biophys. Res. Commun., vol. 320, no. 4, pp. 1271–1276, 2004.

[15] J. Becker-Kettern *et al.*, "*Saccharomyces cerevisiae Forms D-2-Hydroxyglutarate and Couples Its Degradation to D-Lactate Formation via a Cytosolic Transhydrogenase,*" J. Biol. Chem., vol. 291, no. 12, pp. 6036–6058, 2016.

[16] P. Augustin et al., "*Oxidation of the FAD cofactor to the 8-formyl-derivative in human electron-transferring flavoprotein,*" J. Biol. Chem., vol. 293, no. 8, pp. 2829–2840, 2018.

[17] D. Salazar, L. Zhang, G. D. DeGala, and F. E. Frerman, "*Expression and characterization of two pathogenic mutations in human electron transfer flavoprotein*," J. Biol. Chem., vol. 272, no. 42, pp. 26425–26433, Oct. 1997.

[18] H. S. Toogood, A. Van Thiel, N. S. Scrutton, and D. Leys, "*Stabilization of non-productive conformations underpins rapid electron transfer to electron-transferring flavoprotein*," J. Biol. Chem., vol. 280, no. 34, pp. 30361–30366, 2005.

[19] R. Weis, R. Luiten, W. Skranc, H. Schwab, M. Wubbolts, and A. Glieder, "*Reliable high-throughput screening with Pichia pastoris by limiting yeast cell death phenomena*," FEMS Yeast Res., vol. 5, no. 2, pp. 179–189, 2004.

[20] J. H. Schrittwieser et al., "*Biocatalytic organic synthesis of optically pure (S)-scoulerine and berbine and benzylisoquinoline alkaloids*," J. Org. Chem., vol. 76, no. 16, pp. 6703–6714, 2011.

[21] P. Macheroux, "*UV-visible spectroscopy as a tool to study flavoproteins.*," Methods Mol. Biol., vol. 131, pp. 1–7, 1999.

[22] V. Massey, P. Hemmerich, W. R. Knappe, H. J. Duchstein, and H. Fenner, "*Photoreduction of flavoproteins and other biological compounds catalyzed by deazaflavins. Appendix:*

photochemical formation of deazaflavin dimers," Biochemistry, vol. 17, no. 1, pp. 9–17, Jan. 1978.

[23] V. Massey, "*A simple method for the determination of redox potentials.*," in Flavins and Flavoproteins, B. Curti, G. Zanetti, and S. Ronchi, Eds. Como, Italy: Walter de Gruyter, 1991, pp. 59–66.

[24] K. Minnaert, "*Measurement of the equilibrium constant of the reaction between cytochrome c and cytochrome a.*," Biochim. Biophys. Acta, vol. 110, pp. 42–56, 1965.

[25] M. Biasini et al., "*SWISS-MODEL: Modelling protein tertiary and quaternary structure using evolutionary information*," Nucleic Acids Res., vol. 42, no. W1, 2014.

[26] K. Arnold, L. Bordoli, J. Kopp, and T. Schwede, "*The SWISS-MODEL workspace: A web-based environment for protein structure homology modelling*," Bioinformatics, vol. 22, no. 2, pp. 195–201, 2006.

[27] P. Benkert, M. Biasini, and T. Schwede, "*Toward the estimation of the absolute quality of individual protein structure models*," Bioinformatics, vol. 27, no. 3, pp. 343–350, 2011.

[28] T. C. Lehman and C. Thorpe, "*A new form of mammalian electron-transferring flavoprotein*," Arch. Biochem. Biophys., vol. 292, no. 2, pp. 594–599, 1992.

[29] S. G. Mayhew, C. D. Whitfield, S. Ghisla, and M. Schuman-Jörns, "*Identification and properties of new flavins in electron-transferring flavoprotein from Peptostreptococcus elsdenii and pig-liver glycolate oxidase*," Eur. J. Biochem., vol. 44, no. 2, pp. 579–591, 1974.

[30] R. Komuniecki, J. McCrury, J. Thissen, and N. Rubin, "*Electron-transfer flavoprotein from anaerobic Ascaris suum mitochondria and its role in NADH-dependent 2-methyl branched-chain enoyl-CoA reduction*," BBA - Bioenerg., vol. 975, no. 1, pp. 127–131, 1989.

[31] J. K. Demmer, N. Pal Chowdhury, T. Selmer, U. Ermler, and W. Buckel, "*The semiquinone swing in the bifurcating electron transferring flavoprotein/butyryl-CoA dehydrogenase complex from Clostridium difficile*," Nat. Commun., vol. 8, no. 1, 2017.

[32] M. Husain, M. T. Stankovich, and B. G. Fox, "*Measurement of the oxidation-reduction potentials for one-electron and two-electron reduction of electron-transfer flavoprotein from pig liver.*," Biochem. J., vol. 219, no. 3, pp. 1043–1047, 1984.

[33] T. M. Dwyer, L. Zhang, M. Muller, F. Marrugo, and F. Frerman, "*The functions of the flavin contact residues, αArg249 and βTyr16, in human electron transfer flavoprotein*," Biochim. Biophys. Acta - Protein Struct. Mol. Enzymol., vol. 1433, no. 1–2, pp. 139–152, Aug. 1999.

[34] C. P. Pace and M. T. Stankovich, "*Redox properties of electron-transferring flavoprotein from Megasphaera elsdenii*," Biochim. Biophys. Acta (BBA)/Protein Struct. Mol., vol. 911, no. 3, pp. 267–276, 1987.

[35] V. Konjik et al., "*The crystal structure of RosB: Insights into the reaction mechanism of the first member of a family of flavodoxin-like enzymes*," Angew. Chemie - Int. Ed., vol. 56, no. 4, pp. 1146–1151, 2017.

[36] J. M. Robbins, M. G. Souffrant, D. Hamelberg, G. Gadda, and A. S. Bommarius, "*Enzyme-mediated conversion of flavin adenine dinucleotide (FAD) to 8-formyl FAD in formate oxidase results in a modified cofactor with enhanced catalytic properties*," Biochemistry, vol. 56, no. 29, pp. 3800–3807, 2017.

[37] M. Husain and D. J. Steenkamp, "*Electron transfer flavoprotein from pig liver mitochondria. A simple purification and re-evaluation of some of the molecular properties*," Biochem. J., vol. 209, no. 2, pp. 541–545, 1983.

[38] N. J. Watmough, J. Kiss, and F. E. Frerman, "*Structural and redox relationships between Paracoccus denitrificans, porcine and human electron-transferring flavoproteins*," Eur. J. Biochem., vol. 205, no. 3, pp. 1089–1097, 1992.

[39] R. J. Gorelick and C. Thorpe, "*Electron-transferring flavoprotein from pig kidney: Flavin analogue studies*," Biochemistry, vol. 25, no. 22, pp. 7092–7098, 1986.

[40] R. J. Gorelick, L. M. Schopfer, D. P. Ballou, V. Massey, and C. Thorpe, "*Interflavin oxidation-reduction reactions between pig kidney general acyl-CoA dehydrogenase and electron-transferring flavoprotein*," Biochemistry, vol. 24, no. 24, pp. 6830–6839, 1985.

[41] R. Wang and C. Thorpe, "*Reactivity of medium-chain acyl-CoA dehydrogenase toward molecular oxygen*," Biochemistry, vol. 30, no. 32, pp. 7895–7901, 1991.

[42] E. R. DuPlessis, J. Pellett, M. T. Stankovich, and C. Thorpe, "*Oxidase activity of the acyl-CoA dehydrogenases*," Biochemistry, vol. 37, no. 29, pp. 10469–10477, 1998.

[43] N. D. Lenn, M. T. Stankovich, and H. W. Liu, "*Regulation of the redox potential of general acyl-CoA dehydrogenase by substrate binding*," Biochemistry, vol. 29, no. 15, pp. 3709–3715, 1990.

[44] T. C. Lehman and C. Thorpe, "*Alternate electron acceptors for medium-chain acyl-CoA dehydrogenase: Use of ferricenium salts*," Biochemistry, vol. 29, no. 47, pp. 10594–10602, 1990.

[45] H. S. Toogood, D. Leys, and N. S. Scrutton, "*Dynamics driving function - New insights from electron transferring flavoproteins and partner complexes*," FEBS Journal, vol. 274, no. 21. pp. 5481–5504, 2007.

[46] S. Ghisla and C. Thorpe, "*Acyl-CoA dehydrogenases: A mechanistic overview*," European Journal of Biochemistry, vol. 271, no. 3. pp. 494–508, 2004.

[47] R. R. Ramsay, D. J. Steenkamp, and M. Husain, "*Reactions of electron-transfer flavoprotein and electron-transfer flavoprotein: ubiquinone oxidoreductase.*," Biochem. J., vol. 241, pp. 883–892, 1987.

[48] C. M. Byron, M. T. Stankovich, M. Husain, and V. L. Davidson, "*Unusual redox properties of electron-transfer flavoprotein from Methylophilus methylotrophus,*" Biochemistry, vol. 28, no. 21, pp. 8582–8587, 1989.

[49] N. J. Watmough and F. E. Frerman, "*The electron transfer flavoprotein: Ubiquinone oxidoreductases*," Biochimica et Biophysica Acta - Bioenergetics, vol. 1797, no. 12. pp. 1910–1916, 2010.

[50] M. A. Swanson, R. J. Usselman, F. E. Frerman, G. R. Eaton, and S. S. Eaton, "*The iron-sulfur cluster of electron transfer flavoprotein-ubiquinone oxidoreductase is the electron acceptor for electron transfer flavoprotein*," Biochemistry, vol. 47, no. 34, pp. 8894–8901, 2008.

[51] R. J. Usselman, A. J. Fielding, F. E. Frerman, N. J. Watmough, G. R. Eaton, and S. S. Eaton, "*Impact of mutations on the midpoint potential of the [4Fe-4S] +1,+2 cluster and on catalytic activity in electron transfer flavoprotein-ubiquinone oxidoreductase (ETF-QO),*" Biochemistry, vol. 47, no. 1, pp. 92–100, 2008.

3. Biochemical characterization of human D-2-hydroxyglutarate dehydrogenase and two disease related variants reveals the molecular

Biochemical characterization of human D-2-hydroxyglutarate dehydrogenase and two disease related variants reveals the molecular cause of D-2-hydroxyglutaric aciduria

Marina Toplak, Julia Brunner, Julia Schmidt and Peter Macheroux*

Institute of Biochemistry, Graz University of Technology, Petersgasse 12/2, A-8010 Graz, Austria

*to whom correspondence should be addressed:
Prof. Dr. Peter Macheroux
Graz University of Technology
Institute of Biochemisty
Petersgasse 12/2
A-8010 Graz, Austria
Tel.: +43-316-873 6450
Fax: +43-316-873 6952
Email: peter.macheroux@tugraz.at

Keywords: Electron transferring flavoprotein; D-2-hydroxyglutaric aciduria; D-2-hydroxyglutarate; D-lactate.

Abbreviations

CD, circular dichroism; DCPIP, 2,6-dichlorophenyl indophenol; Dld2, D-lactate dehydrogenase 2 from *Saccharomyces cerevisiae*; ETF, electron transferring flavoprotein; ETF-QO, ETF-ubiquinone oxidoreductase; FAD, flavin adenine dinucleotide; GB1, B1 domain of *Streptococcal* protein G; GHB, 4-hydroxybutyrate; hD2HGDH, human D-2-hydroxyglutarate dehydrogenase; hDMGDH, human dimethylglycine dehydrogenase; hMCAD, human medium chain acyl-CoA dehydrogenase; HOT, hydroxyacid-oxoacid transhydrogenase; MADD, multiple acyl-CoA dehydrogenase deficiency

Abstract

D-2-hydroxyglutaric aciduria is a neurometabolic disorder, characterized by the accumulation of D-2-hydroxyglutarate (D-2HG) in human mitochondria. Increased levels of D-2HG are detected in humans exhibiting point mutations in the genes encoding isocitrate dehydrogenase, citrate carrier, the electron transferring flavoprotein (ETF) and its downstream electron acceptor ETF-ubiquinone oxidoreductase or D-2-hydroxyglutarate dehydrogenase (hD2HGDH). However, while the pathogenicity of several amino acid replacements in the former four proteins has been studied rather extensively, hardly anything is known about the effect of certain point mutations on the biochemical properties of hD2HGDH.

Therefore, were combinantly produced wild type hD2HGDH as well as two recently identified disease-related variants (hD2HGDH-I147S and -V444A) and performed their detailed biochemical characterization. We could show that hD2HGDH is a FAD dependent protein, which is able to catalyze the oxidation of both D-2HG and D-lactate to α-ketoglutarate and pyruvate, respectively. The two variants were obtained as apo-proteins and were thus catalytically inactive. The addition of FAD failed to restore enzymatic activity of the variants, indicating that the cofactor binding site is severely compromised by the single amino acid replacements. Further analyses revealed that both variants form aggregates that are apparently unable to bind the FAD cofactor.

Since D-2-hydroxyglutaric aciduria may also result from a loss of function of either the ETF or its downstream electron acceptor ETF-ubiquinone oxidoreductase, ETF may serve as the cognate electron acceptor of reduced hD2HGDH. Here, we show that hD2HGDH directly reduces recombinant human ETF, thus establishing a metabolic link between the oxidation of D-2-hydroxyglutarateand the mitochondrial electron transport chain.

3.1 Introduction

D-2-hydroxyglutaric aciduria (D-2HGA) is a neurometabolic disorder, characterized by a strong accumulation of D-2HG in affected patients [1].The phenotypes associated with increased levels of D-2HG are rather inhomogeneous, with some of the patients suffering from severe disorders such as early-infantile-onset epileptic encephalopathy and cardiomyopathy, as well as from developmental delay and dysmorphic features, while others exhibit much weaker clinical symptoms (1, 2).To date, very little is known about the metabolic processes that lead to the formation and degradation of D-2HG. It was speculated that the main enzyme responsible for the synthesis of D-2HG in humans is the so called hydroxyacid-oxoacid-transhydrogenase (HOT), which catalyzes the α-ketoglutarate dependent oxidation of 4-hydroxybutyrate (GHB) to succinic semialdehyde in the mitochondrial matrix, yielding D-2HG as side product [2]. Therefore, patients suffering from D-2HGA were tested for the hyperactivity of HOT, but none of them showed higher activity of the enzyme as compared to healthy individuals suggesting that enzymes involved in the break-down of D-2HG might be responsible for D-2HGA [3]. This observation brought the only enzyme known to specifically act on D-2HG, i.e. D-2-hydroxyglutarate dehydrogenase (D2HGDH; Uniprot ID: Q8N465; Isoform 1) into the spotlight of research [4,5]. D2HGDH is localized in the mitochondrial matrix and shares high sequence identity with the yeast enzyme D-lactate dehydrogenase 2 (Dld2; Uniprot ID: P46681; 53% identity on amino acid sequence level) and its plant homolog (*Arabidopsis thaliana- (At-)*D2HGDH; Uniprot ID: O23240; 56% identity on amino acid sequence level). Both of these homologs are serviced by an electron transferring flavoprotein (ETF) [6–8] and therefore it appears likely that the human enzyme also delivers electrons directly to ETF. Although this was not shown experimentally thus far, this idea is also in agreement with the increased levels of D-2HG detected in patients suffering from mutations in the genes encoding isocitrate dehydrogenase, citrate carrier, ETF or its downstream electron acceptor ETF-ubiquinone oxidoreductase [9–13].

In addition to the uncertainty revolving around the electron pathway from D-2HG to the mitochondrial electron transport chain, the molecular cause(s) of hD2HGDH deficiency are still unknown. Genetic studies by Struys *et al.*(2005) and Kranendijk *et al.*(2009) revealed several pathogenic mutations in the *d2hgdh* gene of patients with severe phenotypes [1,14], two of which have been investigated in more detail [1]. Struys *et al.*(2005) have shown that two single point mutations at nucleotide position 440 (T→G) and at position 1331 (T→C) lead to missense mutations, causing the replacement of an isoleucine by a serine (Ile147Ser

variant) and a valine by an alanine (Val444Ala variant), respectively. In order to analyze the pathogenicity of the two amino acid replacements, they also determined the enzyme activity of both variants in a radiochemical cell-line based assay, which revealed residual activities of 25% (Val444Ala) and 0%(Ile147Ser) as compared to the wild type protein [1]. Based on their studies, however, they could not explain the reason for the dramatic loss of enzymatic function.

In order to better understand the effect of the two amino acid replacements on the overall activity of hD2HGDH, as well as to find the natural electron acceptor of the protein, we produced recombinant wild type hD2HGDH as well as the Ile147Ser and the Val444Ala variants in *Escherichia coli*. The purified recombinant wild type hD2HGDH possessed a flavin cofactor and exhibited oxidase activity toward D-lactate and D-2HG, but showed a clear preference for the oxidation of D-2HG. In contrast, the two variants were isolated as apo-proteins and were devoid of enzymatic activity. Further analyses revealed that both disease-related variants were unable to bind the FAD cofactor and showed higher tendency toward aggregation. Here, we also demonstrate that reduced hD2HGDH rapidly donates electrons to recombinant human ETF (Uniprot IDs: P13804, α-subunit; P38117, β-subunit), linking D-2HG oxidation directly to the mitochondrial electron transport chain.

Taken together, our study has provided a more detailed understanding of the molecular cause of disease related variants of hD2HGDH and we have firmly established human ETF as the natural electron acceptor of the enzyme. Our findings also provide the bases to rationalize the occurrence of D-2HGA in cases where deficiency of either hETF or of its downstream electron acceptor hETF-ubiquinone oxidoreductase (hETF-QO; Uniprot ID: Q16134) was observed.

3.2 Materials and Methods

3.2.1 Materials

All chemicals and media ingredients were purchased from Sigma-Aldrich (St. Louis, MO, USA), Roth (Karlsruhe, Germany), Merck (Darmstadt, Germany) or Fluka (Buchs, Switzerland) and were of the highest grade commercially available.

All restriction enzymes used were ordered form Thermo Scientific/Fermentas (Waltham, MA, USA) or New England Biolabs (Ipswich, MA, USA) and Ni-NTA columns were obtained from GE Healthcare (Chalfont St. Giles, UK).

3.2.2 Cloning and recombinant production of hD2HGDH

With the initial plan of expressing full-length hD2HGDH (Uniprot ID: Q8N465; Isoform 1; just without the *N*-terminal signal peptide predicted by Signal P [15]) in *Komagataella phaffii* (*Pichia pastoris*), the gene was purchased from Thermo Fisher Scientific (Waltham, MA, USA), codon optimized for expression in the yeast organism. On ordering, additionally, a nucleotide sequence coding for an octahistidine-tag was fused to the 3'end of the gene. Since expression in *Komagataella phaffii* was not successful, a truncated version of the gene lacking the coding sequence of the first 53 amino acid residues at the N-terminus and the C-terminal histidine-tag was generated using PCR (fwd. primer: 5'-TAATCCATGGTCCAGAGATTGCCATTCTCCACTGTTTCC-3' and rev. primer: 5'-ATATGCGGCCGCCTAAGCCTGAGATGGCAAGGTCTTG-3'). After restriction digestion with *Nco*I and *Not*I, the DNA string was inserted into the vector pETM11-His-GB1 TEV, which added nucleotides coding for an additional *N*-terminal hexahistidine-tag, as well as for the fusion protein (solubility enhancer) GB1 (B1 domain of *Streptococcal* protein G; ~8 kDa) (Figure 1).

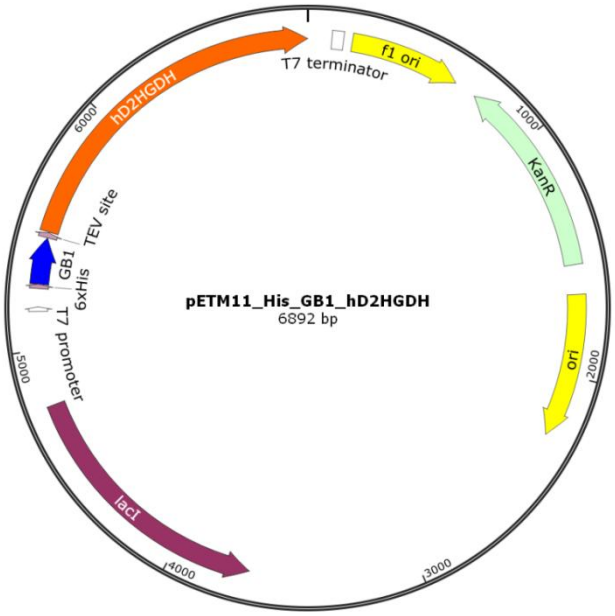

Figure 1: Plasmid map of the pETM11-His-GB1-hD2HGDH wild type construct. In order to allow for the recombinant production of soluble hD2HGDH, the respective gene sequence (*orange*) was fused to the 3'-end of a gene sequence encoding a hexahistidine-tag (*pink arrow*) and the solubility enhancer protein GB1 (*blue*). To be able to cleave off the GB1-tag after purification, a tobacco etch virus (TEV)-site was inserted between the two sequences. In addition, the expression plasmid carries a kanamycin resistance cassette (KanR) for selection, as well as a T7 promoter and a T7 terminator allowing for induction of the gene expression by isopropyl-β-D-thiogalactopyranoside (IPTG).

Having confirmed the construct by sequencing, the recombinant plasmid was transformed with *E. coli* Rosetta (DE3)-pLysS cells for subsequent gene expression.

For production, LB medium containing 50 µg/mL kanamycin as well as 20 µg/mL chloramphenicol for selection was inoculated with an overnight culture to an optical density of approximately 0.1. Then, cultures were left to grow to an optical density at 600 nm (OD_{600}) of about 0.8-0.9 at 37°C and 140 rpm, before adding 100 µM IPTG to induce gene expression. To maximize the protein yield, the cultures were incubated at 20 °C and 140 rpm overnight (about 16 h).

Harvested cells were resuspended in binding buffer (50 mM HEPES, 150 mM NaCl, 10 mM imidazole, pH 7 or 8 + 1 mM DTT) and lysed by sonication with a Labsonic L sonication probe (B. Braun Biotech, Berlin, Germany) for 2 x 5 min. After centrifugation at 38,500 g for 1 h (4 °C), the cleared cell lysate was loaded onto a Ni-NTA column equilibrated with binding buffer (without DTT). Unspecifically bound protein was washed off with wash buffer (50 mM HEPES, 150 mM NaCl, 20 mM imidazole, pH 7 or 8 + 1 mM DTT) and GB1-hD2HGDH was eluted with elution buffer (50 mM HEPES, 500 mM imidazole, pH 7 or 8 + 1 mM DTT). To confirm the presence of the desired protein in the fractions as well as to determine the quality of the purification, SDS-PAGE analysis was used. Fractions containing GB1-hD2HGDH were pooled and buffer was exchanged to 50 mM HEPES, 150 mM NaCl pH 7 or 8 by repeated concentration and dilution using Centripreps® 30 kDa MWCO (Merck Millipore, Burlington, MA, USA).

Because substantial amounts of impurities were detected on the SDS-PAGE right after purification via Ni-NTA chromatography, an additional gel filtration step was introduced, if no TEV-digestion (see below) was performed. The protein was applied to a Superdex200 increase (10/300 GL) column equilibrated with 50 mM HEPES, 150 mM NaCl pH 7 and elution of the protein was followed by monitoring the spectral changes at 280, 375 and 450 nm using a DAD. Presence of GB1-hD2HGDH in the fractions was again confirmed by SDS-PAGE analysis. Fractions containing pure GB1-hD2HGDH were pooled and buffer was exchanged to 50 mM HEPES, 150 mM NaCl pH 7. Concentrated protein (about 100 µM) was flash frozen with liquid nitrogen and stored at -80 °C until further use.

To remove the solubility enhancer (GB1) from hD2HGDH, tobacco etch virus (TEV)-digestion was performed overnight. The protein solution containing the fusion construct was mixed with the protease in a 10:1 (m/m) ratio and incubated at 4°C for 16 h. Then, another affinity-chromatography purification was performed (as described above), yielding

hD2HGDH in the flow-through fraction (and wash fraction with 50 mM imidazole). GB1 and not digested GB1-hD2HGDH, in contrast, remained bound to the column and could only be stripped off with elution buffer. To confirm the presence of the desired protein in the fractions as well as to determine the quality of the purification, again, SDS-PAGE analysis was used. Fractions containing pure hD2HGDH were pooled and buffer was exchanged to 50 mM HEPES, 150 mM NaCl pH 7. Concentrated protein (about 100 µM) was flash frozen with liquid nitrogen and stored at -80 °C until further use.

3.2.3 Recombinant production and purification of hETF

Recombinant production and purification of hETF (Uniprot IDs: P13804, α-subunit; P38117, β-subunit) was carried out as described previously [16].

3.2.4 Protein denaturation and determination of the extinction coefficient of hD2HGDH

To determine the extinction coefficient of hD2HGDH, a spectrum of native as well as of denatured hD2HGDH was recorded as suggested by Macheroux [17]. Assuming that the spectrum of the denatured protein equals the one of free FAD, the extinction coefficient of free FAD (11300 M^{-1} cm^{-1} at 450 nm) could be used to calculate the extinction coefficient of hD2HGDH at 450 nm (11600 ± 300 M^{-1} cm^{-1}).

3.2.5 Photoreduction of hD2HGDH

Photoreduction was performed under anoxic conditions as described by Massey (1978) [18]. A protein solution containing 10 µM hD2HGDH, 2.5 mM EDTA, 7.5 µM methylviologen, and 1 µM 5-deaza-FMN was rendered anaerobic and transferred to a sealable quartz cuvette. After recording a UV-*visible* spectrum between 300 and 800 nm, the sample was irradiated and additional spectra were recorded at a constant temperature of 15 °C, until no further spectral changes were observed. Then, the lid was removed under aerobic conditions to initiate reoxidation of the protein, which again was monitored spectrophotometrically.

3.2.6 Determination of the redox potential of hD2HGDH

The redox potential of hD2HGDH was studied under anoxic conditions using a stopped flow device from Hi-Tech (SF-61DX2) placed in an anaerobic glove box (Belle Technology,

Cambridge, UK) by applying the dye equilibrium method based on the xanthine/xanthine oxidase system, as reported by Massey [19]. Two solutions, one containing ~25 µM hD2HGDH, 500 µM xanthine, and 5 µM methylviologen and a second one with ~20 µM roseoFMN (A_{525}: ~0.2; E°: -252 mV) and ~200 nM xanthine oxidase, were prepared in 50 mM HEPES, 150 mM NaCl pH 7 and mixed using the stopped flow device. Then, reduction of the flavin and the dye was monitored by recording 500 absorption spectra (350 to 700 nm) with a KinetaScanT diode array detector (MG-6560) within 25 min (four measurements). From these data a Nernst plot was generated by plotting the log ([ox]/[red]) of the enzyme as a function of the log([ox]/[red]) of the dye - to determine the log($hD2HGDH_{ox}$/$hD2HGDH_{red}$) and the log(dye_{ox}/dye_{red}) the relative absorption changes at 450 nm and 525 nm, respectively, were used. Using the resulting intercept the redox potential of hD2HGDH could be determined as described by Minnaert [20].

3.2.7 Homology model of hD2HGDH

A homology model of hD2HGDH (Uniprot ID: Q8N465; Isoform 1) was generated with the SWISS-MODEL server [21–23] using the crystal structure of a putative dehydrogenase (RPA1076) from *Rhodopseudomonas palustris* CGA009 as template (pdb: 3pm9). The latter crystal structure was chosen as template, since the protein exhibits the highest sequence identity (~40 % on amino acid sequence level) and coverage with hD2HGDH of all structures deposited in the PDB. The FAD cofactor depicted in the figure was modeled into the predicted structure of hD2HGDH by aligning the two proteins and copying the flavin moiety from the putative dehydrogenase from *Rhodopseudomonas palustris* to the active site of the human D-2-hydroxyglutarate dehydrogenase.

3.2.8 Multiple sequence alignment

Structure-based sequence alignments were performed using the online tool Expresso [24] with amino acid sequences of D2HGDHs from various organisms: *Homo sapiens* (Uniprot ID, Q8N465); *Saccharomyces cerevisiae* (Uniprot ID, P46681); *Rattus norvegicus* (Uniprot ID, P84850); *Arabidopsis thaliana* (Uniprot ID, O23240); *Drosophila melanogaster* (Uniprot ID, Q7K511) and *Rhodopseudomonas palustris* (Uniprot ID, Q6NAV4). The data were exported in “Phylip” format and visualized using SeaView [25] (Supplementary Figure S1).

3.2.9 Reductive and oxidative half-reaction

To study the reductive and oxidative half-reaction (of hD2HGDH), time dependent spectral changes of the flavin absorption were recorded under anoxic conditions using a stopped flow device (Hi-Tech, TgK Scientific, Bradford-on-Avon, UK), placed in a glove box (Belle Technology, Cambridge, UK), and monitored with a KinetikaScanT diode array detector (MG-6560). The following analysis was performed by fitting the data points recorded at 450 nm with the Kinetic Studio Software (TgK Scientific).

For the determination of the reduction rate of hD2HGDH, reduction of the protein-bound FAD cofactor was studied in the presence of eight different D-2-hydroxyglutarate (final concentration: 25 µM to 1,000 µM) and nine D-lactate (final concentration: 0.5 mM to 75 mM) concentrations. A 20 µM enzyme solution (10 µM final concentration) and the substrate solutions were prepared in 50 mM HEPES, 150 mM NaCl pH 7, before mixing them in the stopped flow device and recording the spectral changes between 350 and 700 nm (measurements were performed 4-times at each substrate concentration). The extracted observed rate constants (k_{obs}) were plotted as a function of the respective substrate concentrations to obtain a hyperbolic curve, which allowed determination of the limiting reduction rates (k_{red}) as well as of the dissociation constants (K_d).

To study the effect of product binding on the rate or reoxidation, one sample of reduced hD2HGDH (10 µM) was generated using photoreduction (see above) and a second one by adding about 1.5 eq of D-2-hydroxyglutarate. Then, both samples were mixed with air saturated buffer (20°C) in a stopped flow device and spectral changes between 350 nm and 700 nm were monitored for 1.5 - 3 s and 25 - 50 min, respectively. To obtain bimolecular reoxidation rates, the observed rate constants were divided by the final oxygen concentration in the reaction mixture (final concentration: 140 µM).

3.2.10 Electron transfer from hD2HGDH to hETF

To study the electron transfer from hD2HGDH to hETF, hETF was diluted to a final concentration of 20 µM using 50 mM HEPES, 150 mM NaCl pH 7 and mixed with 2 µM hD2HGDH (in the presence of 1 mM of D-2HG) in a stopped-flow device (Hi-Tech, TgK Scientific, Bradford-on-Avon), placed in an anaerobic glove box (Belle Technology, Cambridge, UK). The resulting time dependent spectral changes were monitored between 350 and 700 nm using a KinetikaScanT diode array detector (MG-6560) for 150 s.

3.2.11 Steady-state kinetics (hD2HGDH)

To determine the kinetic parameters of hD2HGDH under steady-state conditions, a coupled assay with 2,6-dichlorophenyl indophenol (DCPIP) as final electron acceptor was used. Solutions containing 100 nM hD2HGDH and 125 µM DCPIP were prepared in 50 mM HEPES, 150 mM NaCl pH 7 and incubated at 25 °C for 10 min. Then, the reactions were started by adding varying final concentrations of D-2HG (6.25 µM to 1,000 µM) or D-lactate (0.25 mM to 25 mM) and absorbance changes at 600 nm were recorded for 120 s. By plotting the extracted initial rates as a function of the corresponding substrate concentrations the kinetic parameters K_{Mapp} and k_{catapp} could be determined.

3.2.12 Steady-state analysis of the electron transfer from hD2HGDH to hETF

Steady-state parameters for the electron transfer of hD2HGDH to wild type hETF were determined in a coupled assay with DCPIP as final electron acceptor. Buffer (50 mM HEPES, 150 mM NaCl pH 7), hD2HGDH (100 nM), hETF (0.25 to 17.5 µM), and DCPIP (125 µM) were mixed and incubated at 25 °C for 10 minutes. Then, the reaction was started by adding 1 mM D-2-hydroxyglutarate, and the decrease in absorbance at 600 nm was monitored at 25°C for 120 s (measurements at each hETF concentration were performed in triplicate). To determine the kinetic parameters K_{Mapp} and k_{catapp} the extracted initial velocities (normalized to enzyme concentration) were plotted as a function of the respective hETF concentration yielding a hyperbolic curve, which was fitted using the program Origin 7 (OriginLab, Northampton, MA, USA).

3.2.13 Site-directed mutagenesis

The two hD2HGDH-variants were generated from the wild type construct pETM11-GB1-hD2HGDH using PCR-based mutagenesis (for primers see Table 1). Having confirmed the variation in the nucleotide sequence by automated sequencing, the plasmids were transformed with *E. coli* Rosetta (DE3)-pLysS cells for subsequent gene expression. Protein production and purification were then performed as described for the wild type protein (*Cloning and recombinant production of hD2HGDH*).

Table 1: Mutagenesis primers required for the generation of the hD2HGDH-variants in a PCR-based approach (the codon triplets carrying the desired mutations in the nucleotide sequence are shown in bold).

Primer name	Primer sequence
I147S fwd.	5'-CAGTTTTCGACGAGA**TCT**CTTTGTCCACCGC-3'
I147S rev.	5'-CTGGCGGTGGACAAAG**AGA**TCTCGTCG-3'
V444A fwd.	5'-GGTAACTTGCACTTGAAC**GCT**ACTGCTGAGGC-3'
V444A rev.	5'-GGAGAAAGCCTCAGCAGT**AGC**GTTCAAGTGC-3'

3.2.14 Co-production of GB1-hD2HGDH variants and the groES-groEL complex

For co-production of GB1-hD2HGDH and the groES/groEL-complex, pET-M11-GB1-hD2HGDH-I147S and -V444A plasmid DNA was transformed with *E. coli* BL21 (DE3) cells already harboring the pGro7-plasmid.

For protein production, LB medium containing 50 µg/mL kanamycin as well as 20 µg/mL chloramphenicol for selection and 0.5 mg/mL of L-arabinose to initiate chaperone expression was inoculated with an overnight culture to an optical density of approximately 0.1. Then, cultures were left to grow to an optical density at 600 nm (OD_{600}) of about 0.8-0.9 at 37°C and 140 rpm, before adding 100 µM IPTG to induce gene expression. To maximize the protein yield, the cultures were incubated at 20 °C and 140 rpm overnight (about 16 h). Purification was carried out as described above (*2.2 Cloning and recombinant production of hD2HGDH*).

3.2.15 Production of GB1-hD2HGDH variants in the presence of increased riboflavin levels in the culture medium

To study the effect of increased riboflavin levels on protein folding, GB1-hD2HGDH-Ile147S and GB1-hD2HGDH-Val444Ala were again produced as described previously (*2.2* and *2.12*). However, the culture medium was supplemented with 0.1 mM of riboflavin. Additionally, FAD (100 µM) was added to all buffers used in the course of the affinity purification of the proteins.

3.2.16 CD-spectroscopy

In order to study the influence of the two pathogenic amino acid replacements (Ile147Ser and Val444Ala) on protein folding, CD-spectroscopy experiments were performed. hD2HGDH wild type, GB1-hD2HGDH wild type, GB1-D2HGDH-Ile147Ser, and GB1-hD2HGDH-Val444Ala were rebuffered to 50 mM NaH_2PO_4 pH 7 and diluted to final concentrations of 11, 11, 16 and 19 µM, respectively. Then, the protein solutions were transferred to cuvettes (d, 0.1 cm) and CD spectra were recorded between 260 and 190 nm in a JASCO J-1500 spectrophotometer (JASCO Inc., Tokyo, Japan) equipped with a PM-593 detector (Scan speed, 50 nm/min; Interval, 0.2 nm; CD-scale, 200 mdeg/ 1.0 dOD) and averaged over three scans. Subsequent data analysis was performed using the program Spectral Manager (JASCO Inc., Tokyo, Japan), which also allowed prediction of the secondary structure elements using the online program DichroWeb [26–28].

3.2.17 Limited proteolysis

In order to investigate the proteolytic stability of GB1-hD2HGDH wild type and the two variants, the proteins were diluted to a final concentration of ~15 µM using 50 mM HEPES, 150 mM NaCl pH 7 and incubated at 37°C for 5 min. Then, trypsin (Promega, Madison, WI, USA) was added (2 µg/mL) and samples were taken after 0, 30, 60, 90, 120, 150, and 180 min, mixed with Laemmli sample buffer [29], and inactivated at 95°C for 10 min. Finally, SDS-PAGE analysis was performed to determine the fragmentation pattern of the different proteins.

3.3 Results

3.3.1 Production, purification and biochemical characterization of hD2HGDH

Since recombinant production of full-length hD2HGDH (Uniprot ID: Q8N465; Isoform 1) and of a truncated version of the protein lacking the putative mitochondrial targeting sequence ($hD2HGDH_{54}$) was unsuccessful in *E. coli* and in *Komagataella phaffii* (*Pichia pastoris*), a fusion construct with the solubility tag GB1 (B1 domain of *Streptococcal* protein G) was generated. This approach produced soluble fusion protein (GB1-$hD2HGDH_{54}$) in *E. coli* and subsequent purification using affinity chromatography (Ni-NTA) and gel filtration yielded about 3 mg of pure protein from 120 g cell (wet weight). After purification, the *N*-terminal fusion-tag could be removed by means of the tobacco etch virus protease. Although removal

of GB1 had no adverse effect on the solubility and stability of hD2HGDH, this procedure incurred a severe loss of total protein resulting in a final yield of 0.5 mg. Therefore, the “free” hD2HGDH was only prepared for select experiments such as steady-state turnover and interaction studies with human ETF (see below).

The purified protein (with and without GB1) exhibited absorption maxima at 378 nm and 453 nm, indicating the presence of a flavin chromophore. The spectral changes observed upon denaturation of the protein are consistent with FAD being the cofactor (Figure 2A), which is in accordance with previous reports on homologs of hD2HGDH[7,8].

In order to obtain information about the electrochemical properties of hD2HGDH, the enzyme was photoreduced and the redox potential was determined using the xanthine/xanthine oxidase method reported by Massey [19]. Photoreduction of hD2HGDH required the use of significant amounts of the redox mediators 5-deaza-FMN (2.5 µM) and methylviologen (7 µM) yielding fully reduced enzyme (Figure 2B, oxidized: *black*; reduced: *blue*) after 45 min of irradiation. In the course of the reduction, as well as upon reoxidation (Figure 2B, reoxidized: *green*) no radical intermediate was observed, indicating that radical flavin species are not stabilized. Similarly, hD2HGDH was directly reduced to the hydroquinone form in the redox potential experiment. Using roseoFMN as the reporting dye, the flavin chromophore and the dye were fully reduced almost synchronously (Figure 2C),which allowed the determination of the redox potential by plotting the $\log(hD2HGDH_{ox}/hD2HGDH_{red})$ as a function of the $\log(roseoFMN_{ox}/roseoFMN_{red})$. This yielded a redox potential of -196 ± 1 mV, which is significantly more negative than determined for other dehydrogenases (*e.g.*hMCAD: -87 mV[30]).

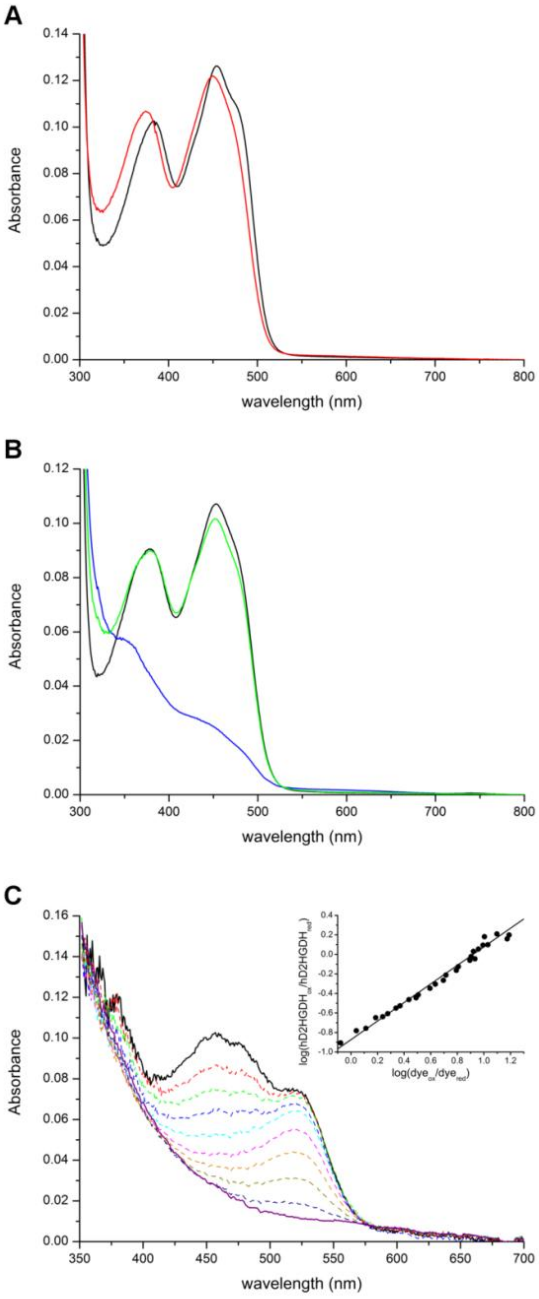

Figure 2: Spectral and electrochemical characterization of (GB1-)hD2HGDH. A, To determine the molar extinction coefficient of hD2HGDH at 450 nm, UV-*visible* absorption spectra of native (*black line*) and denatured (2% SDS; *red line*) hD2HGDH, diluted to a final concentration of 10 µM with 50 mM HEPES, 150 mM NaCl pH 7, were recorded between 300 and 800 nm (25°C). Assuming that the spectrum of denatured hD2HGDH corresponds to the spectrum of free FAD (ε_{450}: 11,300 M^{-1} cm^{-1}), the molar extinction coefficient of hD2HGDH was calculated (ε_{450}: 11,600 ± 300 M^{-1} cm^{-1}). **B**, UV-*visible* absorption spectra (300-800 nm) corresponding to the different flavin redox states observed in the course of the anoxic photoreduction of hD2HGDH (diluted to a final concentration of 10 µM using 50 mM HEPES, 150 mM NaCl pH 7): oxidized (*black line*), fully reduced (*blue line*) and reoxidized (*green line*). **C**, Time-dependent spectral changes of hD2HGDH (~10 µM) and roseoFMN (~10 µM; E°: -222 mV) monitored in the course of the reduction reaction

(25 min), indicating a two-electron reduction of both the FAD cofactor and the dye. All measurements were carried out in 50 mM HEPES, 150 mM NaCl pH 7 at a constant temperature of 25°C. ***Inset***, Based on the relative absorbance changes at 450 and 525 nm, respectively, a Nernst plot was generated by plotting the $\log(hD2HGDH_{ox}/hD2HGDH_{red})$ as a function of the $\log(dye_{ox}/dye_{red})$. From the resulting intercept a redox potential of -196 ± 2 mV was calculated (from four determinations).

3.3.2 Kinetic characterization of hD2HGDH

Detailed kinetic characterization of both GB1-tagged and "free" hD2HGDH revealed that the *N*-terminal fusion tag does not influence the kinetic properties of the protein. hD2HGDH is efficiently reduced by D-2HG as well as by D-lactate, reaching limiting rates with 1 mM D-2HG (k_{red}: 1.9 ± 0.1 s^{-1}; K_D:83 ± 14 µM; Figure 3B) and 75 mM D-lactate (k_{red}: 0.30 ± 0.01 s^{-1}; K_D: 2500 ± 200 µM), respectively (Table 2). It should be noted that when plotting the observed rate constants as a function of the respective substrate concentrations and fitting the results with a hyperbolic function, a y-axis intercept was obtained with both substrates, indicating reversibility of the reduction reaction (k_{-1}: 0.6 ± 0.1s^{-1} and 0.08 ± 0.01s^{-1} for D-2HG and D-lactate, respectively; Figure 3B). Additionally, we found that substrate-induced flavin reduction proceeds in two distinct phases, with the second phase being ~200-fold (2-HG) and ~20-fold (D-lactate), respectively, slower than the first phase (Figure 3A). The fast phase is characterized by the formation of a long wavelength absorption (500-600 nm) and the partial decrease at 350 to 500 nm. In contrast, the second, much slower phase exhibits no spectral changes in the long-wavelength area but only in the absorption indicative of further flavin reduction. (Figure 3A, *black* and *redline*). Interestingly, it was also observed that the amplitude of the two phases strongly depended on the substrate concentration. The amplitude of the first phase increased with increasing substrate concentration with full reduction of the flavin chromophore in a reasonable time frame (up to 150 s) could only be observed with D-lactate.

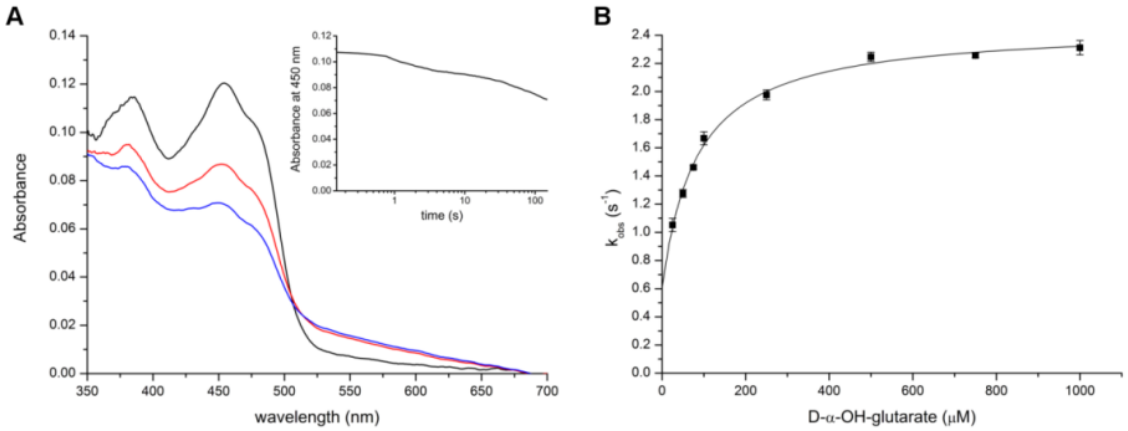

Figure 3: Determination of the reductive rate of hD2HGDH with D-2HG. A, UV-*visible* absorption spectra recorded after mixing ~10 µM hD2HGDH with 1 mM of D2HG in 50 mM HEPES, 150 mM NaCl pH 7 in a stopped-flow device. The *black* line indicates the starting spectrum, while the *blue* line reflects the final spectrum monitored after 150 s (at this substrate concentration full reduction of the protein-bound flavin cofactor could not be achieved). Interestingly, reduction of hD2HGDH proceeds in two distinct phases as indicated by the *red* spectrum and the *inset*. In the first phase, the decrease in absorbance at 450 nm is accompanied by a significant increase in longer wavelength absorbance, which is not observed in the second, much slower phase. **B**, To determine the limiting rate (k_{red}) as well as the dissociation constant (K_D) of D2HG with hD2HGDH, observed rate constants (k_{obs}) for the flavin reduction were extracted and plotted as a function of the corresponding D2HG concentrations (measurements were performed four times at each substrate concentration; standard deviations are indicated by error bars).

Next, we also performed steady-state kinetics to better understand the overall turnover process. In a steady-state assay using 2,6-dichlorophenyl indophenol (DCPIP) as the final electron acceptor, a higher catalytic efficiency of hD2HGDH with D-2HG was observed than with D-lactate ($1.3 \cdot 10^4 \pm 0.2 \cdot 10^4$ M^{-1} s^{-1} *vs* 300 ± 30 M^{-1} s^{-1}). However, the turnover numbers obtained with D-2HG were ~5-times lower than the reduction rates (Table 2), indicating that either product release or the oxidative half-reaction is the rate-limiting process under steady-state conditions.

Table 2: Kinetic parameters of hD2HGDH determined with D-2-hydroxyglutarate and D-lactate under pre steady-state and steady-state conditions (25°C). Reductive rates (k_{red}) and dissociation constants (K_D-values) were determined under pre steady-state conditions by mixing hD2HGDH (10 µM final concentration) with varying concentrations of D-2-hydroxyglutarate (final concentrations: 25 – 1,000 µM) as well as of D-lactate (final concentrations: 0.25 - 75 mM). Both, enzyme and substrate solutions were prepared in 50 mM HEPES, 150 mM NaCl pH 7 and flavin reduction was monitored between 350 and 700 nm for 1.5 to 150 s. Absorbance changes at 450 nm were used to extract observed rate constants (k_{obs}), which were then plotted as a function of the respective substrate concentrations to obtain limiting rates (k_{red}) as well as dissociation constants (K_D) for the interaction of hD2HGDH with the two substrates.

Under steady-state conditions, kinetic characterization of the enzyme was carried out by using DCPIP as final electron acceptor. Buffer (50 mM HEPES, 150 mM NaCl pH 7), hD2HGDH (100 nM) and DCPIP (125 µM) were mixed and incubated at 25°C for 10 min. Then, varying amounts of D-2-hydroxyglutarate (final concentrations: 6.25 µM to 1,000 µM) or D-lactate (final concentrations: 0.25 mM to 25 mM) were added and absorbance changes at 600 nm were recorded for 120 s. By plotting the initial rates as function of the substrate concentrations, k_{catapp} and K_{Mapp} values for the interaction of hD2HGDH with both accepted substrates could be determined.

kinetic parameters	D-2-hydroxyglutarate	D-lactate
k_{red} [s^{-1}]	1.9 ± 0.1	0.30 ± 0.01
k_{-1} [s^{-1}]	0.6 ± 0.1	0.08 ± 0.01
K_D [µM]	83 ± 14	2,500 ± 200
k_{catapp} [s^{-1}]	0.51 ± 0.01	0.39 ± 0.01
K_{Mapp} [µM]	38 ± 3	1,300 ± 100
k_{catapp} / K_{Mapp}(M^{-1} s^{-1})	$1.3 \cdot 10^4 \pm 0.2 \cdot 10^4$	300 ± 30

In addition, we also analyzed the reoxidation of photoreduced- and substrate-reduced protein by molecular oxygen in a stopped-flow apparatus. While photoreduced hD2HGDH was reoxidized within a couple of seconds (k_{ox}: $2.1 \cdot 10^4 \pm 0.1 \cdot 10^4$ M^{-1} s^{-1}), the rate of reoxidation observed for the substrate-reduced enzyme was about 1500-fold lower (k_{ox}: 14 ± 1M^{-1} s^{-1}). Together with the fact that reoxidation of the substrate-reduced enzyme coincided with a decrease in longer wavelength absorption observed in the first phase of the reduction reaction (see above), this finding suggests that the reaction products, *i.e.*α-ketoglutarate or pyruvate, remain bound to the enzyme in order to suppress oxygen reactivity. Interestingly, however, the addition of α-ketoglutarate to photoreduced hD2HGDH did not affect the rate of

reoxidation, indicating that the protein undergoes conformational changes during substrate oxidation, creating a binding pocket for the product.

3.3.3 Electron transfer from hD2HGDH to hETF

It was previously assumed that reduced hD2HGDH may transfer electrons to hETF (Uniprot IDs: P13804, α-subunit; P38117, β-subunit), which is known to service several dehydrogenases in the mitochondrial matrix and thus serves as a central electron acceptor. In order to substantiate this assumption experimentally, we investigated the putative transfer of electrons from reduced hD2HGDH to hETF under steady-state conditions. Briefly, hETF (10 µM) was mixed with 1 µM of hD2HGDH and 1 mM of D2HG in a stopped-flow device and the changes in the UV-*visible* absorption spectrum of hETFwere monitored for 150 s. Within the first 10 s, a strong absorbance increase at 375 nm and a strong decrease at 450 nm were observed (Figure 4A, *black line* to *cyan line*), indicating the formation of an anionic flavin semiquinone species and confirming the successful electron transfer from hD2HGDH to hETF. The radical flavin species, however, was not stable over time and was further reduced to the hydroquinone form within the next 100 s (Figure 4A, *cyan line* to *purple line*). Therefore, it can be concluded that hETF can accept two electrons from hD2HGDH, with the transfer of the second electron being about 10-fold slower than of the first.

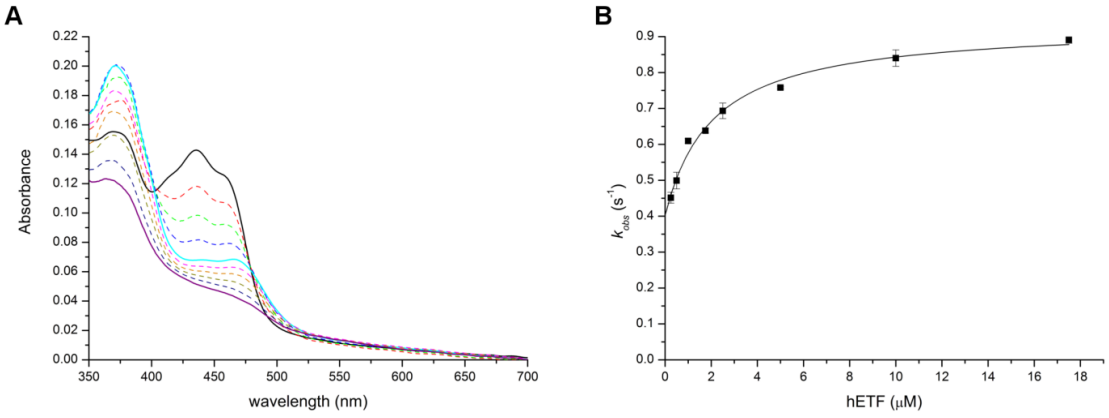

Figure 4: Electron transfer from hD2HGDH to hETF. **A**, Electron transfer from reduced hD2HGDH to hETF was studied under anoxic conditions in 50 mM HEPES, 150 mM NaCl pH 7. 10 µM hETF and 1 µM substrate-reduced hD2HGDH (excess of substrate → 1 mM D-2HG) were mixed in a stopped-flow device and changes in the absorption characteristics of hETF were monitored between 350 and 700 nm for 150 s. Within the first 10 s, formation of an anionic flavin semiquinone species was observed (*black* to *lightblue* line), indicating the transfer

of single electrons from hD2HGDH to hETF. However, the radical species was not stable over time and full reduction to the hydroquinone form was observed after 150 s (*lightblue* line to *purple* line). **B**, The rate of electron transfer from hD2HGDH to hETF was studied using a coupled assay with DCPIP as final electron acceptor. hD2HGDH (100 nM), DCPIP (125 µM) and varying concentrations of hETF (0.25 to 17.5 µM) were mixed in 50 mM HEPES pH 7 and incubated at 25°C for 10 min. Then, D-2HG (1 mM) was added and changes in the absorbance at 600 nm were recorded for 120 s (measurements were performed in triplicate at each substrate concentration). By plotting the extracted initial velocities as a function of the hETF concentrations, a hyperbolic curve was obtained (standard deviations at each substrate concentration are indicated by error bars), which allowed the determination of the limiting rate (k_{catapp}) as well as of the K_{Mapp}-value for the electron transfer from hD2HGDH to hETF (k_{catapp}: 0.53 ± 0.03 s^{-1}; K_{Mapp}: 2.1 ± 0.5 µM).

For a more detailed characterization of the electron transfer process, we then performed a coupled assay with DCPIP as terminal electron acceptor. By studying the rates of electron transfer in the presence of different hETF concentrations, a limiting rate (k_{cat}) as well as a K_M value for the interaction between reduced hD2HGDH and hETF could be obtained (Figure 4B, Table 3).

Table 3: Kinetic parameters determined for the electron transfer from D2HGDH to hETF under steady-state conditions. The steady-state parameters for the electron transfer were determined in a coupled assay involving 1 mM D-2-hydroxyglutarate, 100 nM hD2HGDH, 125 µM DCPIP and varying concentrations of hETF (0.25 to 17.5 µM) in 50 mM HEPES, 150 mM NaCl pH 7. By monitoring the decrease in absorbance of DCPIP at 600 nm for 120 s, initial rates could be obtained and plotted as function of the hETF concentrations to yield the kinetic parameters k_{catapp} and K_{Mapp}.

kinetic parameters	D-2-hydroxyglutarate
k_{catapp} [s^{-1}]	0.53 ± 0.03
K_{Mapp} [µM]	2.1 ± 0.5

The rather low K_M value of 2.1 ± 0.5 µM indicates a relatively high affinity of the reduced donor enzyme to hETF, however, electron transfer looks to be less efficient as compared with other client enzymes (k_{cat}: 0.53 ± 0.03 s^{-1}*vs.* ~2 $s^{-1}$for hDMGDH, hMCAD) under the same assay conditions [16,31].

3.3.4 Production, purificationand characterization of two pathogenic variants of hD2HGDH

Recent studies aiming to understand the molecular causes of D-2-hydroxyglutaric aciduria revealed two pathogenic single nucleotide replacements in the respective gene (c.440T→G and c.1331T→C), leading to single amino acid exchanges in the mature protein (Ile147Ser and Val444Ala; Figure 5A and B).

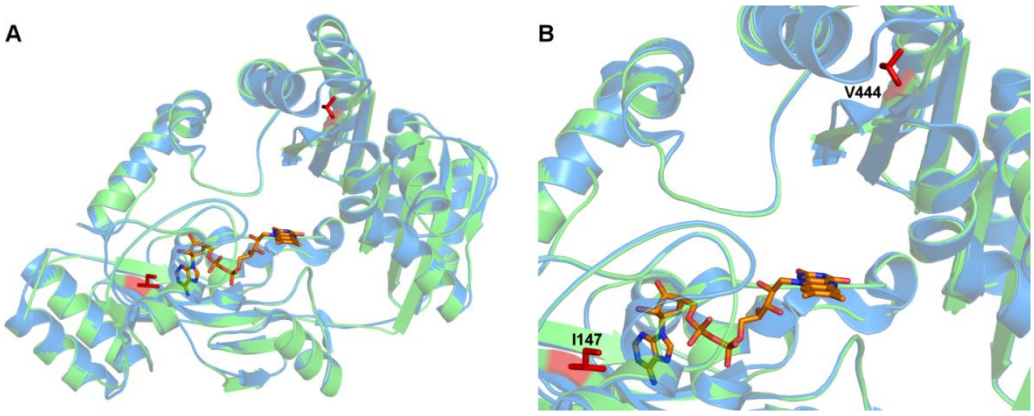

Figure 5:Structural model of hD2HGDH.A, Overall structural model of hD2HGDH (*green*) generated based on the crystal structure of a putative dehydrogenase (RPA1076) from *Rhodopseudomonas palustris* CGA009 (PDB code, 3pm9; *blue*). Putative catalytic and substrate binding residues of the two proteins are shown using *green* and *blue* sticks, respectively. The FAD cofactor is depicted using *orange* sticks. Several patients diagnosed with D-2-hydroxyglutaric aciduria were found to suffer from deficiencies of hD2HGDH, resulting from single pathogenic amino acid replacements of either one of the two amino acid residues displayed as *red* sticks (Ile147 and Val444); Ile147 and Val444 were found to be replaced by a serine (Ile147Ser) or an alanine (Val444Ala), respectively. **B**, Close-up view of the active site with the two important amino acid residues altered in patients suffering from D-2-hydroxyglutarate dehydrogenase deficiency shown as *red* sticks (Ile147 and Val444).According to the model, both Ile147 and Val444 are too distant from the FAD cofactor and the substrate binding site in order to be involved in flavin binding or D-2HG oxidation.

It was shown that both protein variants exhibit much lower activity (Ile147Ser: 0% and Val444Ala: 25%) as compared with the wild type in a cell-line based assay. However, the reasons for the dramatic loss in catalytic activity remained elusive [1]. In order to address this question, we recombinantly produced both variants with an *N*-terminal GB1-tagin *E. coli*. In contrast to the wild type protein, both variants were obtained as apo-proteins, indicating that they exhibited severely impaired flavin binding properties. Since hD2HGDH requires the flavin cofactor for proper enzymatic function, this fact explains the loss in catalytic activity

found in a radiochemical assay performed by Struys *et al.* (2005)[1].The presence of an excess of FAD, *i.e.* 50 and 500 µM FAD failed to restore the catalytic activity of the variant proteins. For both variants residual activities in the range of 0.1% of the wild type enzyme were obtained indicating that flavin binding was seriously compromised by the single amino acid replacements.

To further assess the structural properties of the variant proteins the CD-spectrum of the wild type and the two protein variants were recorded. This analysis revealed no significant difference in secondary structure elements between the wild type and the two variant proteins (Figure 6A and Table 4), indicating some other factor to be responsible for the reduced FAD binding affinity and enzymatic activity. Therefore, we decided to also investigate the proteolytic stability of the variants compared to wild type hD2HGDH. Interestingly, both of them showed a strongly reduced susceptibility for proteolytic degradation as compared to the wild type (Figure 6B), which is a strong indication for the variants to be aggregated. This supposition was further tested by subjecting purified samples of wild type and variant proteins to analytical size-exclusion chromatography. As shown in Figure 6C, this clearly demonstrated that the two variants form aggregates, whereas the wild type protein is a dimer in solution.

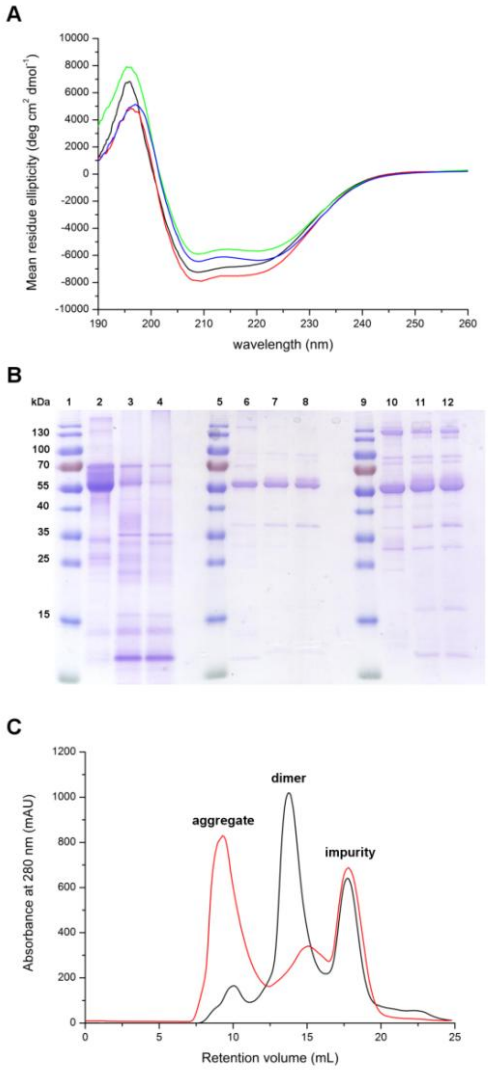

Figure 6: Biochemical and biophysical characterization of hD2HGDH wild type, GB1-hD2HGDH wild type, GB1-hD2HGDH-I147S and GB1-hD2HGDH-V444A. A, CD-spectra obtained with hD2HGDH wild type (*black* line), GB1-hD2HGDH wild type (*red* line), GB1-hD2HGDH-I147S (*green* line), and GB1-hD2HGDH-V444A (*blue* line). The proteins were rebuffered to 50 mM NaH_2PO_4 pH 7 and diluted to a final concentration of 11, 11, 16, and 19 µM, respectively. Then, the solutions were transferred to cuvettes (d, 0.1 cm) and CD-spectra were recorded at 20 °C between 260 and 190 nm and averaged over three scans. **B**, SDS-PAGE analysis of the limited proteolysis experiment performed with GB1-hD2HGDH wild type, GB1-hD2HGDH-I147S, and GB1-hD2HGDH-V444A. In lanes 1, 5, and 9 PageRuler® prestained protein ladder (Thermo Fisher Scientific) is depicted, whereas in the remaining lanes the fragmentation pattern of GB1-hD2HGDH wild type (lane 2-4), GB1-hD2HGDH-I147S (lane 6-8), and GB1-hD2HGDH-V444A (lane 10-12) after 0, 90, and 180 min is shown. **C**, Chromatogram obtained in the course of the gel filtration of GB1-hD2HGDH wild type (*black* line) and GB1-hD2HGDH-I147S (*red* line) using a Superdex200 increase column (10/300 GL) equilibrated with 50 mM HEPES, 150 mM NaCl pH 7. The elution pattern indicates the wild type protein to be a dimer in solution, whereas the variants seem to form aggregates.

Table 4: Secondary structure prediction for hD2HGDH wild type, GB1-hD2HGDH wild type, and the two protein variants GB1-hD2HGDH-I147S and GB1-hD2HGDH-V444A. Wild type and variant proteins were diluted to a final concentration of 11 and 16/19 µM, respectively, using 50 mM NaH_2PO_4 pH 7. Then, CD-spectra were recorded between 260 and 190 nm, which allowed subsequent secondary structure prediction using the online program DichroWeb[26–28].

Secondary structure	hD2HGDH wild type	GB1-hD2HGDH wild type	GB1-hD2HGDH-I147S	GB1-hD2HGDH-V444A
α-helix (%)	21	24	19	20
β-sheet (%)	26	24	30	28
turn (%)	14	14	13	13
random (%)	39	39	37	38

*the CD-spectra were analyzed using the program CDSSTR [32,33] and the SP175 reference dataset [34] between 190 and 240 nm.

3.4 Discussion

3.4.1 Kinetic characterization of hD2HGDH

The successful recombinant production of hD2HGDH as fusion construct with the solubility enhancer GB1 in *E. coli* enabled the detailed biochemical characterization of hD2HGDH and allowed to establish its suspected interaction with the human electron transferring flavoprotein (hETF). Kinetic characterization revealed that hD2HGDH is able to efficiently catalyze the oxidation of D-2HG as well as of D-lactate, though the reduction rates determined with the latter substrate were almost a factor of 5 lower as compared with D-2HG (k_{red}: 1.9 ± 0.1 s^{-1}; 0.39 ± 0.05 s^{-1}, respectively). Also, the dissociation constants obtained for D-lactate were much higher than with D-2HG, indicating that D-2HG is more efficiently oxidized by the enzyme. Interestingly, reversibility of the reduction reaction was observed with both substrates as indicated by the significant k_{-1}-rates obtained under rapid reaction conditions (Figure 3B, Table 2). This finding is in agreement with the slightly more positive reduction potential of the D-lactate/pyruvate couple (-190 mV) as compared with the midpoint potential of the flavin cofactor bound to hD2HGDH (-196 mV), which causes substrate oxidation to be rather unfavorable.

Similar kinetic properties have previously been found in classical acyl-CoA dehydrogenases, which are arguably among the best characterized electron donors of many electron transferring flavoproteins [35,36]. These enzymes have been shown to tightly bind the

reaction products in the active site in order to shift the chemical equilibrium toward substrate oxidation [35,37–39], which is indicated by the formation of a charge-transfer complex between the protein-bound reduced FAD and the reaction products. The fact that reduction of the FAD-cofactor in hD2HGDH also coincides with a significant increase in longer-wavelength absorption (Figure 3A), suggests that hD2HGDH employs a similar strategy to make substrate conversion more efficient. Also the observation that the increase in longer-wavelength absorption was more pronounced when the enzyme was reduced by D-2HG, is in agreement with this hypothesis and may be explained assuming that α-ketoglutarate is bound more tightly to hD2HGDH than pyruvate. The higher affinity of α-ketoglutarate to hD2HGDH also provides an explanation for the much slower second phase of flavin reduction observed with D-2HG than with D-lactate, as this phase presumably reflects the decay of the charge-transfer complex to reduced dehydrogenase and released product, i.e. either □-ketoglutarate or pyruvate [38,40].

Interestingly, steady-state experiments involving hD2HGDH and D-2HG revealed an overall turnover-rate (k_{catapp}) that was 4-5-times lower than the limiting rate of reduction (Table 2), suggesting that either product release or the oxidative half-reaction was rate-limiting under these conditions. This is in line with the low reoxidation rates obtained with substrate-reduced hD2HGDH as compared with photoreduced enzyme, indicating that binding of the reaction products may not only affect the chemical equilibrium of the enzymatic turnover but may also influence oxygen reactivity.

How flavoenzymes exert control over the reactivity of the reduced cofactor with dioxygen is a longstanding topic in this research field [41–44]. Mostly, oxygen reactivity is an intrinsic feature of the proteins [41,44–46], however, in the case of classical client dehydrogenases, *e.g.* the family of acyl-CoA dehydrogenases, a similar concept of product-controlled oxygen reactivity has already been described [37–39]. In these enzymes, product binding leads to an increased hydrophobicity in the active site, thereby impeding the stabilization of superoxide species required for the reoxidation of reduced flavin cofactors by molecular oxygen [47]. Recently, we could also show that Dld2 from *Saccharomyces cerevisiae* controls oxygen reactivity by product binding [8]. However, in contrast to acyl-CoA dehydrogenases the reduced activity toward dioxygen appears to be the result of conformational changes that take place in the course of substrate binding and conversion to the oxidized product [8]. Since only the presence of α-ketoglutarate was not sufficient to prohibit reoxidation of reduced hD2HGDH by molecular oxygen and considering that the enzyme is an ortholog of Dld2, it is

very likely that hD2HGDH controls oxygen reactivity in a similar way as the yeast counterpart.

3.4.2 Electron transfer to hETF

The hETF services at least thirteen different dehydrogenases in the mitochondrial matrix, including the acyl-CoA dehydrogenases required for fatty acid and amino acid degradation [16]. Based on the observation that D-2HG accumulates as a result of defects in either the hETF or its final electron acceptor ETF-QO [9], hD2HGDH was also proposed to be a client enzyme of hETF, however, the interaction was not tested experimentally so far. In the present study, we could clearly demonstrate that reduced hD2HGDH is indeed capable of donating electrons to hETF and thus this enzyme can be safely added to the list of hETF clients. While oxygen reactivity is strongly suppressed in substrate-reduced hD2HGDH (see above *3.2* and *4.1*), electron transfer to hETF readily occurs as could be shown by mixing hETF with catalytic amounts of hD2HGDH and an excess of D-2HG in a stopped-flow device (Figure 4A, Scheme 1). Spectral analysis of the reduction of hETF by hD2HGDH revealed a fast transfer of single electrons, resulting in the generation of an anionic flavin semiquinone (Figure 4A, *light blue* line), which was subsequently further reduced to the hydroquinone (Figure 4A, *purple* line), albeit at a 10-times slower rate (Scheme 1).

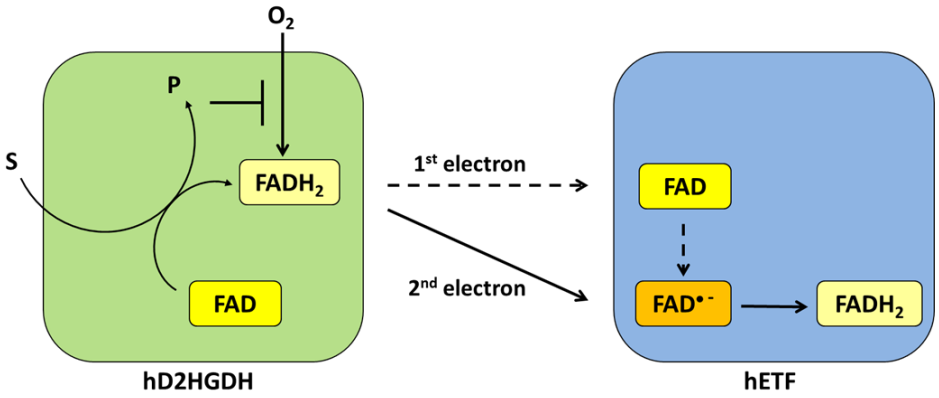

Scheme 1: Electron transfer reactions between hD2HDGH and hETF. Reduction of the FAD cofactor bound to hD2HGDH by the substrate (S) leads to fully (two-electron) reduced FAD and the product (P), which is still bound to the enzyme to prevent reaction with oxygen. However, hD2HGDH rapidly reduces the FAD cofactor of hETF by one-electron transfer leading to the anionic FAD semiquinone, which undergoes slower reduction to the fully reduced FAD (bottom line shown in the blue square).

This behavior is quite similar to the interaction of hETF with other clients such as the acyl-CoA dehydrogenases [39,48–50]. Like hD2HGDH, substrate reduced acyl-CoA dehydrogenases exhibit rather poor reactivity toward molecular oxygen, but undergo rapid one-electron transfer reactions with hETF [38,48]. Whether the mechanisms used to guarantee successful electron delivery to hETF are the same in both enzymes is presently unclear. Given the differences in the three-dimensional structure of the family of acyl-CoA dehydrogenases (acyl-CoA dehydrogenase-fold) and of D-lactate/D-2-hydroxyglutarate dehydrogenase (*p*-cresol methylhydroxylase-fold), it is conceivable that the molecular mechanisms enabling successful electron transfer are also distinct. In any case, being able to control oxygen reactivity is important to ensure the delivery of electrons to the mitochondrial electron transport chain and at the same time limits the production of undesired reactive oxygen species, such as hydrogen peroxide.

Interestingly, the overall turnover rates determined for the electron transfer from hD2HGDH to hETF are in a similar range, but slightly lower as compared with other client dehydrogenases (0.53 ± 0.03 s^{-1} vs ~2 s^{-1} of hDMGDH and hMCAD). However, it should be noted that the interaction of hETF with hD2HGDH is tighter as compared with other donor dehydrogenases (K_M = 2.1 ± 0.5 µM *vs* ~70 µM and ~8 µM for hDMGDH and MCAD, respectively) [16,31], which requires the use of very low hETF concentrations (lowest hETF concentration: 250 nM *vs* 100 nM hD2HGDH) in the turnover assay. Therefore, it is possible that reduced hD2HGDH to some extent directly transfers electrons to DCPIP, thereby seemingly lowering the turnover rates for the electron transfer from hD2HGDH to hETF. This interpretation is also in line with the fact that by applying a hyperbolic fit to the data points, a y-axis intercept at a k_{obs} of ~0.4 s^{-1} was obtained, which is in the same range as the limiting rate (k_{catapp}) determined for the oxidation of D-2HG by hD2HGDH in the DCPIP assay (see above *3.2*).

3.4.3 Disease related variants

Recently, two disease-causing mutations in the *hd2hgdh* gene have been identified in patients suffering from D-2HGA [1]. Although it was shown that the enzymatic activity of the resulting protein variants (hD2HGDH-Ile147Ser and hD2HGDH-Val444Ala) was severely reduced, the reason for the loss in protein function remained elusive, in particular because the position(s) of the amino acid replacement(s) as well as the conservative nature of the

exchange(s) did not provide a straight forward explanation [1]. Thus, we produced the two variants in *E. coli* to investigate the loss of activity in more detail. Both variants were isolated as apo-proteins and the addition of FAD could not reconstitute the holo-protein. This finding was surprising because neither one of the positions where the amino acid replacements have occurred appears to be involved in FAD binding (Figure 5). In order to better understand the lack of FAD binding, we performed CD-spectroscopy and limited proteolysis experiments as well as size-exclusion chromatography. We could clearly show that while the secondary structure elements largely remained unaffected by the single amino acid replacements (Figure 6A and Table 4), their quaternary structures were strongly impaired (Figure 6B and C). Size exclusion chromatography, for example, revealed that both variants exhibit an increased tendency toward aggregate formation, whereas the wild type enzyme is a dimer in solution. This fact is also in agreement with the results obtained from the limited proteolysis experiment, which revealed a reduced susceptibility of the variants to proteolytic degradation, and may explain the decreased binding affinity of the FAD cofactor as compared to the wild type enzyme.

The findings are also very well in line with the observation of Struys *et al.*(2005) that the replacement of Ile147 by a serine results in a complete loss in enzymatic activity, but they do not explain the residual activity of 25% determined for the Val444Ala variant [1]. However, there are several reasons, why different results could have been obtained in our study, as compared to Struys *et al.* [1]. Firstly, the completely diminished oxidase activity observed in our studies might result from the recombinant production of the protein in *E. coli*. While humans employ a set of chaperones in order to ensure properly-folded proteins, the latter are absent in the bacterial expression system. On the other hand, co-production of the chaperon in complex GroES/GroEL in *E. coli* failed to reduce the amount of catalytically inactive aggregate. Apart from the presence of molecular chaperones, also the availability of free FAD was reported to affect protein folding and activity[51,52]. Studies by Saijo *et al.*[51] and Cornelius *et al.*[52], for example, have shown that increasing the levels of riboflavin in the culture media reduced the aggregation of defective MCAD and ETF-QO variants, resulting in a higher activity of these proteins. However, in the case of the two hD2HGDH variants the amount of aggregate could not substantially be reduced by riboflavin supplementation in the culture medium. Nevertheless, since vitamin B_2 supplementation has been successfully used for the treatment of milder forms of multiple acyl-CoA dehydrogenase deficiency (MADD)

and glutaric aciduria type I and II [53–55], it is conceivable that increased riboflavin levels may have a beneficial effect on the activity of the variant proteins *in vivo*.

3.5 Conclusions

In the present study, we have established the kinetic parameters for the oxidation of D-lactate and D-2HG by hD2HGDH, which have clearly identified D-2HG as the preferred substrate. We have also shown that product binding to the reduced enzyme suppresses the reactivity with oxygen and turns the enzyme into a dehydrogenase. Moreover, we have provided experimental evidence that substrate-reduced enzyme transfers electrons to hETF and thus oxidation of D-2HG is coupled to the mitochondrial electron transport chain. Finally, our results also explain the lack of enzymatic activity in two disease-related variants discovered in patients suffering from D-2HGA.

3.6 Author contributions

MT, JB and JS cloned the genes, produced the proteins and performed the biochemical characterization of hD2HGDH wild type and the variants; MT, JB and PM designed the biochemical experiments and interpreted the data; MT and PM wrote the manuscript.

3.7 Conflict of interest

The authors declare no conflict of interest.

3.8 Acknowledgements

We would like to thank Eva Frießer for her help with the production as well as with the purification of GB1-hD2HGDH wild type and the variants and Dr. Gustav Oberdorfer for his assistance with the CD-spectroscopy experiments. This work was supported by a grant from the Austrian Science Fund (FWF) through grant W901 (Doctoral Program "Molecular Enzymology"). The authors are also grateful for the support by the interuniversity program in natural sciences (NAWI Graz).

3.9 References

[1] E. A. Struys, "*Mutations in the D-2-hydroxyglutarate dehydrogenase gene cause D-2-hydroxyglutaric aciduria*," Am J Hum Genet, vol. 76, pp. 358–360, 2005.

[2] E. E. Kaufman, T. Nelson, H. M. Fales, and D. M. Levin, "*Isolation and characterization of a hydroxyacid-oxoacid transhydrogenase from rat kidney mitochondria*," J. Biol. Chem., vol. 263, no. 32, pp. 16872–16879, 1988.

[3] E. A. Struys, N. M. Verhoeven, H. J. Brink, W. V. Wickenhagen, K. M. Gibson, and C. Jakobs, "*Kinetic characterization of human hydroxyacid-oxoacid transhydrogenase: Relevance to D-2-hydroxyglutaric and γ-hydroxybutyric acidurias*," J. Inherit. Metab. Dis., vol. 28, no. 6, pp. 921–930, 2005.

[4] Y. Achouri, G. Noël, D. Vertommen, M. H. Rider, M. Veiga-da-Cunha, and E. van Schaftingen, "*Identification of a dehydrogenase acting on D-2-hydroxyglutarate*," Biochem. J., vol. 381, no. 1, pp. 35–42, 2004.

[5] M. K. M. Engqvist, C. Eßer, A. Maier, M. J. Lercher, and V. G. Maurino, "*Mitochondrial 2-hydroxyglutarate metabolism*," Mitochondrion, vol. 19, no. PB, pp. 275–281, 2014.

[6] J. Becker-Kettern et al., "*Saccharomyces cerevisiae Forms D-2-Hydroxyglutarate and Couples Its Degradation to D-Lactate Formation via a Cytosolic Transhydrogenase*," J. Biol. Chem., vol. 291, no. 12, pp. 6036–6058, 2016.

[7] M. Engqvist, M. F. Drincovich, U. I. Flügge, and V. G. Maurino, "*Two D-2-hydroxy-acid dehydrogenases in Arabidopsis thaliana with catalytic capacities to participate in the last reactions of the methylglyoxal and β-oxidation pathways*," J. Biol. Chem., vol. 284, no. 37, pp. 25026–25037, 2009.

[8] M. Toplak, J. Brunner, C. R. Tabib, and P. Macheroux, "*Closing the gap: yeast electron-transferring flavoprotein links the oxidation of D-lactate and D-α-hydroxyglutarate to energy production via the respiratory chain*," FEBS J., p. febs.14924, 2019.

[9] M. Kranendijk, E. A. Struys, G. S. Salomons, M. S. Van der Knaap, and C. Jakobs, "*Progress in understanding 2-hydroxyglutaric acidurias.*," J. Inherit. Metab. *Dis.*, vol. 35, no. 4, pp. 571–87, Jul. 2012.

[10] H. Watanabe et al., "*Identification of the D-enantiomer of 2-hydroxyglutaric acid in glutaric aciduria type II*," Clin. Chim. Acta, vol. 238, no. 2, pp. 115–124, 1995.

[11] M. Kranendijk et al., "*IDH2 mutations in patients with D-2-hydroxyglutaric aciduria,"* Science,

vol. 330, no. 6002. p. 336, 2010.

[12] B. Nota et al., "*Deficiency in SLC25A1, encoding the mitochondrial citrate carrier, causes combined D-2- and L-2-hydroxyglutaric aciduria*," Am. J. Hum. Genet., vol. 92, no. 4, pp. 627–631, 2013.

[13] C. Mühlhausen et al., "*Combined D2-/L2-hydroxyglutaric aciduria (SLC25A1 deficiency): clinical course and effects of citrate treatment*," J. Inherit. Metab. Dis., vol. 37, no. 5, pp. 775–781, 2014.

[14] M. Kranendijk et al., "*Evidence for genetic heterogeneity in D-2-hydroxyglutaric aciduria*," Hum. Mutat., vol. 31, no. 3, pp. 279–283, 2010.

[15] T. N. Petersen, S. Brunak, G. von Heijne, and H. Nielsen, "*SignalP 4.0: discriminating signal peptides from transmembrane regions*," Nat. Methods, vol. 8, no. 10, pp. 785–786, 2011.

[16] P. Augustin et al., "*Oxidation of the FAD cofactor to the 8-formyl-derivative in human electron-transferring flavoprotein*," J. Biol. Chem., vol. 293, no. 8, pp. 2829–2840, 2018.

[17] P. Macheroux, "*UV-visible spectroscopy as a tool to study flavoproteins.*," Methods Mol. Biol., vol. 131, pp. 1–7, 1999.

[18] V. Massey, P. Hemmerich, W. R. Knappe, H. J. Duchstein, and H. Fenner, "*Photoreduction of flavoproteins and other biological compounds catalyzed by deazaflavins. Appendix: photochemical formation of deazaflavin dimers*," Biochemistry, vol. 17, no. 1, pp. 9–17, Jan. 1978.

[19] V. Massey, "*A simple method for the determination of redox potentials.*," in Flavins and Flavoproteins, B. Curti, G. Zanetti, and S. Ronchi, Eds. Como, Italy: Walter de Gruyter, 1991, pp. 59–66.

[20] K. Minnaert, "*Measurement of the equilibrium constant of the reaction between cytochrome c and cytochrome a.*," Biochim. Biophys. Acta, vol. 110, pp. 42–56, 1965.

[21] M. Biasini et al., "*SWISS-MODEL: Modelling protein tertiary and quaternary structure using evolutionary information*," Nucleic Acids Res., vol. 42, no. W1, 2014.

[22] K. Arnold, L. Bordoli, J. Kopp, and T. Schwede, "*The SWISS-MODEL workspace: A web-based environment for protein structure homology modelling*," Bioinformatics, vol. 22, no. 2, pp. 195–201, 2006.

[23] P. Benkert, M. Biasini, and T. Schwede, "*Toward the estimation of the absolute quality of*

individual protein structure models," Bioinformatics, vol. 27, no. 3, pp. 343–350, 2011.

[24] F. Armougom et al., "*Expresso: Automatic incorporation of structural information in multiple sequence alignments using 3D-Coffee*," Nucleic Acids Res., vol. 34, no. WEB. SERV. ISS., 2006.

[25] M. Gouy, S. Guindon, and O. Gascuel, "*Sea view version 4: A multiplatform graphical user interface for sequence alignment and phylogenetic tree building*," Mol. Biol. Evol., vol. 27, no. 2, pp. 221–224, 2010.

[26] A. Lobley, L. Whitmore, and B. A. Wallace, "*DICHROWEB: An interactive website for the analysis of protein secondary structure from circular dichroism spectra*," Bioinformatics, vol. 18, no. 1, pp. 211–212, 2002.

[27] L. Whitmore and B. A. Wallace, "*DICHROWEB, an online server for protein secondary structure analyses from circular dichroism spectroscopic data*," Nucleic Acids Res., vol. 32, no. WEB SERVER ISS., 2004.

[28] L. Whitmore and B. A. Wallace, "*Protein secondary structure analyses from circular dichroism spectroscopy: Methods and reference databases*," Biopolymers, vol. 89, no. 5, pp. 392–400, 2008.

[29] U. K. Laemmli, "*Cleavage of structural proteins during the assembly of the head of bacteriophage T4*," Nature, vol. 227, no. 5259, pp. 680–685, 1970.

[30] G. J. Mancini-Samuelson, V. Kieweg, K. M. Sabaj, S. Ghisla, and M. T. Stankovich, "*Redox properties of human medium-chain Acyl-CoA dehydrogenase, modulation by charged active-site amino acid residues*," Biochemistry, vol. 37, no. 41, pp. 14605–14612, 1998.

[31] H. S. Toogood, A. Van Thiel, N. S. Scrutton, and D. Leys, "*Stabilization of non-productive conformations underpins rapid electron transfer to electron-transferring flavoprotein*," J. Biol. Chem., vol. 280, no. 34, pp. 30361–30366, 2005.

[32] L. A. Compton and W. C. Johnson, "*Analysis of protein circular dichroism spectra for secondary structure using a simple matrix multiplication*," Anal. Biochem., vol. 155, no. 1, pp. 155–167, 1986.

[33] N. Sreerama and R. W. Woody, "*Estimation of protein secondary structure from circular dichroism spectra: Comparison of CONTIN, SELCON, and CDSSTR methods with an expanded reference set*," Anal. Biochem., vol. 287, no. 2, pp. 252–260, 2000.

[34] J. G. Lees, A. J. Miles, F. Wien, and B. A. Wallace, "*A reference database for circular*

dichroism spectroscopy covering fold and secondary structure space," Bioinformatics, vol. 22, no. 16, pp. 1955–1962, 2006.

[35] E. R. DuPlessis, J. Pellett, M. T. Stankovich, and C. Thorpe, "*Oxidase activity of the acyl-CoA dehydrogenases*," Biochemistry, vol. 37, no. 29, pp. 10469–10477, 1998.

[36] N. D. Lenn, M. T. Stankovich, and H. W. Liu, "*Regulation of the redox potential of general acyl-CoA dehydrogenase by substrate binding*," Biochemistry, vol. 29, no. 15, pp. 3709–3715, 1990.

[37] H. S. Toogood, D. Leys, and N. S. Scrutton, "*Dynamics driving function - New insights from electron transferring flavoproteins and partner complexes*," FEBS Journal, vol. 274, no. 21. pp. 5481–5504, 2007.

[38] S. Ghisla and C. Thorpe, "*Acyl-CoA dehydrogenases: A mechanistic overview,"* European Journal of Biochemistry, vol. 271, no. 3. pp. 494–508, 2004.

[39] B. D. Johnson and M. T. Stankovich, "*Influence of two substrate analogues on thermodynamic properties of medium-chain acyl-CoA dehydrogenase,*" Biochemistry, vol. 32, no. 40, pp. 10779–10785, 1993.

[40] N. Ravi Kumar and D. K. Srivastava, "*Facile and restricted pathways for the dissociation of octenoyl-CoA from the medium-chain fatty acyl-CoA dehydrogenase (MCAD)-FADH2-octenoyl-CoA charge-transfer complex: Energetics and mechanism of suppression of the enzyme's oxidase activity,*" Biochemistry, vol. 34, no. 29, pp. 9434–9443, 1995.

[41] V. Massey and S. Ghisla, "*The mechanism of action of flavoprotein - catalyzed reactions,*" in Biological Oxidations, vol. 34, H. Sund and V. Ullrich, Eds. Berlin: Springer, 1983, pp. 114–139.

[42] A. Mattevi, "*To be or not to be an oxidase: challenging the oxygen reactivity of flavoenzymes*," Trends in Biochemical Sciences, vol. 31, no. 5. pp. 276–283, 2006.

[43] P. Chaiyen, M. W. Fraaije, and A. Mattevi, "*The enigmatic reaction of flavins with oxygen,*" Trends in Biochemical Sciences, vol. 37, no. 9. pp. 373–380, 2012.

[44] E. Romero, J. R. Gómez Castellanos, G. Gadda, M. W. Fraaije, and A. Mattevi, "*Same substrate, many reactions: Oxygen activation in flavoenzymes,*" Chemical Reviews, vol. 118, no. 4. pp. 1742–1769, 2018.

[45] Y. Lindqvist, C. I. Branden, F. S. Mathews, and F. Lederer, "*Spinach glycolate oxidase and yeast flavocytochrome b2 are structurally homologous and evolutionarily related enzymes with*

distinctly different function and flavin mononucleotide binding," J. Biol. Chem., vol. 266, no. 5, pp. 3198–3207, 1991.

[46] D. Zafred et al., "*Rationally engineered flavin-dependent oxidase reveals steric control of dioxygen reduction,*" FEBS J., vol. 282, no. 16, pp. 3060–3074, 2015.

[47] C. Thorpe and J.-J. Kim, "*Structure and mechanism of action of the acyl-CoA dehydrogenases,*" FASEB J., vol. 9, no. 9, pp. 718–725, 1995.

[48] R. J. Gorelick, L. M. Schopfer, D. P. Ballou, V. Massey, and C. Thorpe, "*Interflavin oxidation-reduction reactions between pig kidney general acyl-CoA dehydrogenase and electron-transferring flavoprotein,*" Biochemistry, vol. 24, no. 24, pp. 6830–6839, 1985.

[49] J. Reinsch, A. Katz, J. Wean, G. Aprahamian, and J. T. McFarland, "*The deuterium isotope effect upon the reaction of fatty acyl-CoA dehydrogenase and butyryl-CoA.,*" J. Biol. Chem., vol. 255, no. 19, pp. 9093–9097, 1980.

[50] C. L. Hall and J. D. Lambeth, "*Studies on electron transfer from general acyl-CoA dehydrogenase to electron transfer flavoprotein.*," J. Biol. Chem., vol. 255, no. 8, pp. 3591–3595, 1980.

[51] T. Saijo, J. J. P. Kim, Y. Kuroda, and K. Tanaka, "*The roles of threonine-136 and glutamate-137 of human medium chain Acyl- CoA dehydrogenase in FAD binding and peptide folding using site-directed mutagenesis: Creation of an FAD-dependent mutant, T136D,*" Arch. Biochem. Biophys., vol. 358, no. 1, pp. 49–57, 1998.

[52] N. Cornelius et al., "*Molecular mechanisms of riboflavin responsiveness in patients with ETF-QO variations and multiple acyl-CoA dehydrogenation deficiency,*" Hum. Mol. Genet., vol. 21, no. 15, pp. 3435–3448, 2012.

[53] R. A. Chalmers, M. D. Bain, and J. Zschocke, "*Riboflavin-responsive glutaryl CoA dehydrogenase deficiency,*" Mol. Genet. Metab., vol. 88, no. 1, pp. 29–37, 2006.

[54] B. J. Henriques, R. K. Olsen, P. Bross, and C. M. Gomes, "*Emerging roles for riboflavin in functional rescue of mitochondrial β-oxidation flavoenzymes*," Curr. Med. Chem., vol. 17, no. 32, pp. 3842–3854, 2010.

[55] S. Missaglia, D. Tavian, L. Moro, and C. Angelini, "*Characterization of two ETFDH mutations in a novel case of riboflavin-responsive multiple acyl-CoA dehydrogenase deficiency*," Lipids Health Dis., vol. 17, no. 1, p. 254, 2018.

4. Supplement: 8-formyl FAD modification in yETF variants

4.1 Methods

If not further described, the experimental procedures were performed as it is described in chapter 2. “Closing the gap: Yeast electron transferring flavoprotein links the oxidation of D-lactate and D-α-hydroxyglutarate to energy production via the respiratory chain”.

4.1.1 Site directed mutagenesis

yETF variants were generates as described in *2.3.10 Site directed mutagenesis*. The variants, as well as their primer sequences are listed in Table 1.

Table 1: Mutagenesis primers used to generate yETF variants. Codon triplets carrying the mutations are shown in bold.

Variant	Type	Primer Sequence
αN269A	Fwd.	5′–CGTGCAAGCGTTGATAATGGCCTGTGTGAT**GCT**AGCCTGCAGATTGG–3′
	Rev.	5′–GCAACAACTTTACCGGTCTGACCAATCTGCAGGCT**AGC**ATCACACAGG–3′
αQ272A	Fwd.	5′–GATAATAGCCTG**GCT**ATTGGTCAGACCGG–3′
	Rev.	5′–CTGACCAAT**AGC**CAGGCTATTATCACAC–3′
βE169A	Fwd.	5′–CTGGATAATGGTCGTGTTCAGGTTACCCGT**GCA**ATCGATGATGGTG–3′
	Rev.	5′–GGCTTGCTTCAATAACTTCTTCACCATCATCGAT**TGC**ACGGGTAACC–3′
βF19I	Fwd.	5′–GCGTATTCTGGTTCCGGTTAAACGTGTTGTTGAT**ATT**CAGATTAAACCG–3′
	Rev.	5′–CGGTCAGGGTTTTATTCACACGCGGTTTAATCTG**TAA**ATCAACAACACG–3′
βF19Y	Fwd.	5′–GCGTATTCTGGTTCCGGTTAAACGTGTTGTTGAT**TAT**CAGATTAAACCG–3′
	Rev.	5′–CGGTCAGGGTTTTATTCACACGCGGTTTAATCTG**ATA**ATCAACAACACG–3′

Additionally, the following variants including two or three mutations were generated:

yETF-βF19Y-αN269A
yETF-βF19Y-αQ272A
yETF-βF19Y-αQ272A-αN269A
yETF-βF19Y-βE169A.

These variants were generated using the same procedure as the variants with a single mutation. The templates used for the polymerase chain reactions included one (or in case of the triple mutant two) mutation(s).

4.2 Results

4.2.1 Photoreduction of yETF variants

Photoreductions were performed for all yETF variants and monitored using UV-Vis spectroscopy. The spectral changes observed in two additional variants (yETF-αAsn269Ala (A) and yETF-βPhe19Tyr-βGlu169Ala (B)) are shown in Figure 8.

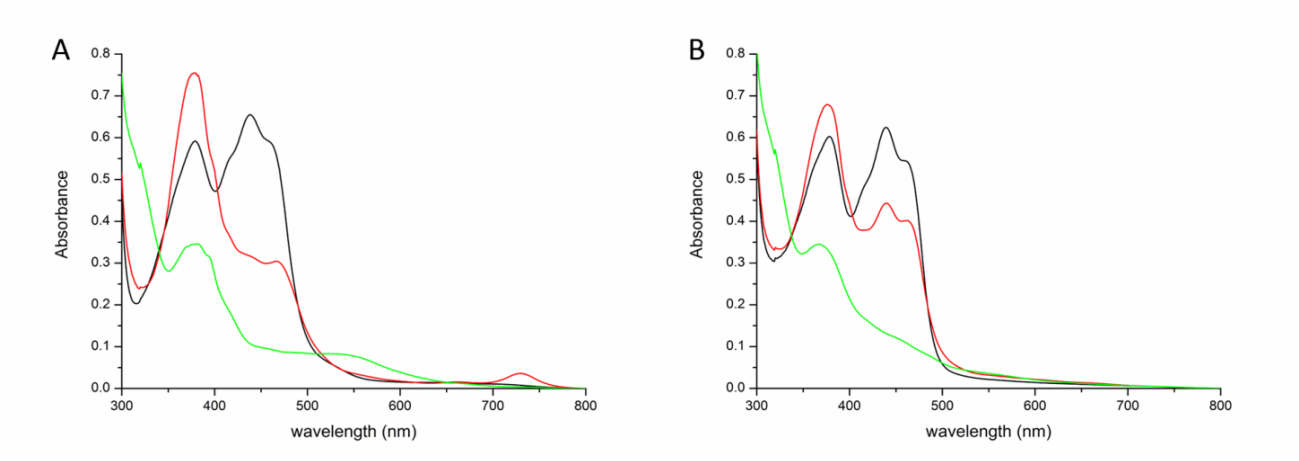

Figure 8: Photoreduction of yETF-αAsn269Ala (A) and yETF-βPhe19Tyr-βGlu169Ala (B) under anoxic conditions. UV/Vis absorption spectra were recorded in a range of 300-800 nm. The spectra show the oxidized FAD (black line), the anionic semiquinone (red line), as well as the reduced FAD (green line).

4.2.2 Formation of 8-formyl-FAD in yETF variants

8-formyl-FAD (8f-FAD) content observed in yETF wild type and selected variants (A) in comparison with the equivalent hETF variants (B) is shown in Figure 9.

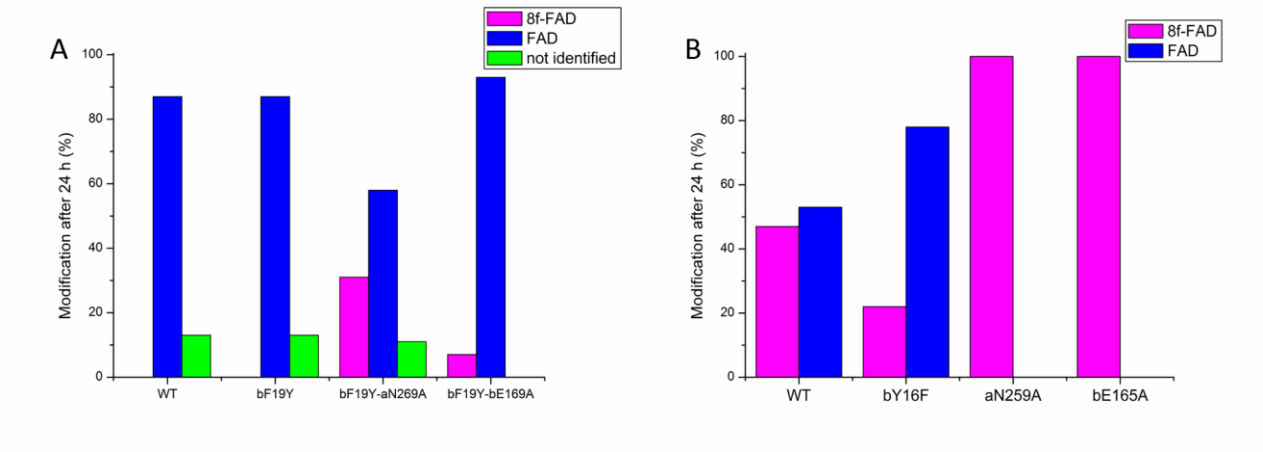

Figure 9: 8f-FAD modification of yETF variants (A) and hETF variants (B). yETF-βF19Y has the same amino acid residues in the binding pocket as hETF-WT, allowing these variants to be compared. yETF-βF19Y-αN269A can be compared to hETF-αN259A and yETF-βF19Y-βE169A can be compared to hETF-βE165A.

The observed modifications of all yETF variants analyzed are shown in Table 2.

Table 2: Cofactor modification of yETF variants after 24 hours. Column 2 describes the percentage of unmodified FAD, while column 3 shows the amount of 8-formyl-FAD modification. An unknown flavin modification could also be observed, which is indicated in column 4.

Variants	FAD [%]	8-formyl-FAD [%]	Not identified [%]
Wilde type	87	0	13
αN269A	74	26	0
αQ272A	96	0	4
βE169A	72	0	28
βF19I	74	0	26
βF19Y	88	0	12
βF19Y-αN269A	58	37	5
βF19Y-αQ272A	94	6	0
βF19Y-αQ272A- αN269A	92	0	8
βF19Y-βE169A	93	7	0

4.3 Conclusion

The photoreduction experiments, as well as the time-dependent analyses of the formation of 8f-FAD in yETF variants show that there is no correlation between the 8f-FAD formation in hETF and yETF. In hETF, the exposure of the cofactor to the surrounding solution leads to the formation of 8f-FAD, whereas this effect cannot be observed for yETF. Additionally, yETF shows a modification that could not be identified, which was never observed in hETF.

Additionally, the absorption changes monitored during the photoreduction of yETF wild type and the variants were very similar. Even though a semiquinone state is formed, it is not as stable in hETF. With time, every yETF variant could be reduced to the hydroquinone form.

In conclusion, no variant of yETF was able to simulate the modification occurring in hETF. Therefore the ETF of *Saccharomyces cerevisiae* could not be used to gain more information on the mechanism o 8f-FAD formation in hETF.